DOT/FAA/TC-13/43

Federal Aviation Administration
William J. Hughes Technical Center
Aviation Research Division
Atlantic City International Airport
New Jersey 08405

General Aviation Accident Prevention—Basic Envelope Protection Phase III: Flight Test Results and Recommendations for Future Envelope Protection Systems

September 2014

Final Report

This document is available to the U.S. public through the National Technical Information Services (NTIS), Springfield, Virginia 22161.

U.S. Department of Transportation
Federal Aviation Administration

NOTICE

This document is disseminated under the sponsorship of the U.S. Department of Transportation in the interest of information exchange. The U.S. Government assumes no liability for the contents or use thereof. The U.S. Government does not endorse products or manufacturers. Trade or manufacturers' names appear herein solely because they are considered essential to the objective of this report. The findings and conclusions in this report are those of the author(s) and do not necessarily represent the views of the funding agency. This document does not constitute FAA policy. Consult the FAA sponsoring organization listed on the Technical Documentation page as to its use.

This report is available at the Federal Aviation Administration William J. Hughes Technical Center's Full-Text Technical Reports page: actlibrary.tc.faa.gov in Adobe Acrobat portable document format (PDF).

Technical Report Documentation Page

1. Report No.	2. Government Accession No.	3. Recipient's Catalog No.
DOT/FAA/TC-13/43		

4. Title and Subtitle	5. Report Date
GENERAL AVIATION ACCIDENT PREVENTION – BASIC ENVELOPE PROTECTION, PHASE III: FLIGHT TEST RESULTS AND RECOMMENDATIONS FOR FUTURE ENVELOPE PROTECTION SYSTEMS	September 2014
	6. Performing Organization Code
7. Author(s)	8. Performing Organization Report No.
John Wilson and Mark Peters	
9. Performing Organization Name and Address	10. Work Unit No. (TRAIS)
Sensis Corporation Seagull Technology Center 1700 Dell Avenue Campbell, CA 95008	
	11. Contract or Grant No.
12. Sponsoring Agency Name and Address	13. Type of Report and Period Covered
U.S. Department of Transportation Federal Aviation Administration Central Region—Small Airplane Directorate FAA Central Regional Office 901 Locust Street Kansas City, MO 64106	Final Report
	14. Sponsoring Agency Code ACE-114

15. Supplementary Notes

The Federal Aviation Administration William J. Hughes Technical Center Aviation Research Division COR was Robert J. McGuire.

16. Abstract

This report discusses the development of a means to reduce loss-of-control (LOC) accidents in the general aviation fleet. A full-time stability augmentation and envelope protection system for retrofit or forward fit to existing cable-controlled aircraft was developed and flight-tested in a Cessna R182 aircraft. Two features of the system were found to be of great potential value for eliminating LOC accidents: (1) stall warning and protection using direct angle-of-attack measurement, including visual, auditory, and tactile warnings; and (2) roll stability augmentation with or without overbank protection, including an always-on tendency to return to wings-level flight without compromising manual roll control feel. Flight test results, overall impressions, and detailed recommendations for future design and certification standards for such systems are included in this report.

17. Key Words	18. Distribution Statement
Flight control, Loss of control, Autopilots, Envelope protection, Stability augmentation, General aviation, Light aircraft	This document is available to the U.S. public through the National Technical Information Service (NTIS), Springfield, Virginia 22161. This document is also available from the Federal Aviation Administration William J. Hughes Technical Center at actlibrary.tc.faa.gov.

19. Security Classif. (of this report)	20. Security Classif. (of this page)	21. No. of Pages	22. Price
Unclassified	Unclassified	169	

Form DOT F 1700.7 (8-72) Reproduction of completed page authorized

TABLE OF CONTENTS

			Page
EXECUTIVE SUMMARY			x
1.	INTRODUCTION		1
	1.1	Background	1
2.	FULL-TIME ENVELOPE PROTECTION SYSTEM CONCEPT		2
	2.1	Sensing Considerations	2
	2.2	Display and Annunciation Considerations	3
	2.3	Servo Design Considerations	3
3.	SIMULATOR TESTS		3
4.	FLIGHT TEST PLATFORM AND EQUIPMENT		5
	4.1	System Overview	6
		4.1.1 Pilot Inputs	7
		4.1.2 Actuation	7
		4.1.3 Sensors	7
		4.1.4 Computers	7
		4.1.5 Pilot Cues	7
	4.2	Experimental Pallet	8
	4.3	Sensors	9
		4.3.1 The ADAHRS	9
		4.3.2 The AoA Module	10
		4.3.3 The G-Limit Module	14
	4.4	Actuators	16
		4.4.1 Servos	16
		4.4.2 Yoke Buzzers	22
	4.5	Displays	24
	4.6	Computers	28
		4.6.1 Computer Problems	31

5. HARDWARE-IN-THE-LOOP SIMULATION 32

6. FLIGHT CONTROL SOFTWARE 32

6.1 Operating System 32
6.2 Data Acquisition Libraries 33
6.3 Dataflow To and From the Flight Control Computer 33

7. AUTOPILOT STANDARD-MODE ALGORITHMS 35

7.1 Lateral Autopilot 35

7.1.1 Wing Leveler 35
7.1.2 Heading Capture 36

7.2 Longitudinal Autopilot 39

7.2.1 Vertical Speed Mode 39
7.2.2 The FLC Mode 40
7.2.3 Altitude Hold and Capture 43
7.2.4 Control Surface Deflections 43

7.3 Standard Autopilot Modes Not Implemented 44

8. STABILITY AUGMENTATION ALGORITHMS 44

8.1 Lateral Stability Augmentation 44

8.1.1 Tactile Consequences of the Control Law 45
8.1.2 Tactile Consequences of Servo Mechanizations 47

8.2 Longitudinal Stability Augmentation 47

9. ENVELOPE PROTECTION ALGORITHMS 49

9.1 Lateral Envelope Protection 49
9.2 Longitudinal Envelope Protection 51

9.2.1 Stall 52
9.2.2 Overpitch 53
9.2.3 Overspeed 53

9.3 Mode Switching 54

10. MANUALLY-ENGAGED UNUSUAL ATTITUDE RECOVERY DESIGN 55

10.1 Bank Angle Control 56
10.2 Pitch Recovery Control 56
10.3 Outer Loop Logic 58

11. FLIGHT TEST RESULTS 60

11.1 Standard Autopilot Functions 60

11.1.1 Wing Leveler 60
11.1.2 Heading Capture and Hold 61
11.1.3 Vertical Speed Hold 62
11.1.4 Flight Level Change 63
11.1.5 Vertical Speed Hold With Automatic Switch to FLC 64

11.2 Stability Augmentation 65

11.2.1 Unaugmented Spiral Mode 66
11.2.2 Lateral Stability Augmentation 67
11.2.3 Unaugmented Phugoid Mode 68
11.2.4 Longitudinal Stability Augmentation 69
11.2.5 Combined Lateral and Longitudinal Stability Augmentation 70

11.3 Envelope Protection 71

11.3.1 Overbank 71
11.3.2 Stall 73
11.3.3 Overpitch 75
11.3.4 Overspeed 76

11.4 Unusual Attitude Recovery 77

11.4.1 Unusual Attitude Recovery 77

12. DISCUSSION 79

12.1 Utility and Relative Importance of Features 79
12.2 Stall Protection 79
12.3 Roll Stability Augmentation/Overbank Protection 80
12.4 Other Features 81

13. RECOMMENDATIONS REGARDING FUTURE DESIGNS AND CERTIFICATION STANDARDS 81

13.1 Key Functional Capabilities 81
13.2 Philosophical Considerations 82

13.3 High-Level Design Principles 82
13.4 Desirable Design Attributes 83

13.4.1 Servo Design 83
13.4.2 Lateral Protection 84
13.4.3 Longitudinal Protection 86
13.4.4 Unusual Attitude Recovery 87
13.4.5 Tactile Feedback 88
13.4.6 Additional Considerations 88

14. REFERENCES 88

APPENDICES

A—Flight Control Software Description
B—Derivation of Aircraft Equations of Motion
C—Linear Force Model
D—Linearization of Longitudinal Dynamics
E—Linearization of Lateral Dynamics
F—Aircraft Model Numerical Data
G—Linear Analysis of Control Modes
H—Experimental Servo Component Details
I—Flight Test Hazard Analysis
J—Preflight Checklist for Experimental Test Flights
K—Flight Test DVD

LIST OF FIGURES

Figure		Page
1	Cessna R182 Simulator	4
2	Cessna R182 Simulator Instrument Panel	5
3	Cessna R182 Aircraft Used for Flight Test	6
4	Functional Block Diagram of Flight Test Instrumentation	6
5	Experimental Pallet Installed in Baggage Area of Cessna R182	8
6	The ADAHRS Used in Flight Test	9
7	Alpha Systems Two-Port AoA Probe Installed on Test Aircraft	11
8	Dynon Two-Port AoA Probe Installed on Test Aircraft	12
9	Experimental AoA Module	13
10	Linear Fit for AoA vs. Normalized Probe Pressures	14
11	The G-Limit Disconnect Module	15
12	Alpha Prototype Servo Mounted Alongside Control Loader on Simulator	16
13	Alpha Prototype Servo CAD Image	17
14	Beta Prototype Servo CAD Image	18
15	Output Sprocket of ARC Certified Servo With Integrated Shear Pin	19
16	Flight Servo Attached to Elevator Cable Controls in Aircraft	20
17	Modified ARC Servo Initially Used for Aileron Control During Flight Tests	21
18	Flight Servo Mounted in Cabin Ceiling for Aileron Control	22
19	Experimental Yoke Buzzers Mounted on Test Aircraft Yokes	23
20	Close-up View of Yoke Buzzer Showing Eccentric Weight on Motor Shaft	24
21	Experimental PFD and MCP in Test Aircraft	25
22	The PFD Display Screenshot	26
23	Engineering/Test MCP	27
24	Graphics Computer (top) and Flight Control Computer (bottom)	28
25	Jetway Mini-ITX IPC Motherboard With VIA CN700 Chipset	29
26	National Instruments NI-PCI-6221 Data Acquisition Card	29
27	The ZOTAC™ GF9300-I-E Motherboard Used for the Graphics Computer	30
28	The M3-ATX-HV Power Converter	30
29	Corsair Solid-State 32GB Hard Drive	31
30	Input/Output Signals for Flight Computers	34
31	Lateral Bank Angle Control	36
32	Simple Ramp Shaping Function for Bank Angle Control	36
33	Heading Control	37
34	Heading Control Using Bank Angle	38
35	Vertical Speed Controller	39
36	Ramp Shaping Function Used With the Vertical Speed Controller	40
37	Speed Capture for FLC Mode	41
38	Logic for Engaging Vertical Speed Mode During FLC Mode	42
39	Altitude Hold and Capture	43
40	Controller for Commanding Control Surface Deflections	44
41	Bank Angle Stability Augmentation	45

42	The Type of Actuator Control Law Influences the Tactile Feel	46
43	Difference in Tactile Feel Between Torque and Position-Based Control Laws	46
44	Longitudinal Stability Augmentation Used on the Simulator	48
45	Trim Impact on the Controller	48
46	Gradual Torque Increases Can Be Missed	50
47	Bank Angle Envelope Control Used in the Simulator	51
48	Bank Angle Envelope Control Using Hysteresis	51
49	Stall Prevention	52
50	Overpitch Envelope Protection	53
51	Overspeed Envelope Protection	54
52	Accelerated Stall Can Trigger Underpitch	55
53	Wing Leveling Algorithm Used for Recovery	56
54	Pitch Control Law Used for Recovery	57
55	Control Law for Fine Pitch Control	58
56	Logic Used to Determine Transition to Fine Pitch Control	58
57	Logic Used to Orchestrate Roll and Pitch Control	59
58	Logic Used to Determine Transition to Autopilot	59
59	Wing Leveler	61
60	Heading Capture and Hold	62
61	Descent at Commanded Vertical Speed	63
62	Flight Level Change	64
63	Vertical Speed Hold With Automatic Switch to FLC	65
64	Unaugmented Spiral Mode	66
65	Spiral Entry With Lateral Stability Augmentation On	67
66	Unaugmented Phugoid Mode	68
67	Pitch Up Maneuver With Longitudinal Stability Augmentation	69
68	Spiral Entry With Lateral and Longitudinal Stability Augmentation On	70
69	Overbank With Envelope Protection On	72
70	The PFD Annunciation of a Right-Hand Overbank Condition	73
71	Incipient Stalls With Envelope Protection On	74
72	The PFD Annunciation of Incipient Stall	75
73	Overpitch With Envelope Protection On	76
74	Overspeed With Envelope Protection On	77
75	Unusual Attitude Recovery	78

LIST OF ABBREVIATIONS AND ACRONYMS

6-DOF	6-degrees-of-freedom
ADAHRS	Air Data Attitude and Heading Reference System
AHRS	Attitude and Heading Reference System
AoA	Angle of attack
ARC	Aircraft Radio Corporation
CAD	Computer-aided design
CFIT	Controlled flight into terrain
Comedi	Control and Measurement Device Interface
EOM	Equation of Motion
FCON	Flight control
FLC	Flight Level Change
GA	General Aviation
GPS	Global Positioning System
IAS	Indicated air speed
I/O	Input/output
IMC	Instrument meteorological conditions
KIAS	Knots Indicated air speed
LOC	Loss of control
MCP	Mode control panel
MSL	Mean sea level
NASA	National Aeronautics and Space Administration
PI	Proportional plus integral (feedback control)
PID	Proportional plus integral plus derivative (feedback control)
PFD	Primary flight display
POSIX	Portable Operating System Interface
RF	Radio frequency
RTAI	RealTime Application Interface
RTHAL	Real Time Hardware Abstraction Layer
UDP	User Datagram Protocol
VFR	Visual flight rules
VHF	Very high frequency

EXECUTIVE SUMMARY

This report discusses the development of a means to reduce loss-of-control (LOC) accidents in the general aviation (GA) fleet. A full-time stability augmentation and envelope protection system for retrofit or forward fit to existing cable-controlled aircraft was developed and flight-tested in a Cessna R182 aircraft. In addition to full-time stability augmentation compatible with pilot manual control, the system provided visual, auditory, and tactile warnings in the event that the aircraft crossed certain flight envelope boundaries. The system also exerted aileron and elevator inputs in a direction appropriate for recovering the aircraft to a safe flight condition. In all cases, the pilot maintained the ability to continue effective, simultaneous manual control inputs with the system engaged. The system was fully compatible with the existing cable controls of the aircraft. Numerous lessons were learned that are relevant to good design practices and desirable certification standards for such systems. These lessons are documented in this report.

Aircraft LOC remains a significant contributor to fatal accidents in GA, and causes the majority of fatal accidents in commercial air transport. The LOC accidents are dominated by two initiating phenomena: stall and excessive bank. Stall is the initial cause of LOC in a number of common scenarios, including stall-spin accidents at pattern altitude, departure stalls, and accelerated stalls during aggressive maneuvering. Excessive bank leads to LOC accidents associated with continued visual flight rules (VFR) into instrument meteorological conditions (IMC) accidents by pilots unable to fly by reference to instruments. Associated with such accidents is pilot disorientation, either prior to, during, or following the excessive banked condition and resulting spiraling dive.

Accordingly, we found that two particular capabilities among those implemented in this work stood out as extremely valuable: stall protection and overbank protection. Active envelope protection to warn and protect against imminent stall (including visual, auditory, and tactile annunciations in concert with servo engagement to prevent inadvertent exceedance of critical angle of attack (AoA)) can prevent stall-induced LOC accidents. Additionally, the inclusion of AoA awareness aids based on measured AoA is both practical and extremely valuable for a typical GA aircraft. The AoA awareness may be provided by visual, auditory, and tactile means. Tactile means are very effective in alerting the pilot of incipient stall in conditions with high levels of distraction.

Lateral stability augmentation via an always-on, torque-limited controller that does not adversely affect manual control feel of the aircraft has potentially great value in reducing the incidence of VFR-into-IMC LOC accidents. In addition to stability augmentation, a more forceful lateral envelope protection capability using higher torque limits for highly-overbanked conditions is practical and potentially advantageous.

In general, the technology to make AoA awareness, stability augmentation, and envelope protection systems accessible at an affordable cost for light GA aircraft is now available. Encouraging retrofit of the existing fleet and inclusion of such systems on a forward-fit basis for

new GA aircraft has the potential to substantially decrease the future incidence of GA LOC accidents.

1. INTRODUCTION.

This report discusses phase III, the final phase of work that focused on defining and developing flight envelope protection concepts and systems for light general aviation (GA) aircraft. Flight tests of a full-time, pilot-in-the-loop, automatic flight envelope protection system were conducted in a Cessna R182 aircraft. The system provided full-time stability augmentation, plus visual, auditory, and tactile warnings in the event that the aircraft state crossed certain envelope boundaries. In addition, the system exerted aileron and elevator inputs in a direction appropriate for recovering the aircraft to a safe flight condition. In all cases, the pilot maintained the ability to continue effective, simultaneous manual control inputs with the system engaged. The system was fully compatible with the existing cable controls of the aircraft. Numerous lessons were learned that are relevant to good design practices and desirable certification standards for such systems. These lessons are documented in this report.

1.1 BACKGROUND.

Aircraft loss of control (LOC) remains a significant contributor to fatal accidents in GA as well as commercial air transport. The LOC accidents account for approximately 38% of all GA aircraft accidents or approximately 100 accidents and 185 lives lost each year [1]. The LOC may occur as a result of disorientation during operation in instrument meteorological conditions (IMC), during low-speed operation in the pattern due to an uncoordinated stall and subsequent spin, or as a result of other conditions in flight.

To reduce LOC accidents, previous research programs have sought to simplify the task of flying the airplane through some form of advanced flight control (FCON). These research programs have generally focused on implementations that require fly-by-wire capability [2]. Although very effective, such approaches, thus far, have been considered impractical for light aircraft, which are typically controlled with cable and pulley actuation. Fly-by-wire systems would likely be difficult to retrofit into existing older GA aircraft or to certify in new production aircraft based on existing type certificates because these aircraft use cable-and-pulley actuation FCON systems. Recently, however, selected envelope protection functions have begun to appear as additional features in existing autopilot systems for cable-controlled aircraft.

With a focus on systems that could be retrofit or forward fit to existing aircraft with cable-and-pulley actuated FCONs, a full-time, always-on autopilot was developed that provides automatic protection against excursions outside the aircraft's normal operational envelope. This concept was developed to allow the pilot to continuously remain in full manual control of the aircraft while the autopilot simultaneously monitors for unsafe conditions, provides warnings if such conditions develop, and contributes control inputs to automatically assist the pilot in returning the aircraft to a safe flight condition.

Previous reports describe initial conceptual work for LOC prevention and the development and use of a dedicated simulator facility to further explore full-time automatic envelope protection [3 and 4]. This report documents the results of flight tests carried out in a Cessna R182 aircraft, including full-time envelope protection and stability augmentation using an experimental autopilot connected to the aircraft cable control system. The system flown operated as an

always-on system that allowed the pilot to maintain normal manual control, while intervening with visual, auditory, and tactile warnings in the event the aircraft passed beyond defined envelope boundaries and providing control inputs to assist in a return to a safe flight condition.

2. FULL-TIME ENVELOPE PROTECTION SYSTEM CONCEPT.

In approaching the question of how to best prevent aircraft LOC accidents, an automatic assistant that would intervene if the aircraft entered a dangerous flight regime was determined to be an effective approach. Considering the typical categories of aircraft LOC accidents, a full-featured system should provide intervention for stall in wings-level flight, accelerated stall, and overbanked conditions. In addition, the system should protect against overpitched conditions, overspeed, and over-g.

Any intervention the system provided should follow the general design principles of clearly notifying the pilot of the condition and what the system was doing to correct it; applying control forces in a manner that was not disconcerting to the pilot; and continuously permitting the pilot to exercise full authority over the controls in any direction desired.

Providing these characteristics in a system that can be retrofit to existing aircraft in the fleet and can be generally compatible with reversible cable-and-pulley connected primary FCONs, leads to a number of system and servo design considerations, as described further in sections 2.1 through 2.3.

2.1 SENSING CONSIDERATIONS.

For a full-featured automatic envelope protection system, an Attitude and Heading Reference System (AHRS) with Air Data Computer capability is considered essential. The cost of solid-state AHRS and Air Data Attitude and Heading Reference System (ADAHRS) units is becoming increasingly affordable to the class of aircraft for which a full-featured envelope protection system would be targeted. In addition, angle-of-attack (AoA) sensing is required for effective stall protection. Inexpensive AoA sensing is readily available in the experimental aircraft market and should readily migrate into the certified aircraft market. The AoA estimation schemes based on sensed aircraft acceleration cannot afford the same degree of accuracy of direct sensing of AoA, because the aircraft acceleration obtained at a certain dynamic pressure and AoA is dependent on aircraft weight, which is typically unknown.

Although an ADAHRS with AoA sensing is the ideal sensing suite for the full-featured automatic envelope protection system developed and reported herein, subsets of sensors can play an important role in systems that provide a lesser suite of features. For example, a very effective and low cost system for eliminating certain types of LOC accidents might be a simple AoA sensor with appropriate display and annunciation to alert the pilot to the imminent approach of critical AoA and wing stall, with no automatic control features.

2.2 DISPLAY AND ANNUNCIATION CONSIDERATIONS.

For a full-time envelope protection system to provide proper awareness to the pilot of its interventions, it is beneficial to include annunciations in more than one sensory modality. For practical reasons, this test focused on the visual and auditory annunciations through visual symbologies on a primary flight displays (PFDs) and auditory annunciations with verbal notifications through the audio system. Tactile feedback to the pilot was largely limited to the forces felt through the control yoke as a consequence of control inputs by the envelope protection system. However, by the end of the flight test, additional tactile notification for certain circumstances was found to be advantageous.

2.3 SERVO DESIGN CONSIDERATIONS.

To meet the design goal of providing control inputs from the automatic envelope protection and stability augmentation systems through the cable-controlled primary flight control system, without interfering with the pilot's full manual-control authority, certain servo performance attributes not characteristic of typical autopilot servos were required. In particular, when engaged and operating, the servos for this system had to be functionally back-drivable by the pilot. If the pilot wished to push back against the envelope protection system and move the controls in a direction opposite to the sense of the servo applied forces, the servos would have to be designed to permit that. In addition, the servos had to simultaneously be capable of sufficiently high torques that could provide control inputs on the same order as those of a human pilot. The need to meet these two fundamental design requirements has substantial implications for servo design, which is discussed in greater detail in section 13.4.1.

3. SIMULATOR TESTS.

Prior to implementation in an actual test aircraft, a human-in-the-loop cockpit simulator of a Cessna R182 (figure 1) was constructed to test the feasibility of a full-time envelope protection system in a cable-controlled aircraft.

Figure 1. Cessna R182 Simulator

The simulator featured a refurbished, salvaged Cessna R182 fuselage cab with electric control actuators to create realistic stick force gradients, a flat metal instrument panel with flat panel displays, and a 180-degree surround out the window display. Particular attention was paid to the tactile elements associated with the stick force gradients associated with the aircraft. Figure 2 shows a photograph of the instrument panel. Both a traditional steam-gauge primary flight instrument presentation and a modern PFD presentation were developed and used in the simulator.

Figure 2. Cessna R182 Simulator Instrument Panel

This ground simulator was used to provide an initial feasibility demonstration and development platform in preparation for testing full-time envelope protection in an actual aircraft. Details of the simulator construction and the findings from simulator trials can be found in reference 4. In summary, the simulator allowed validation of the essential concept of a full-time, always-on envelope protection system that would contribute control forces to the cable-and-pulley flight control system of a light aircraft, while still allowing the pilot to maintain simultaneous manual control of the aircraft. In addition, initial first-cut algorithms were developed for both stability augmentation and envelope protection features, and concepts for visual and auditory annunciation were explored. The simulator provided confidence that it was feasible to develop a similar experimental always-on envelope protection system to be flight-tested in an actual aircraft was feasible.

4. FLIGHT TEST PLATFORM AND EQUIPMENT.

Flight tests of the envelope protection and stability augmentation system were conducted in a 1978 Cessna R182 (shown in figure 3).

Figure 3. Cessna R182 Aircraft Used for Flight Test

4.1 SYSTEM OVERVIEW.

Figure 4 provides a functional block diagram of the flight test equipment installation.

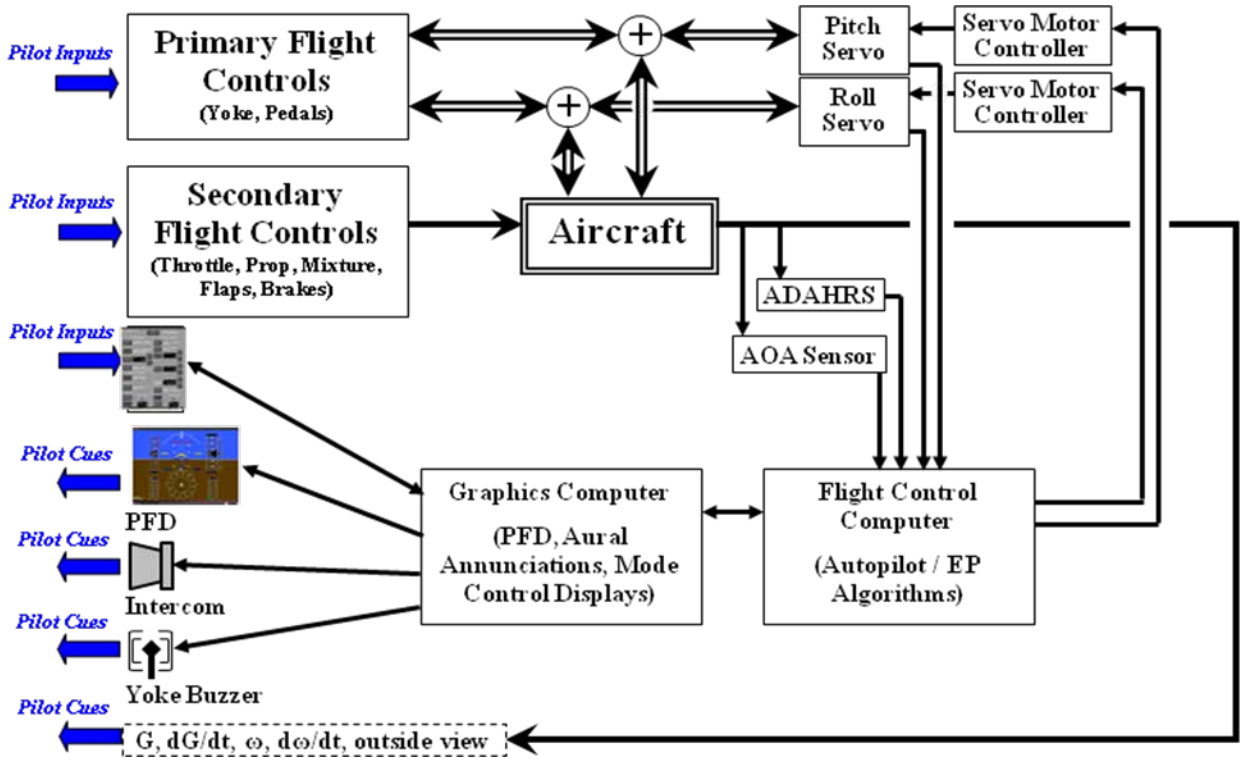

Figure 4. Functional Block Diagram of Flight Test Instrumentation

Figure 4 shows pilot inputs to the system and system outputs to the pilot, emphasizing the pilot-in-the-loop nature of the system.

4.1.1 Pilot Inputs.

Pilot inputs to the system include manipulation of the primary and secondary flight control and to the system mode control panel (MCP). Primary and secondary flight controls are all unaltered certified equipment included in the Cessna R182. Primary flight controls include the yoke, which is directly connected mechanically by cables and pulleys to the ailerons, elevator, and the pedals, which are connected by cables and pulleys to the rudder. Figure 4 does not show the elevator trim, which can be controlled by the pilot with a trim wheel or by using a yoke-mounted electric trim. Secondary flight controls include throttle, prop control, mixture, flaps, and wheel brakes.

4.1.2 Actuation.

The primary flight controls directly actuate the aileron, elevator, and rudder. Attached to the aileron and elevator cable control system are an experimental pitch servo (for elevator) and an experimental roll servo (for aileron.) These are the sole means of actuation afforded to the experimental envelope protection and stability augmentation system. Servo motor controllers supply electrical commands to the servos, and torque sensors within the servos provide measured servo output torque to the flight control computer. Section 4.4.1 describes the servos in more detail.

4.1.3 Sensors.

Sensors in the system include an off-the-shelf experimental ADAHRS, a custom AoA system using an experimental Dynon probe with custom electronics, and, for safety purposes, a separate g-limit module that disconnects power from the experimental servos in the event of a g-exceedance in the aircraft vertical axis.

4.1.4 Computers.

Two separate computers running real-time Linux are used: one for measurement and feedback control and the other devoted to graphics, audio annunciations, and user inputs for the MCP and PFD. All of the algorithms and system software for these functions were designed and developed by the project team.

4.1.5 Pilot Cues.

The visual system outputs to the pilot are the PFD (with custom symbologies to support envelope protection features) and the MCP (chiefly designed as an engineering tool to turn features of the envelope protection and stability augmentation system on and off while in flight). Audio system outputs to the pilot are verbal English-language annunciations synthesized by the graphics computer and fed into the aircraft intercom system. In the last phase of flight tests, a mechanical yoke buzzer was added to the yokes to provide a tactile vibration to the pilot’s hands during stall and overpitch envelope protection alerts.

In addition, the system diagram in figure 4 emphasizes the importance of feedback to the pilot of the resulting aircraft dynamics of this pilot-in-the-loop automated system. These feedback parameters include aircraft accelerations, acceleration rates of change, angular rates, angular accelerations, and outside visual cues. All of these feedback parameters affect performance and pilot perceptions of system acceptability.

4.2 EXPERIMENTAL PALLET.

Figure 5 shows a photograph of the experimental equipment pallet mounted in the baggage area of the test aircraft. Section 4.2 provides a brief review of the components in the experimental hardware. Sections 4.3, 4.4, 4.5, and 4.6 describe the sensors, the actuators, the displays, and the computers that comprised the system.

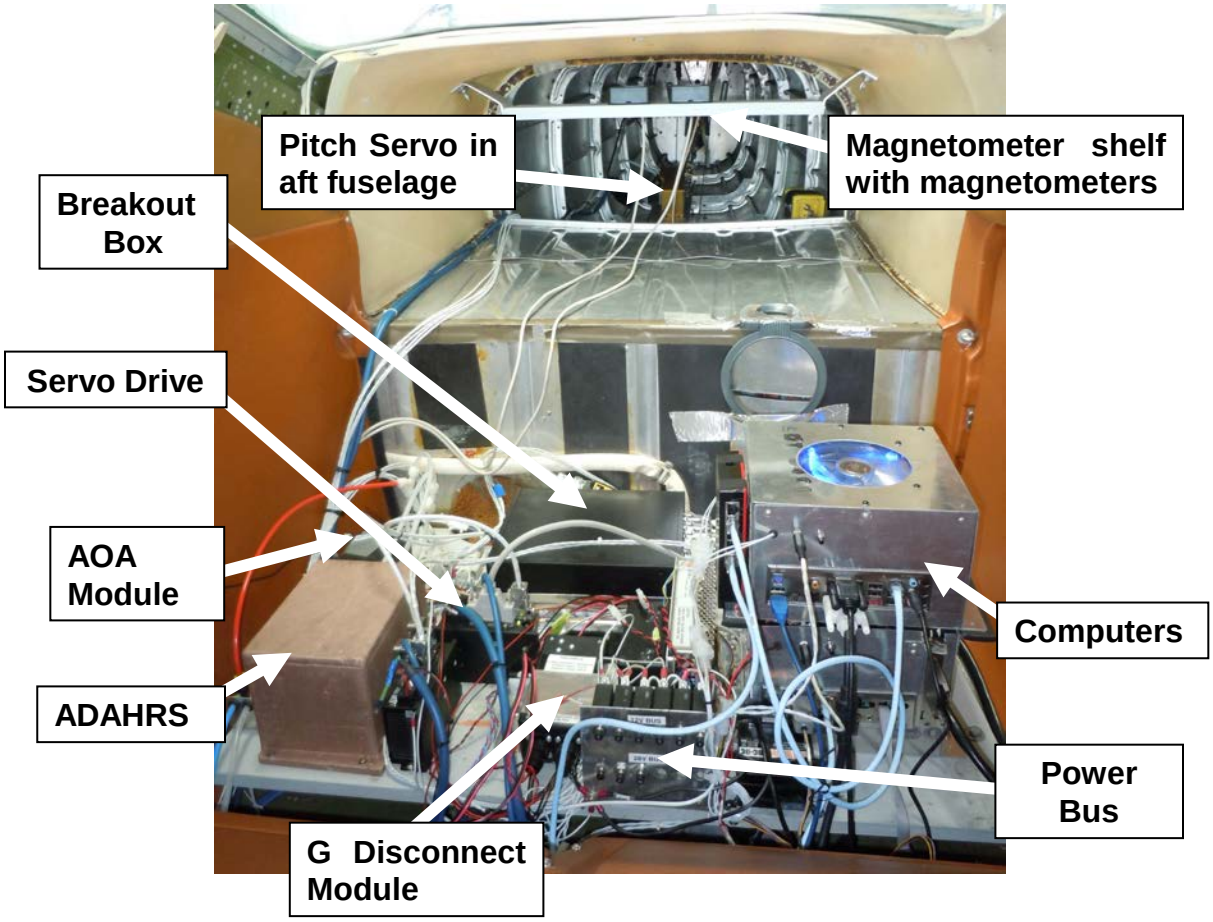

Figure 5. Experimental Pallet Installed in Baggage Area of Cessna R182

The pallet itself was fabricated from 1-in.-thick cabinet-grade seven-ply plywood. It was shimmed using precisely cut tapered blocks of walnut wood to achieve a surface level with respect to the aircraft zero-pitch reference to within 0.2 degrees. The shims were bolted to four

hard points in the floor of the aircraft baggage area, and the pallet was fastened into drilled and tapped holes in the walnut shims with machine screws.

The major items of labeled equipment are seen on the pallet. Figure 5 also shows the experimental pitch servo, which is just visible in the aft fuselage. The servo, computers, and sensors on the pallet are discussed in sections 4.3, 4.4.1, and 4.6.

Figure 5 also shows a separate shelf in the upper part of the area above the hat shelf. This is for the dual magnetometers used by the dual ADAHRS unit. The shelf was constructed of the same material as the pallet and was mounted to cargo-net hardpoints with aluminum brackets. This location was chosen for its magnetic cleanliness and convenient proximity to the main pallet.

4.3 SENSORS.

4.3.1 The ADAHRS.

The Dual Horizon ADAHRS used for the experimental equipment was manufactured by Grand Rapids Technologies (shown in figure 6).

Figure 6. The ADAHRS Used in Flight Test

This ADAHRS was chosen for a combination of acceptable performance characteristics, ease of interface, and low cost. The ADAHRS software load was provided through special arrangements with Grand Rapids Technologies to provide higher-than-normal output rates. The outputs from

the ADAHRS were received at approximately 37 Hz instead of the typical 15 Hz provided by the commercially available product.

The Dual Horizon ADAHRS was selected with the anticipation that compare logic could be used to protect against the experimental flight control system following certain types of errors in the ADAHRS outputs (e.g., from sensor failures within the ADAHRS). Because of the technical limitations of the computer equipment used on the test aircraft, it was not possible to collect data simultaneously from both ADAHRS outputs, so the dual capability was not used. However, no ADAHRS failures affected flight control during the test program.

In this installation, the Grand Rapids Technologies Dual Horizon ADAHRS did exhibit one unfortunate characteristic. Its pitch and roll outputs were dramatically affected by radio frequency (RF) interference in the 123 MHz band, where typical transmissions from the aircraft on UNICOM frequencies would be made. This necessitated adding RF shielding around the unit and avoiding transmissions during tests of the envelope protection system. However, transmissions were typically not needed, except during takeoff and landing, when the experimental system was disengaged, so any residual RF effects on the ADAHRS were of no practical importance. The RF susceptibility of the unit was not communicated to the manufacturer and no efforts were made to discover its root cause.

It was also discovered that the ADAHRS was not capable of a reliable in-flight restart, even when operating in nominal straight-and-level flight. However, this limitation was of no practical importance during flight test as there was no need to power-cycle the experimental system.

In spite of these limitations, this ADAHRS performed acceptably and provided reliable and accurate aircraft state data, sufficient to support closed-loop aircraft control with good quality results.

4.3.2 The AoA Module.

The AoA measurement is vitally important for envelope protection systems, and it was not typically provided by installed systems on GA aircraft at the time of this research (at least among the certified fleet). However, it has become increasingly common in experimental aircraft and the components necessary to yield good AoA measurement are inexpensive.

Two separate commercial off-the-shelf probes were examined to provide differential air pressures that vary with AoA. Figure 7 shows the Alpha Systems probe, which was the first probe installed and tested on the test aircraft. As shown in the figure, this probe provides pressure from two ports, one angled downward and one angled upward with respect to the nominal-level free-stream direction. As AoA increases, so does pressure from the lower orifice, while pressure from the upper orifice decreases. This probe is sold as part of a complete AoA system with various available displays and is acceptable for installation on certified aircraft with a mechanic's signature.

Figure 7. Alpha Systems Two-Port AoA Probe Installed on Test Aircraft

Whereas this probe with the associated indicator electronics and the display provides extremely useful AoA information as designed, investigation revealed that the pressure from the upper port became somewhat erratic at very high AoAs (above 15 degrees, the nominal power-off stall AoA of the wing). At these very high AoAs, between 15 and 17 degrees, it was difficult to find a relationship between the measured pressures and actual AoA that appeared to be quantitatively dependable for the research purposes envisioned.

For this reason, an alternative dual-port probe was installed on the test aircraft (shown in figure 8). The probe is manufactured by Dynon for use with its EFIS systems for experimental aircraft, which include AoA information. The Dynon probe has a forward-facing orifice that provides pitot pressure similar to any ordinary pitot tube would. In addition, it has a second orifice that is canted downward. It is important to note that, as mounted on the test aircraft, both of these probes were distanced farther forward and below the leading edge of the aircraft wing than was the case for the Alpha Systems probe.

Figure 8. Dynon Two-Port AoA Probe Installed on Test Aircraft

Compared to the Alpha Systems probe, pressures obtained from the Dynon probe proved inherently superior for extracting AoA information at very high AoAs. At AoAs as high as 17 degrees, no erratic behavior of the measured pressures was observed, and calibrating the probe to provide aircraft AoA information was straightforward. Therefore, the Dynon probe was selected for the test aircraft. In addition to its other benefits, the Dynon probe also included one ordinary forward-facing orifice to furnish pitot pressure, which was an advantage because tapping into the aircraft primary pitot-static system was no longer necessary to support the air-data capabilities of the ADAHRS.

The custom electronics used to provide AoA information is shown in figure 9. The key elements of the electronics included a static pressure sensor (simply vented to cabin pressure, but to be connected to a proper static source in a nonexperimental configuration), two differential pressure sensors (one for each probe orifice), and a single-board computer with active directions to read the outputs of the pressure sensors. For convenience of calibration only, the module also included a Global Positioning System (GPS) receiver and a dual-axis tilt sensor.

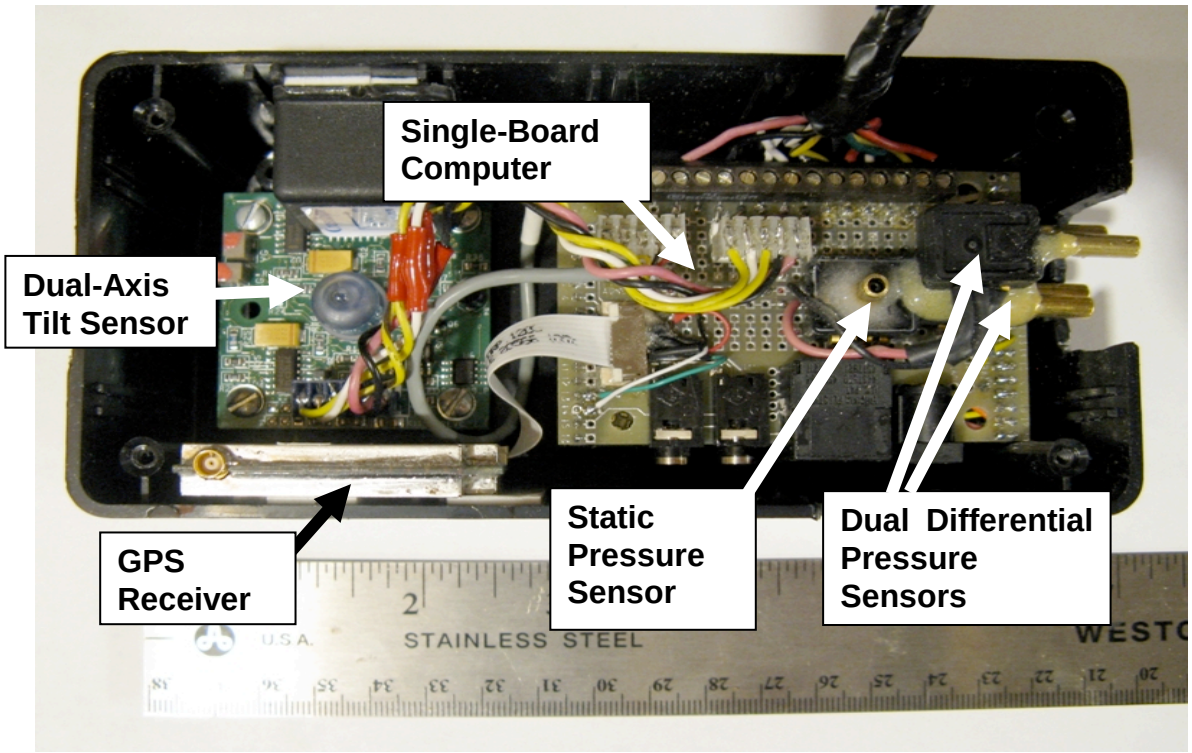

Figure 9. Experimental AoA Module

Calibration was accomplished by taking a rich set of flight data in nominally straight-and-level flight over a variety of airspeeds, from edge-of-stall with power on at the low end of the range (high AoA) to a cruise configuration at the high airspeed range (low AoA). A calibration procedure automatically identified nominally static conditions (i.e., nominally unaccelerated flight with no rapid change of aircraft pitch) and calculated AoA as the difference between aircraft pitch (as measured by the tilt sensor) and aircraft flight path angle (as provided by velocity outputs from the GPS receiver).

Although data taken in this manner do exhibit significant noise (much more than would be expected from wind-tunnel measurements, for example), with enough redundant data, a reliable relationship can be derived between pressure differences normalized in any number of different ways and AoA.

For the flight test experiments, AoA was calculated using a simple linear fit to the difference between the two dynamic pressures from the two orifices, normalized by the dynamic pressure from the forward-facing orifice. Figure 10 shows the derived fit with the flight data used to obtain. The data leading to this fit were taken with a variety of flap extensions. Placement of the probe well outboard of the flaps minimized the influence of flap position on local AoA. Thus, the probe provided information on the AoA of the outboard wing, which is important for stall protection purposes.

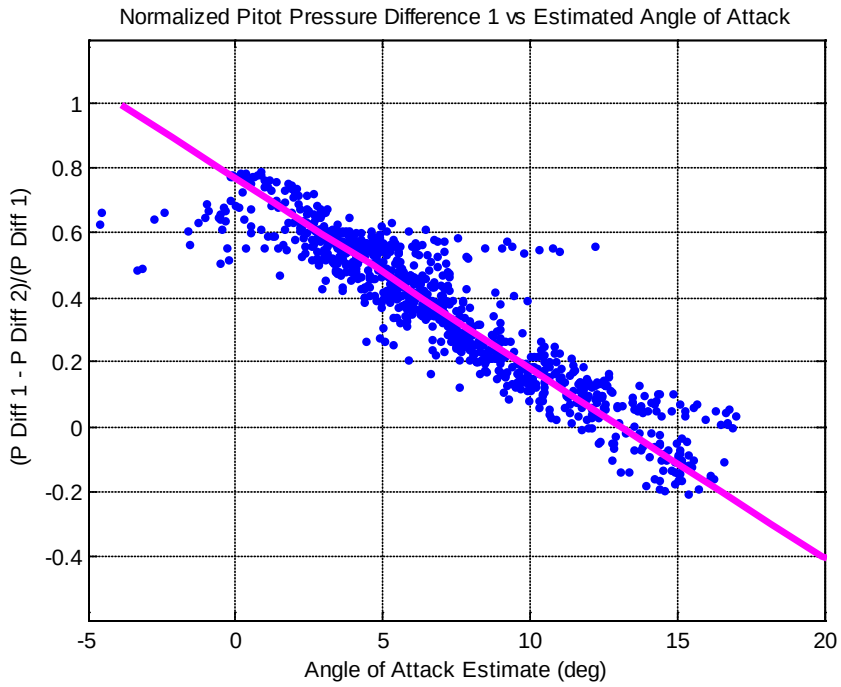

Figure 10. Linear Fit for AoA vs. Normalized Probe Pressures (May 2011 data)

4.3.3 The G-Limit Module.

As an added safety mechanism for flight test purposes, a separate and independent mechanism was designed to automatically remove power from the experimental servos in the event that certain g-levels were encountered by the aircraft.

This system was designed to be as simple as possible, with no microprocessor or software involved. It consisted of a pair of high-current relays (one providing electrical power to each servo) controlled by two g-sensors: one for the positive *z* axis of the aircraft and one for the negative *z* axis. For the purposes of this flight test, the positive g-limit was chosen at +2.4 g and the negative g-limit at -0.9 g. Exceeding either of these limits resulted in the respective g-sensor tripping, which caused both relays to disengage and removed electrical power from both experimental servos.

Figure 11 shows the inside of the g-sensor.

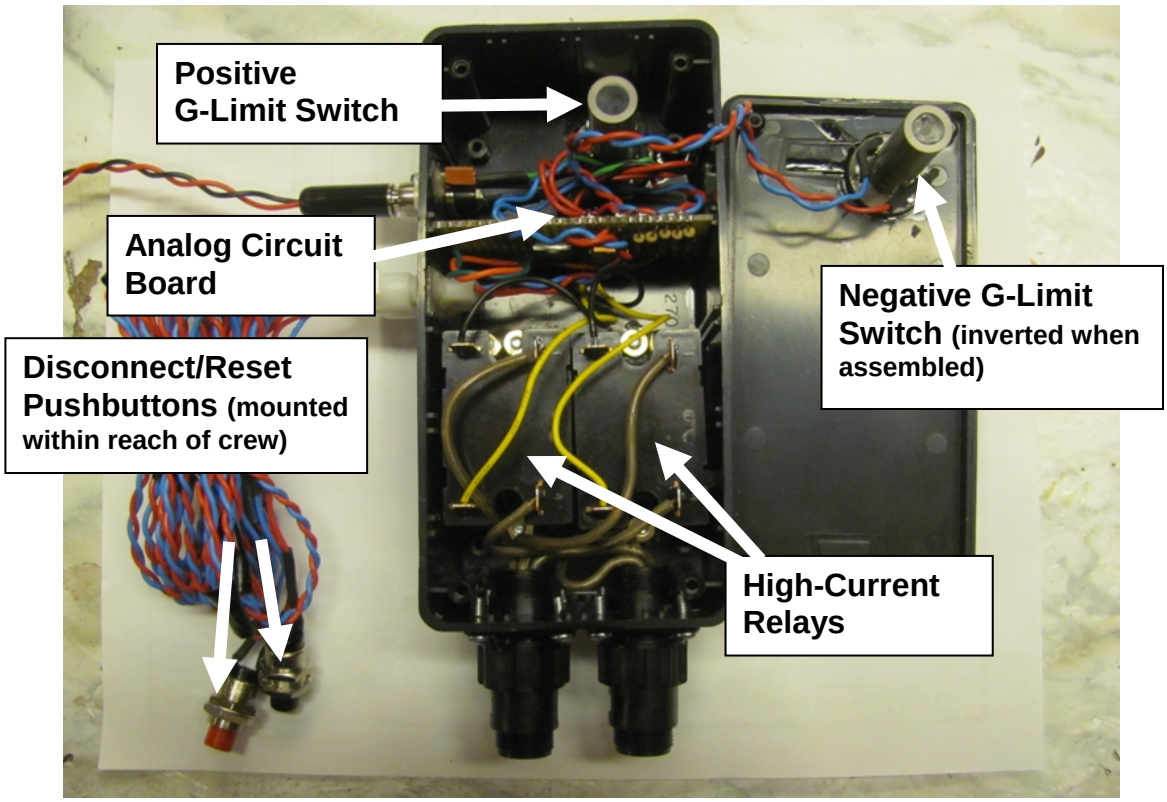

Figure 11. The G-Limit Disconnect Module

In addition to the automatic servo power-off function, this module was also equipped with a manual disconnect/reset push button pair, mounted within reach of the pilot and flight test engineer on the pedestal supporting the experimental MCP. If needed, the red disconnect button was used in flight to quickly remove power from the servos. Also, the disconnect button was used to remove power from the servos for phases of flight during which the experimental protocol required it (in this case, all flight operations below 3,000 ft above ground level).

Early in the development of the flight software, the g-limit module automatically removed power from the servos during flight tests on two or three occasions. For developmental purposes, it was a beneficial addition to the system because it provided a guaranteed protection against inadvertent overstressing of the airframe. Later in flight tests, it was found that the g-load at which the positive g-limit switch would trip was, unfortunately, closer to +2.0 g rather than the desired and specified +2.4 g. This was an impediment to carrying out a few of the flight test maneuvers (in particular, manually-selected unusual attitude recovery with significant initial vertical descent rate).

Some sort of g-limiting is beneficial for any automatic flight control system, but, for a mature system with a solid-state acceleration sensing capability (such as within an AHRS or ADAHRS), a separate g-limit module, such as the one discussed, would likely be considered an unnecessary complication. However, this added safety feature was useful during the software development phase of experimental flight tests.

4.4 ACTUATORS.

4.4.1 Servos.

The servos used in the test aircraft were custom designed and fabricated for this project. Off-the-shelf candidate servos were considered, but none of the existing designs met the criteria for use in the project, mainly because they did not have sufficient capacity to work well in a pilot-in-the-loop cable-control system. The key capability required to enable such use is the functional back-drivability of the servo; that is, the servo would need to yield to the pilot manual inputs to allow the pilot to maintain full control authority, even while the servo was adding forces to the cable control system. At the same time, the servo had to be capable of delivering torques of the same magnitude as the pilot to be effective in the system envisioned.

Figure 12 shows the first iteration of the servo design, mounted on the aircraft simulator for initial testing purposes, alongside a control loader linear motor that is part of the simulator.

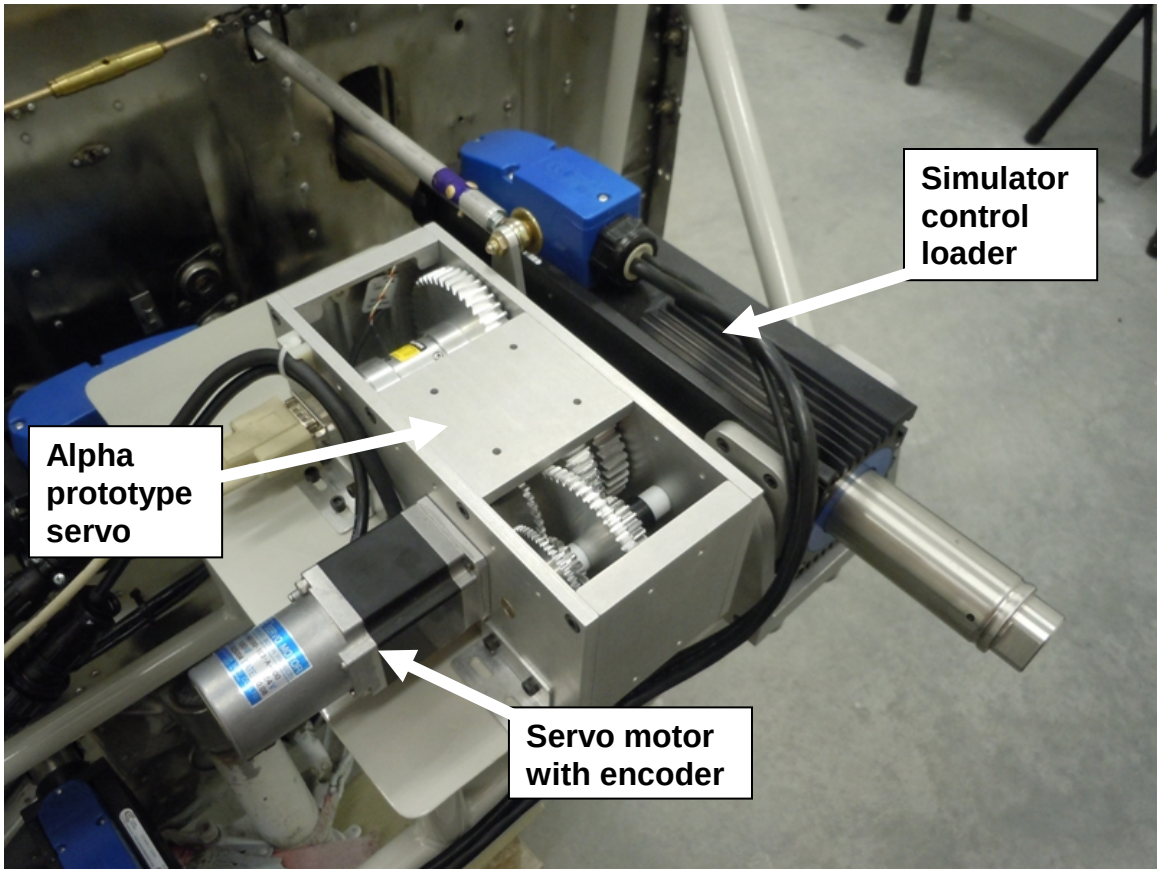

Figure 12. Alpha Prototype Servo Mounted Alongside Control Loader on Simulator

Figure 13 shows a computer-aided design (CAD) drawing of the alpha prototype servo's internals, including motor, gear train, output torque sensor, and output arm.

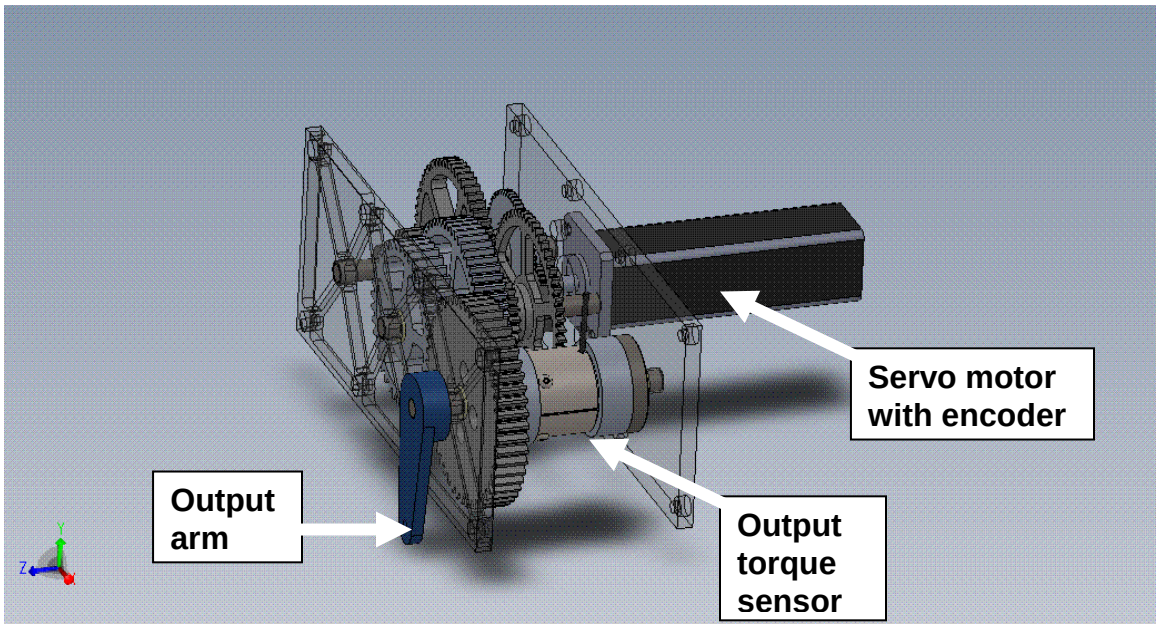

Figure 13. Alpha Prototype Servo CAD Image

The alpha prototype servo served as a testbed for testing and refining concepts prior to proceeding with the final design of the flight servo. The initial design required few changes, but those made were significant. These included: (1) adding a gear train engagement/disengagement mechanism, including a microswitch to enable verification that the gear train was actually engaged; (2) adding a potentiometer to the system to provide initial output shaft orientation to initialize the encoder for subsequent servo position measurements; (3) changing the servo output arm to an output sprocket with integrated shear pin; and (4) decreasing the gear train's overall gear ratio.

Figure 14 shows a CAD image of the beta prototype servo used for flight tests.

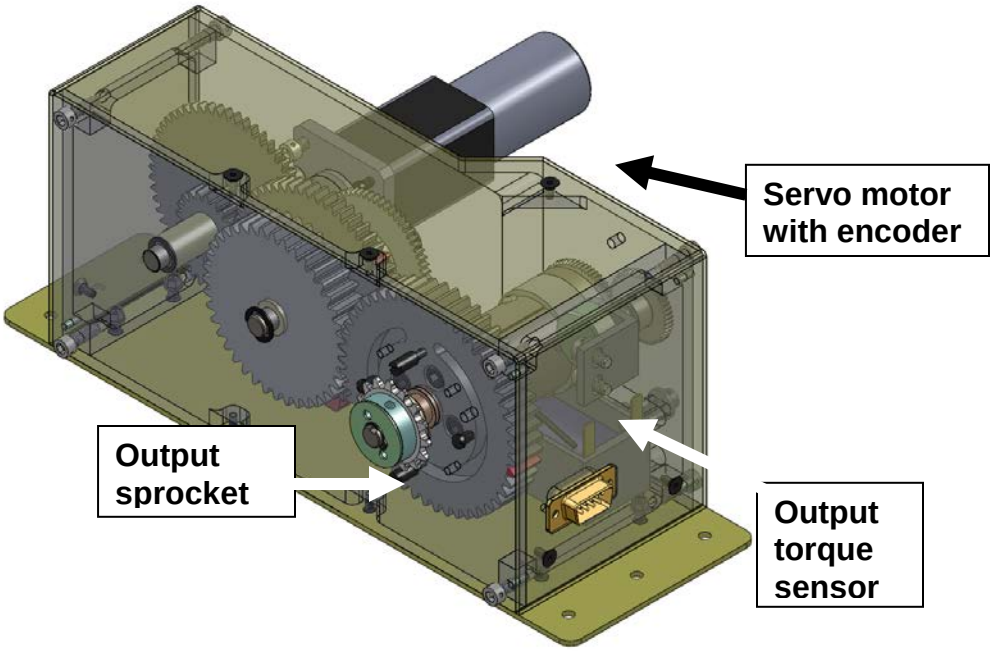

Figure 14. Beta Prototype Servo CAD Image

The change from an output arm to an output sprocket was influenced by experimental work with a legacy-certified servo, the Aircraft Radio Corporation (ARC) servo common in Cessna R182 autopilots. There were many benefits with the design of this servo from the 1970s, including the output sprocket with integrated shear pin (shown in figure 15). This sprocket was used for the output of the flight servos because of the ready availability of spares, the simplicity of mating the chain-cable assembly already compatible with this sprocket to the cable controls of the test aircraft, and, most importantly, the well-proven design, including an appropriate shear pin. Because of the smaller lever arm of the sprocket in comparison to the output arm of the alpha prototype, it was also decided to decrease the overall gear train's gear ratio by a factor of 3, from 101.25:1 to 33.25:1. The peak torque of the flight prototype servo was estimated to be about 166 in.-lb, which is far greater than the maximum anticipated need for the flight test program.

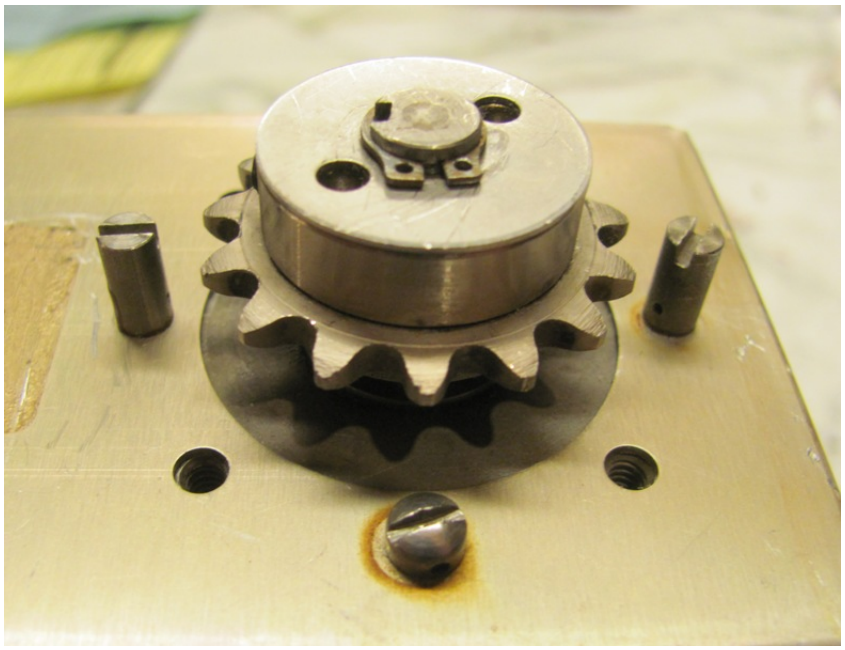

Figure 15. Output Sprocket of ARC Certified Servo With Integrated Shear Pin

Additional technical details of the experimental flight servo components are provided in appendix F.

Figure 16 shows the experimental flight servo mounted in the aft fuselage of the test aircraft with its output connected to the elevator cable controls. This aspect of the experimental test equipment had been a major challenge to conceive and design properly, but the end result was ideal in many respects. By using existing holes in the fuselage formers and mounting holes for the nearby marker beacon antenna in the fuselage bottom, a custom-fabricated sheet-metal mounting system was devised that necessitated no new holes in any part of the aircraft structure for the experimental system. The proven Cessna/ARC servo output sprocket and cable-chain system was used in combination with STec cable clamps to connect the servo output to the elevator cables of the test aircraft.

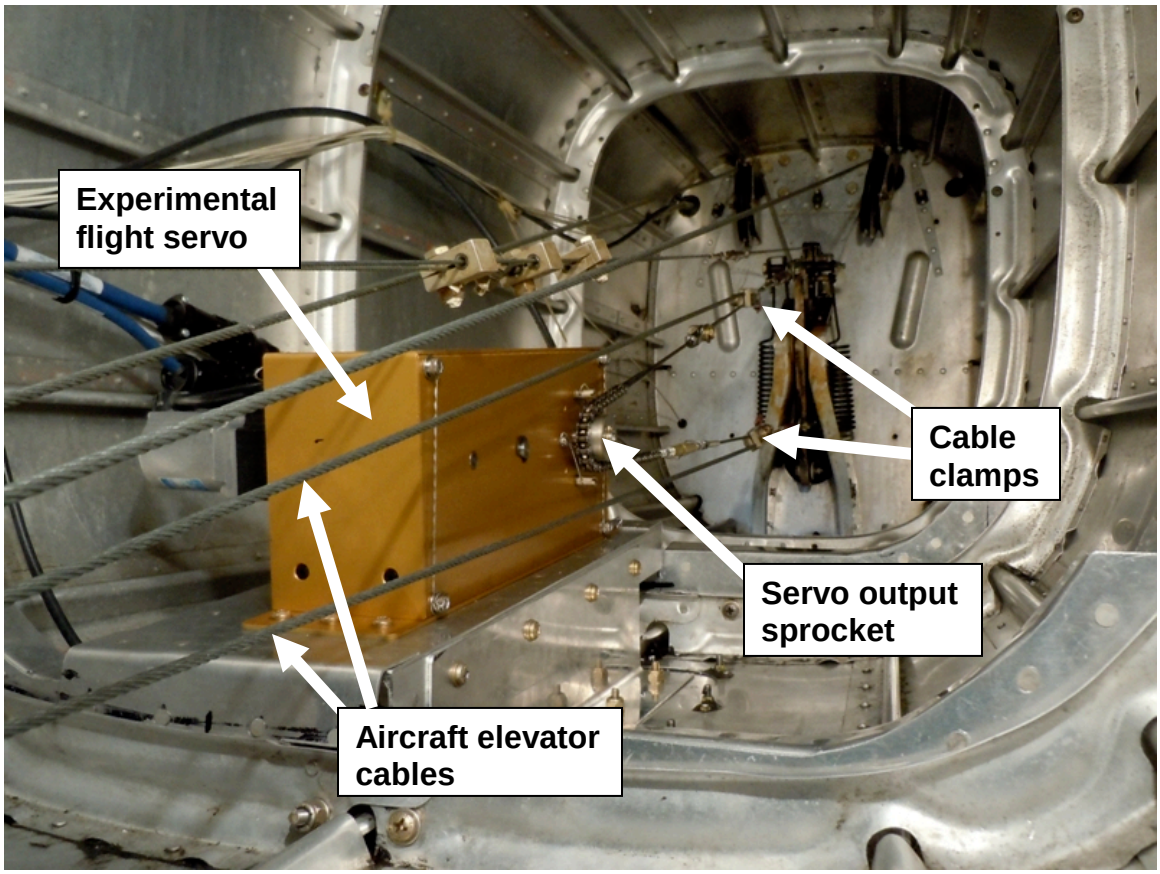

Figure 16. Flight Servo Attached to Elevator Cable Controls in Aircraft

Two copies of the flight servo were fabricated to provide a simultaneous capability to fly the system both in the ground simulator and in the aircraft in flight and to supply spares in case components of the flight servo needed to be replaced. Soon after the equipment was fully operational in the test aircraft, an iron-bird simulation capability was created to allow the full system to be flown in the cockpit while in the hangar, obviating the continuing need for the full ground-based simulator itself. However, the second flight servo became invaluable soon thereafter.

For aileron control during the initial sequence of flight tests, a certified ARC servo was modified to provide four times the usual torque by adding a second 4:1 gear in the system, in addition to the existing single 4:1 gear between the motor and output shaft in the stock servo. In addition, to provide position sensing, a ten-turn thin-film potentiometer was added to the servo. The modified servo is shown in figure 17.

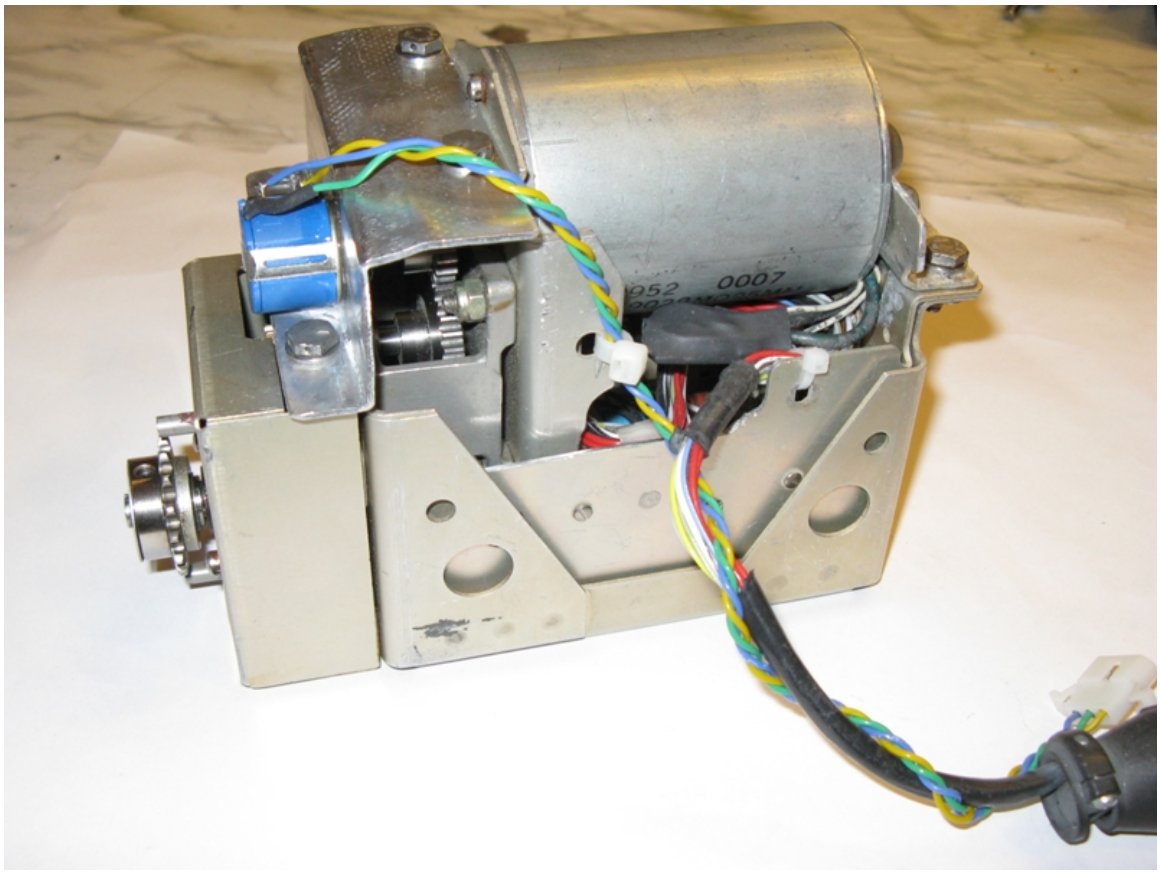

Figure 17. Modified ARC Servo Initially Used for Aileron Control During Flight Tests

This servo remained mechanically compatible with the in-wing mounting system of the original ARC servo used for the test aircraft's ARC 300A single-axis autopilot; therefore, it was simple to pull the certified servo out and replace it with the modified experimental servo (being driven by the experimental equipment rather than by the certified autopilot).

The first of the four-flight test series was carried out using this servo for aileron control. It proved generally satisfactory, but after some debate regarding the need to do so, it was decided to find a way to use the second copy of the custom flight servo designed for the program for aileron control in future flight tests. This was motivated by four considerations: (1) direct output torque measurement available from the custom servo, (2) quieter and more precise output position sensing available from the custom servo's encoder, (3) somewhat higher torque capability from the custom servo, and (4) some degree of cogging felt in the roll control using the modified ARC servo.

However, aileron control was not considered when the custom servo was designed, so its external envelope was too large to allow it to be mounted in the aircraft wing, and reducing its size to allow it to fit would have been a substantial undertaking. After careful consideration, a location was found in the ceiling of the aircraft cabin that would allow mating the experimental servo to the aileron control cable. A special cog assembly was fabricated to allow redirection of a slightly lengthened chain-cable assembly (with several chain links added), and existing hard points in the

aft wing carry-through structure were used to mount the servo. The cable output was attached to the aileron cable using STec cable clamps (as in the case of the elevator servo).

Figure 18 shows the flight servo mounted in the ceiling area of the test aircraft cabin and mated to the aileron control cable.

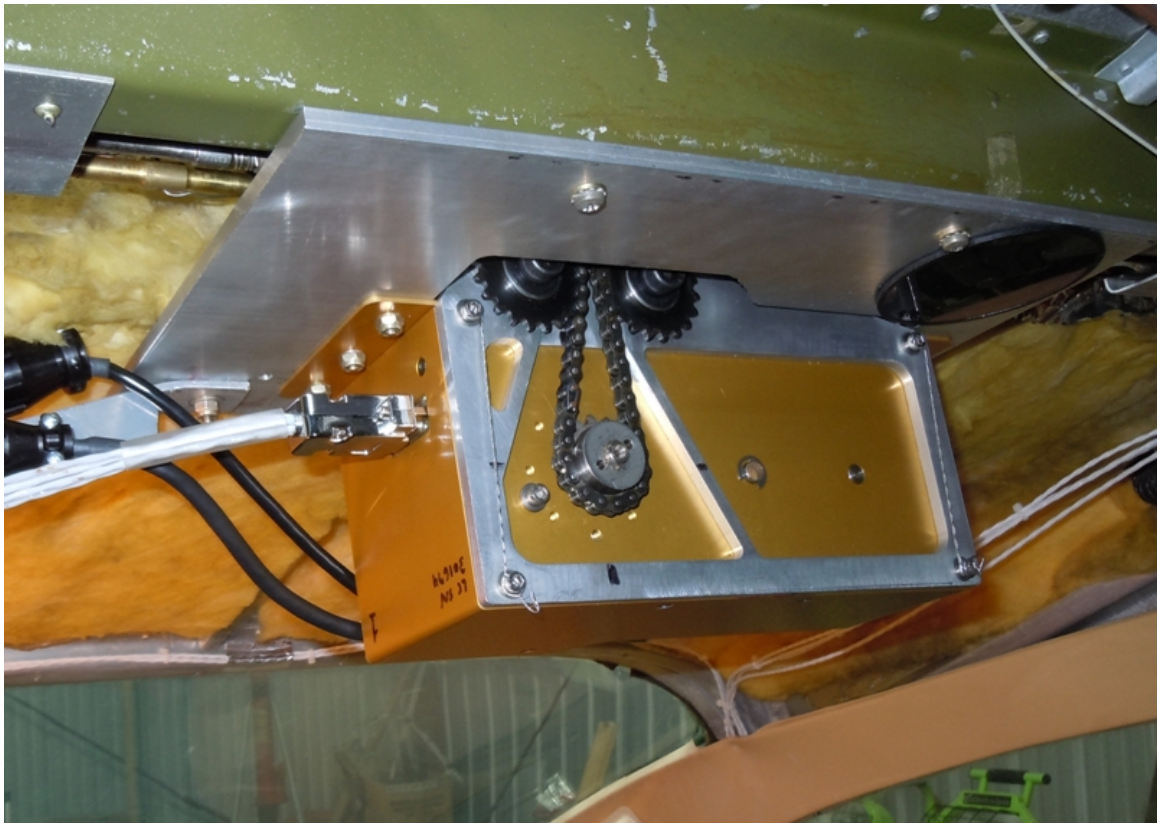

Figure 18. Flight Servo Mounted in Cabin Ceiling for Aileron Control

4.4.2 Yoke Buzzers.

Following the third set of flight tests, it was determined that an additional means of giving tactile feedback to the pilot was needed to provide an alert function for certain flight conditions (in particular, an imminent stall). Accordingly, a pair of yoke buzzers was developed in prototype form and used during the final set of test flights. The yoke buzzers are shown in figures 19 and 20.

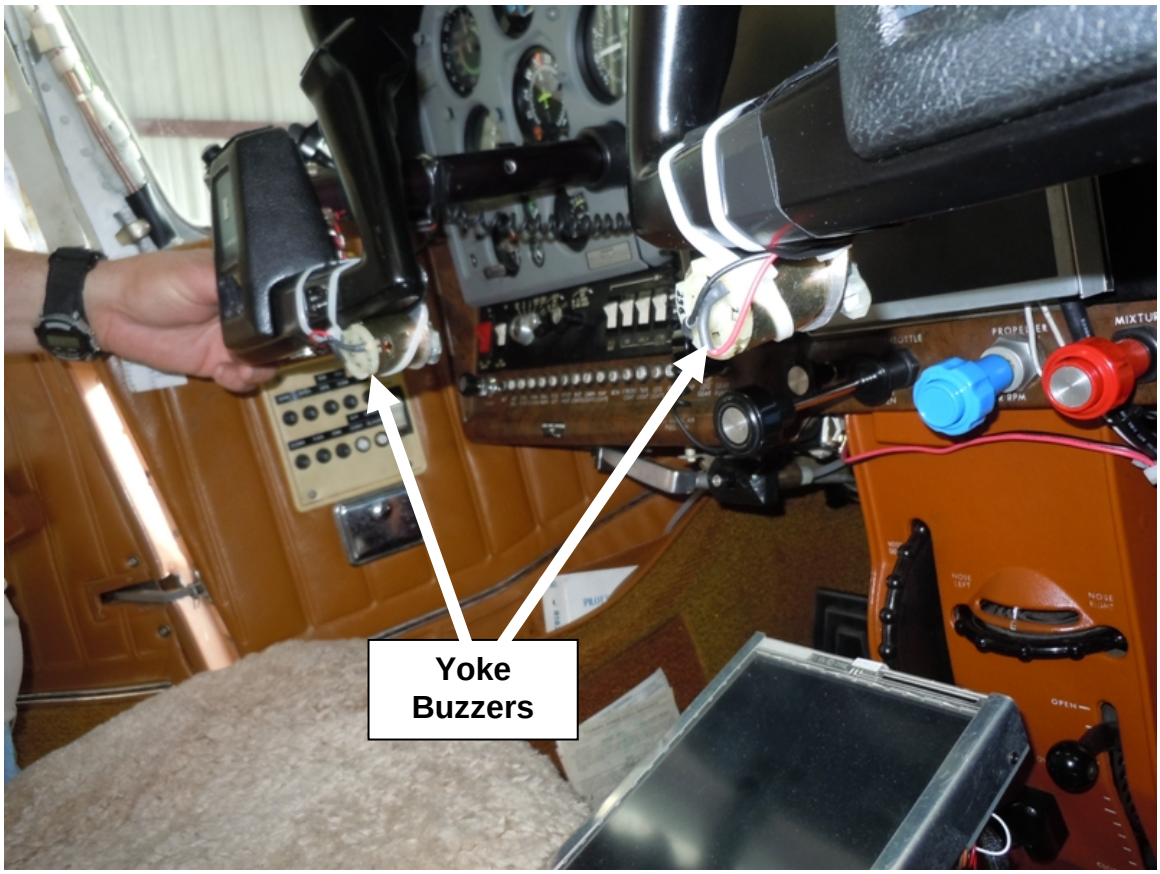

Figure 19. Experimental Yoke Buzzers Mounted on Test Aircraft Yokes

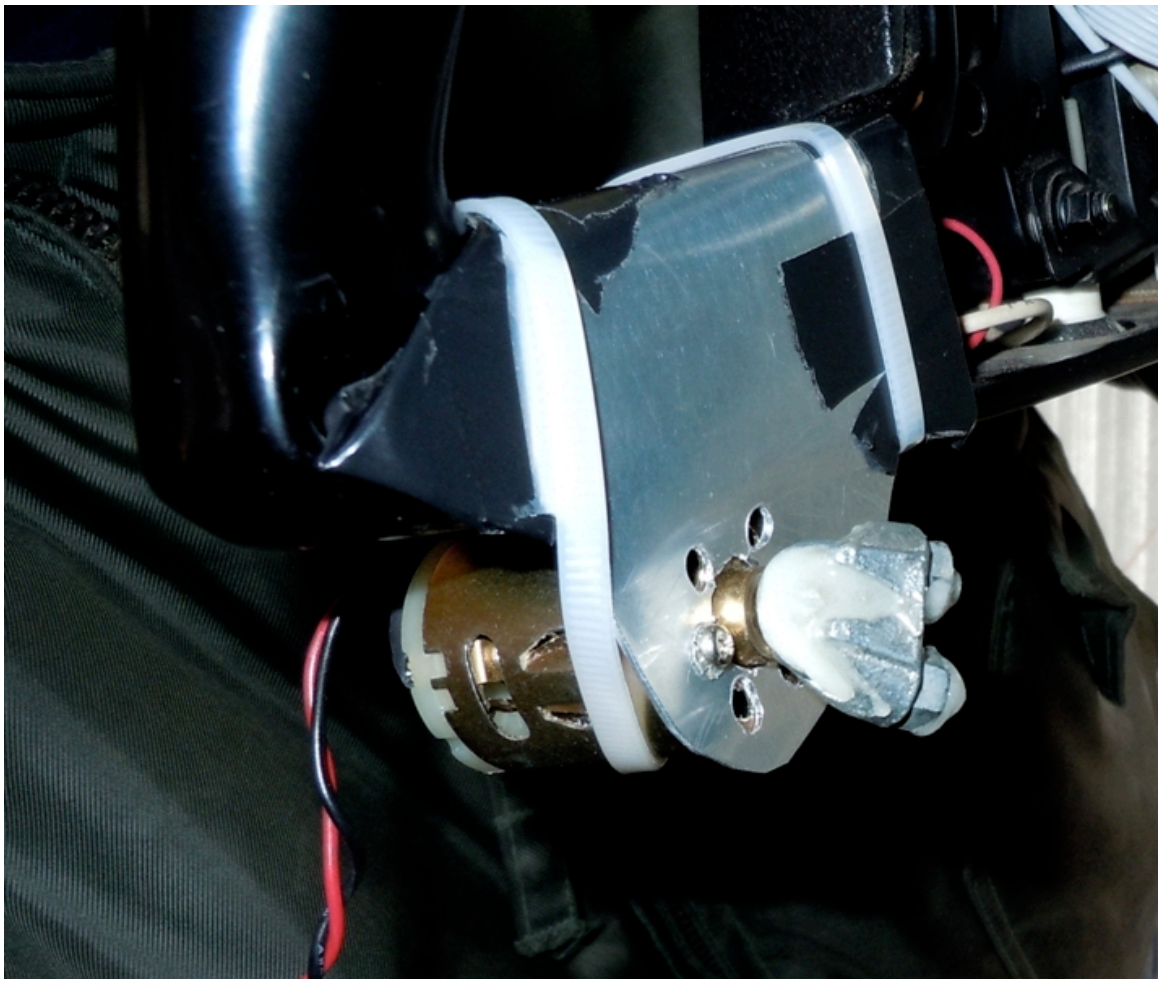

Figure 20. Close-up View of Yoke Buzzer Showing Eccentric Weight on Motor Shaft

The experimental yoke buzzers were designed to provide a noticeable vibration of the yoke, which would be impossible to ignore by a pilot touching the yoke. The buzzers consisted of an inexpensive DC motor with an eccentric weight attached. A single buzzer attached to one yoke failed to provide any noticeable sensation on the opposite-side yoke, thus one buzzer for each yoke was used. The buzzers were firmly but temporarily attached to the yoke using a thin aluminum mounting fixture shaped to conform to the yoke shape and tightened onto the yoke with nylon cable ties, as shown in figures 19 and 20.

When powered on, the buzzers caused a yoke vibration at a frequency and amplitude that could not be ignored by the pilot, even in the noisy, vibration-filled environment of the aircraft in flight. Regardless of distractions, the buzzers were found to be an extremely effective means of alerting the pilot to an impending stall.

4.5 DISPLAYS.

In the flight test aircraft, an experimental PFD display was temporarily mounted on rails covering the lower portion of the radio stack. A touchscreen MCP used for controlling the mode of

operation of the experimental autopilot and envelope protection system was mounted on a center pedestal fastened to the seat rails. Figure 21 shows these displays mounted in the test aircraft.

Figure 21. Experimental PFD and MCP in Test Aircraft

Figure 22 is a screenshot of the PFD display. In addition to typical PFD symbology, this display included AoA and g-indicators at the lower left and lower right of the display. In addition, several novel symbologies were added in connection with the envelope protection features of the system.

Figure 22. The PFD Display Screenshot

One unique feature present at all times on the display was a stall margin indicator. This indicator moved parallel to the pitch ladder, and the distance between it and the top of the aircraft-symbol chevron was indicative of the remaining AoA margin before wing stall. The wing was at critical AoA when the stall margin indicator touched the point of the chevron. This symbol provided an at-a-glance depiction of the margin available prior to wing stall.

Control of the functional status of the experimental autopilot, stability augmentation, and envelope protection system during flight was affected through a touch-screen engineering/test MCP (shown in figure 23).

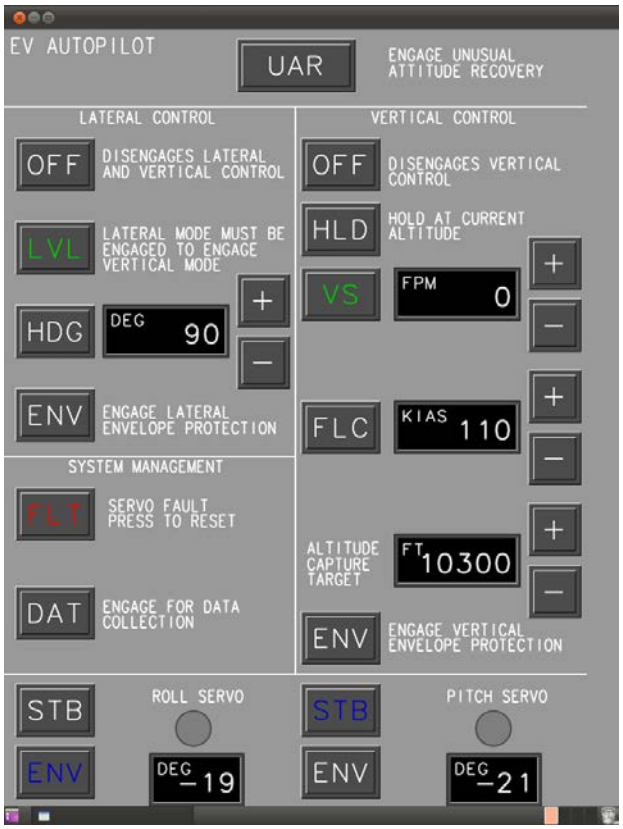

Figure 23. Engineering/Test MCP

This MCP was not part of the examination of pilot-system interactions, but rather a tool for controlling the equipment mode of operation during flight tests. The MCP was divided into five sections as shown in the figure. The individual functions within the sections were as follows:

- Lateral Control—Basic autopilot lateral functions, plus on-off control of lateral stability augmentation and envelope protection features.

- Vertical Control—Basic autopilot vertical functions, plus on-off control of vertical stability augmentation and envelope protection features.

- Unusual Attitude Recovery—A single button at the top of the display to manually engage unusual attitude recovery.

- System Management—A single button to fault (power-off) servos in software and to clear automatically-engaged servo fault states, plus button to start and stop data collection.

- Envelope Protection Submode Selection—Four buttons at the bottom of the display to individually enable any combination of stability augmentation/envelope protection functions for lateral/vertical features, plus servo position readouts and engagement indicators.

4.6 COMPUTERS.

A flight-control computer and a graphics computer were used to run the experimental system in the test aircraft. They were housed in custom sheet-metal enclosures as shown in figure 24.

Figure 24. Graphics Computer (top) and Flight Control Computer (bottom)

The flight control computer gathered data from all sensors, ran the feedback-control algorithms, and commanded the servos and yoke buzzers. The graphics computer generated graphics for the PFD and the mode-control touchscreen display, handled pilot requests from the MCP, relayed mode commands and status to the flight control computer, and generated audio annunciations for the aircraft intercom system.

The flight control computer was custom-built using a Jetway™ Mini-ITX IPC (Integrated Processor) motherboard running a VIA CN700 chipset, as shown in figure 25. Industrial boards designed for a high operating temperature range (0° to 60°C) were used, and were known to function well when running the real-time Linux kernel. The board needed one PCI slot to support the National Instruments™ NI-PCI-6221 data acquisition board (see figure 26).

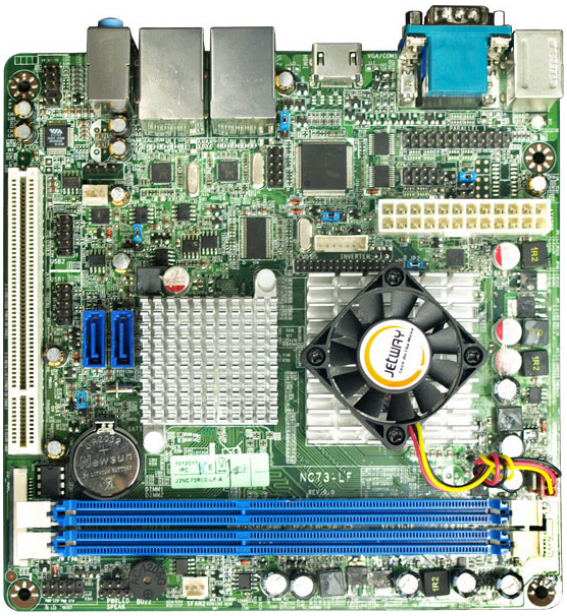

Figure 25. Jetway Mini-ITX IPC Motherboard With VIA CN700 Chipset

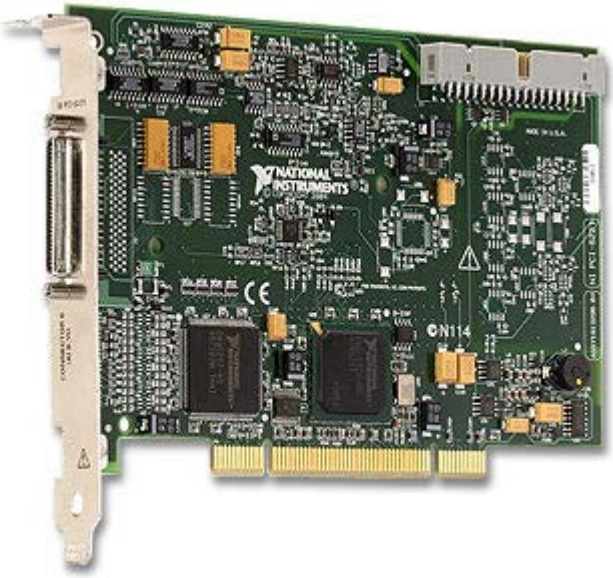

Figure 26. National Instruments NI-PCI-6221 Data Acquisition Card

The graphics computer was created using a ZOTAC™ GF9300-I-E motherboard (see figure 27). This motherboard was specifically chosen for its on board NVIDIA™ GeForce 9300 video chipset. NVIDIA™ chipsets are known for their solid support of OpenGL graphics, which was what the library used to generate all of the graphics. The motherboard supported LGA775 socket-type processors and a mid-range Intel™ processor. The graphics computer ran a version of standard (not real time) Ubuntu Linux using the Gnome desktop environment.

Figure 27. The ZOTAC™ GF9300-I-E Motherboard Used for the Graphics Computer

Both computers were powered by a small DC/DC M3-ATX-HV power supply to accept 6V to 34V input and provide the appropriate power to the motherboard, as shown in figure 28.

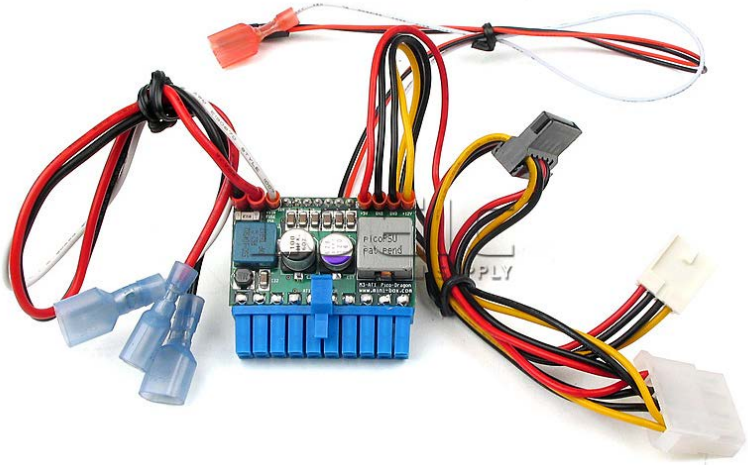

Figure 28. The M3-ATX-HV Power Converter

Each computer used a single Corsair® solid state 32GB hard drive, as shown in figure 29.

Figure 29. Corsair Solid-State 32GB Hard Drive

4.6.1 Computer Problems.

The computers exhibited unique failures in the airplane environment. The graphics computer, not a high-temperature range machine, had the tendency to shut down when operating during hot days, on which temperatures could exceed 100°F. This problem was so pervasive that special enclosures were constructed to facilitate additional cooling. These enclosures were constructed from 2024T3 sheet metal and riveted together. The enclosures supported large cooling fans that circulated the air around the motherboards and allowed for airflow underneath them. The new enclosures reduced the cooling problem considerably.

The graphics computer tended to be sensitive to vibration. It shut down periodically when the aircraft touched down and, in some cases, when the landing gear was retracted. The final bump of the gear coming into the gear well (under the computer pallet) was enough to shut down the computer. In this case, the solution was to cushion the computer enclosure with a 1/8″ piece of weather stripping.

Both computers were sensitive to dirty power and, in some cases, failed to boot or exhibited other errors that were difficult to decipher. These problems subsided when cleaner power was used. Whereas the computer DC/DC converters within the computers were chosen for their ability to run off 28V, ultimately 12V power was used from the main 12V DC/DC converter (originally needed for the displays). This power converter was much more robust and was designed to provide clean filtered power at 12V exactly (which was an absolute requirement for the LCD displays) and when used for the computers the problems subsided.

Both computers had problems with memory and SATA connectors (used to connect to the hard drives) coming loose. The loose hard drive connections were easy to troubleshoot because the drive would not show up when the computer would post. Loose memory chips were more insidious and several motherboards were replaced before the problem was determined to be loose memory, which did not have to be very loose and usually was not visible. These problems were solved by using RTV to hold the memory in place and lacing cord or tie wraps to ensure the SATA connectors would not come loose.

5. HARDWARE-IN-THE-LOOP SIMULATION.

Prior to initial flight tests, the components as installed in the aircraft system were used to carry out hardware-in-the-loop testing of autopilot, stability augmentation, and envelope protection features. These tests were conducted using a Cessna R182 aircraft simulation model running on a computer external to the aircraft. Measured flight control surface positions resulting from servo actuation were relayed to the simulation model, which simulated aircraft dynamics and returned aircraft state information to the flight-control computers in the aircraft. This type of test was invaluable in uncovering and resolving algorithmic, software, and hardware issues before flight, ultimately making development of the entire autopilot system safer and more efficient.

6. FLIGHT CONTROL SOFTWARE.

The flight control code contains the software functions that run the autopilot and envelope protection functions. The purpose of this section is to present an overview of the flight control code architecture. Details of the software implementation can be found in appendix A of this report.

The flight control code was a single process running on the flight control computer. The code is written in C and runs under an open-source version of real-time Linux. To the extent possible when writing in C, which does not inherently support true object-oriented coding, the code as written was implemented in an object-oriented fashion.

6.1 OPERATING SYSTEM.

The operating system for the flight control computer is a version of Linux Fedora 7.0 modified to support real-time operations. An older version of Linux was chosen specifically to ensure hardware compatibility. To have real-time capability, the Linux kernel was modified using RealTime Application Interface (RTAI) libraries.

The RTAI libraries are free open-source code. It stemmed from the need for a tool to support a varied set of internal research activities related to advanced active controls for generic aero-servo-elastic systems, including large space structures, acoustics, and flexible manipulators, while using standard 32-bit personal computers. Originally developed for DOS machines, using Linux as a general-purpose operating system led to the idea of adding hard real-time capabilities to it. The RTAI has since become widely used worldwide within the academic community.

The RTAI expands Linux to real-time by patching the Linux kernel with a generic Real Time Hardware Abstraction Layer (RTHAL). The RTHAL performs the following primary functions:

- Gathers all the pointers to the time-critical kernel internal data and functions into a single structure. This allows the easy trapping of all the kernel functionalities that are important for real-time applications, so that they can be dynamically substituted by RTAI when hard real-time is needed.

- Reworks the related Linux functions, data structures, and macros to make it possible to use them to initialize RTHAL pointers for normal Linux operations.

The related patch is quite simple and changes or adds about a hundred lines to the Linux kernel. A full description of RTAI can be found at https://www.rtai.org.

6.2 DATA ACQUISITION LIBRARIES.

Data acquisition was performed using a National Instruments NI-PCI-6221 board which was installed in the PCI slot of the flight control computer. The software used with the card is usually the proprietary National Instruments code which is not available for Linux. To overcome this limitation, an open-source library, the Control and Measurement Device Interface (Comedi) library was used to access data from the board within the software.

The Comedi project is an ongoing project that develops open-source drivers, tools, and libraries for data acquisition. The Comedi library is a collection of drivers for a variety of common data acquisition plug-in boards. The drivers are implemented as a core Linux kernel module providing common functionality and individual low-level driver modules. The Comedi features integrated real-time support (compatible with RTAI) for many hardware devices and a high-level library to make code incorporation less difficult.

6.3 DATAFLOW TO AND FROM THE FLIGHT CONTROL COMPUTER.

This section describes the dataflow through the flight-control system. Figure 30 shows the major components of the system, including the flight control computer (center) with the graphics computer center mounted directly above.

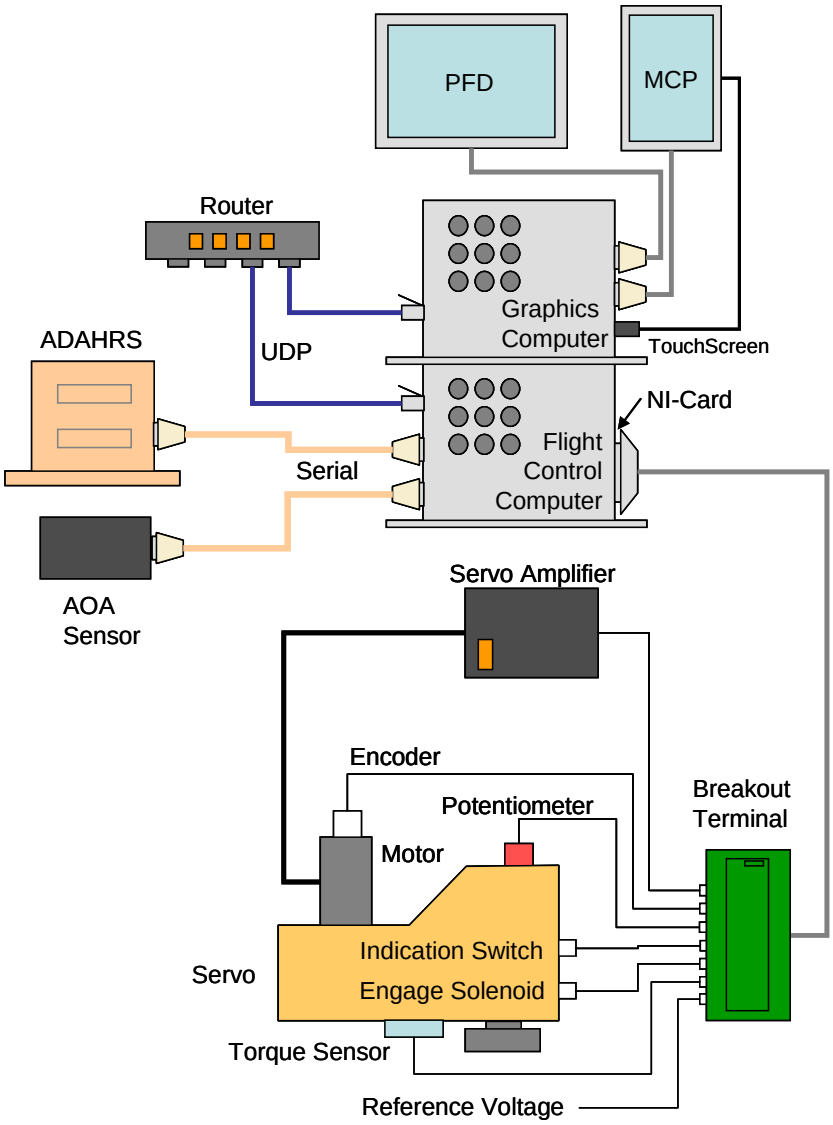

Figure 30. Input/Output Signals for Flight Computers

The flight control computer takes in data from Ethernet communications, serial communications, and individual analog/digital signals through a National Instruments data acquisition card. The attitude and air data are collected from the ADAHRS in the form of serial messages collected at one of the two available serial ports. The AoA data and GPS position data are collected from the AoA sensor model through the second serial port.

The graphics computer sends operator inputs to the flight computer through Ethernet communications using User Datagram Protocol (UDP) messages. In turn, the flight control computer sends status data and aircraft state data to the graphics computer in the form of UDP messages.

The remainder of the data is transmitted using a National Instruments (NI-PCI-6221) data acquisition card, which is installed on a PCI slot for the flight-control computer's motherboard.

A multipin cable connects the data acquisition card to a breakout terminal block, which makes the pins accessible to individual wires. The six main signals to and from each servo are:

1. Servo drive signal
2. Position encoder
3. Position potentiometer
4. Engage solenoid
5. Engage indication switch
6. Torque sensor

The servo drive signal sends a signal to the motor drive, which controls the current flow to the servo motor. The motor has an encoder on the back of it, which is used for servo position measurements. Additionally, there is a potentiometer that measures position. The servo has a solenoid-actuated dropout gear, which must be engaged for the servo to operate. A contact switch provides information on whether the the dropout gear is engaged. Finally, there is a torque sensor, which measures the torque at the servo's output shaft. The system includes a reference voltage measurement for A/D conversion of analog signals.

Complete details of the software implementation used for the flight control system, including envelope protection and stability augmentation functions, are given in appendix A of this report.

7. AUTOPILOT STANDARD-MODE ALGORITHMS.

This section discusses the implementation of the basic autopilot modes (modes that are common to most high-end autopilots). These functions drive the aircraft to a particular state and do not allow simultaneous pilot interaction. Autopilot functions are always user-activated and do not have the capacity to self-engage, although they might self-disengage in some circumstances. The autopilot is separated into lateral and longitudinal modes of operation.

7.1 LATERAL AUTOPILOT.

The lateral autopilot has two modes of operation: (1) a wing leveler (bank angle controller) and, (2) heading capture algorithm.

7.1.1 Wing Leveler.

The wing leveler is a bank angle controller that is set to always command a wings-level state. The block diagram is shown in figure 31. Bank angle error is used to generate an aileron command to level the aircraft. Exclusive proportional control would be ideal for this control law, due to the natural integrating relationship between aileron deflection and bank angle. However, in cases where a roll bias exists (e.g., uneven fuel load), pure proportional control can fail to achieve a wings-level condition. To correct for this problem, a small amount of integrator control is added to remove any unexpected roll bias. The commanded aileron deflection is then sent to the actuator controller, which commands the surface to the desired position.

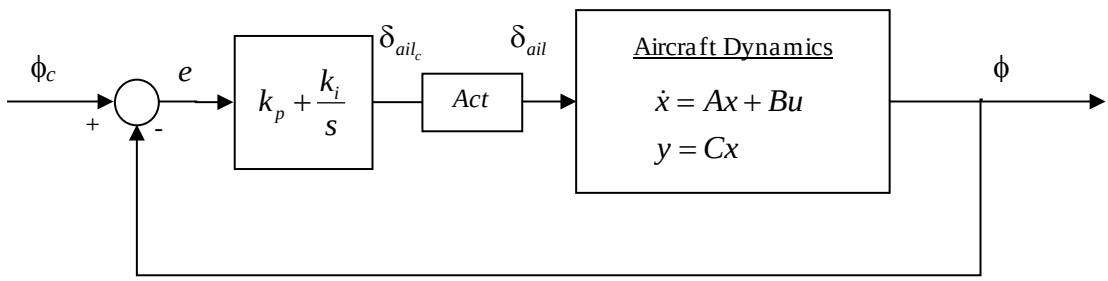

Figure 31. Lateral Bank Angle Control

One problem with the bank angle controller, as shown in figure 31, is that the controller would behave aggressively when large bank angle changes were commanded. This problem, typical of linear control laws, was solved with a simple shaping algorithm on the input. Figure 32 shows the basic shaping algorithm. When a large bank angle change is commanded that exceeds some specified error bound, $\Delta\phi_{c_{\max}}$, a ramped commanded bank angle, $\Delta\phi_{c_r}$, is used instead, which approaches the actual commanded value at a predefined rate. The end result is a control law that establishes a steady roll rate and captures the target bank angle smoothly.

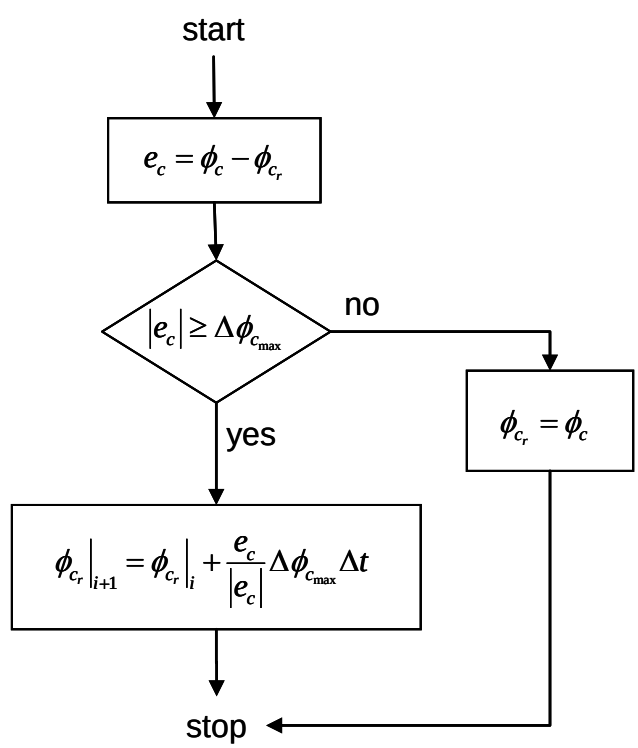

Figure 32. Simple Ramp Shaping Function for Bank Angle Control

7.1.2 Heading Capture.

The purpose of the heading capture algorithm is to turn an aircraft to capture and maintain a desired heading. In theory, this is one of the easier control laws to construct. However, in

practice, it turned out to be the hardest of the standard autopilot algorithms to perfect. Through the evolution of the algorithm, increasingly more-sophisticated techniques were applied to yield better performance. The final iterations of the heading capture algorithm worked adequately, but still exhibited some degree of undesirable attributes. Clearly, a heading capture algorithm for a production autopilot would require more analysis to perfect. Two types of systems were implemented: a rate-based controller and an attitude-based bank angle controller.

7.1.2.1 Turn Rate Controller.

Initially, a turn rate controller was implemented. In this case, a proportional heading loop is cascaded with a turn rate controller, as shown in figure 33. The inner loop, turn rate control uses proportional plus integral (PI) control to capture a particular turn rate. The commanded turn rate is calculated based on heading error. To prevent excessive turn rates, the commanded turn rate is bounded at some maximum turn rate (often 3°/sec) for instrument procedures.

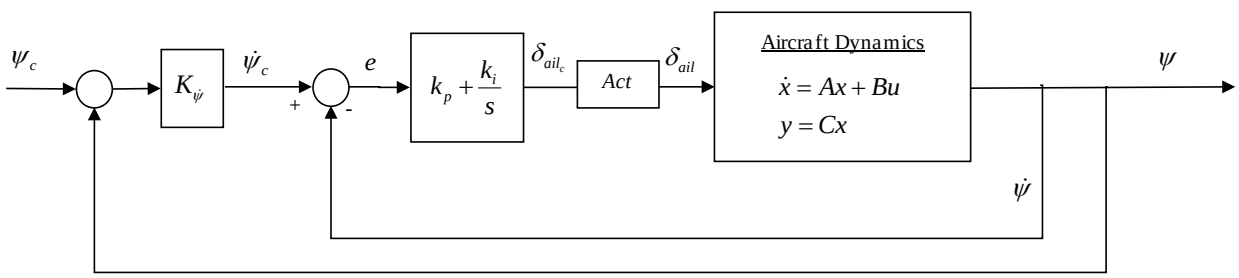

Figure 33. Heading Control

Assuming the inner loops track commanded turn rate well, a smooth capture of the proper heading is a natural outcome of this type of controller because it results in a linear reduction of turn rate as a function of heading error. The turn rate controller worked, but it did not have a crisp performance. The inner loop would generally capture the commanded turn rate in time, but too slowly to track well. Because the controller did not track turn rate well, the bank angle would tend to hunt to maintain the commanded turn rate. The poor tracking of turn rate during capture meant that the system would often overshoot or undershoot the target, depending on the speed of the aircraft. Essentially this controller emulated a rate-based autopilot, which is known to perform poorly when compared with attitude-based autopilots.

7.1.2.2 Heading Capture Using a Bank Angle Controller.

A better method to manage heading was to use the bank angle controller, which made use of the bank angle measurement. The bank angle controller leave as is established a bank angle and then rolled out on a specified heading. To capture a given heading, the bank angle was commanded as a function of heading error, as shown in equation 1 and figure 34.

$$\phi_d = k_\psi \left(\psi_d - \psi\right); \left|\phi_d\right| < \phi_{\max} \tag{1}$$

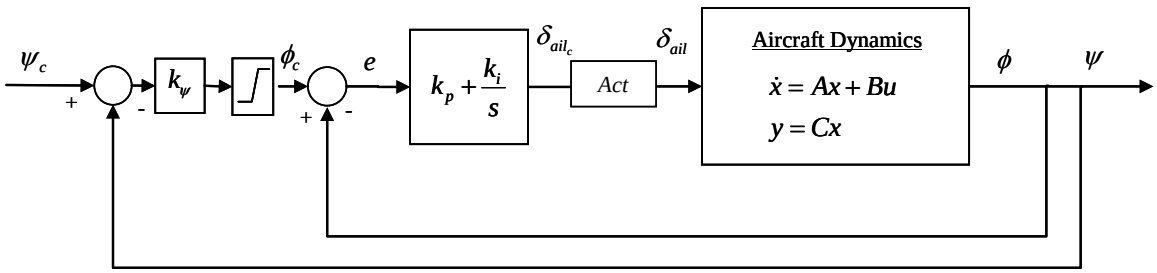

Figure 34. Heading Control Using Bank Angle

This heading capture algorithm had two persistent problems: (1) the capture algorithm would not roll out on a heading consistently well, and would overshoot or undershoot and, (2) the bank angle controller would experience slight roll oscillations that would become more pronounced as the aircraft slowed down.

The problem with using bank angle is that the linear relationship of equation 1 does not work well as a capture algorithm because turn rate does not vary linearly with bank angle. Essentially, the algorithm worked for a single airspeed when the rollout lead was appropriate, but would undershoot and overshoot at all other airspeeds. At low speed, when the turn rate was much faster for a given bank angle, overshoot was a big problem.

Several fixes were applied to the system. The first was to schedule the bank angle (ϕ_{max}) based on the airspeed of the aircraft. Thus, the aircraft at 60 kts would have a maximum bank angle of approximately 10°, which linearly increased to a maximum of approximately 25° as the aircraft approached 110 kts. The second fix was to vary the capture gain, k_ψ. In this case, the key was to measure the turn rate of the aircraft so that the gain, k_ψ, would be scaled up or down based on how fast the aircraft was turning. A smaller k_ψ resulted in the rollout starting sooner. The problem with this approach is that it also impacts the capture dynamics. For instance, a low k_ψ might not capture and maintain heading as well as the nominal value. Therefore, once the heading error was acceptably low, k_ψ would need to be returned to its nominal value to complete the capture and maintain the hold. However, even these solutions did not yield perfect results. Ultimately, the linear relationship in equation 1 was removed and replaced with one that more accurately reflects the dynamics between turn rate and bank angle, as shown in equation 2.

$$\phi_c = \sin^{-1}\left(\frac{\dot{\psi} V_{IAS}}{g}\right) \tag{2}$$

The bank angle could then be varied explicitly as a function of the desired turn rate, which in turn was a function of the heading error.

The final problem with the heading controller was that at low speed it would oscillate in roll. During simulation, this was not a big problem, but, in the aircraft, it was uncomfortable for the occupants. To correct this problem, gain scheduling was applied to stiffen the gains at low speed. The bank angle controller used for heading capture was the only instance in which gain scheduling was applied for this system.

Regardless of the method used for turning, the direction of the turn must be determined. Turn direction is chosen to minimize the turn angle required from the current heading to reach the desired heading.

7.2 LONGITUDINAL AUTOPILOT.

The longitudinal autopilot has three main functions:

1. Vertical speed
2. Flight level change (FLC)
3. Altitude hold/capture

7.2.1 Vertical Speed Mode.

The vertical speed controller feeds back altitude rate error to a PI controller, which commands a given elevator position (see figure 35). The commanded elevator is then sent to the actuator controller, which drives the elevator to the desired position.

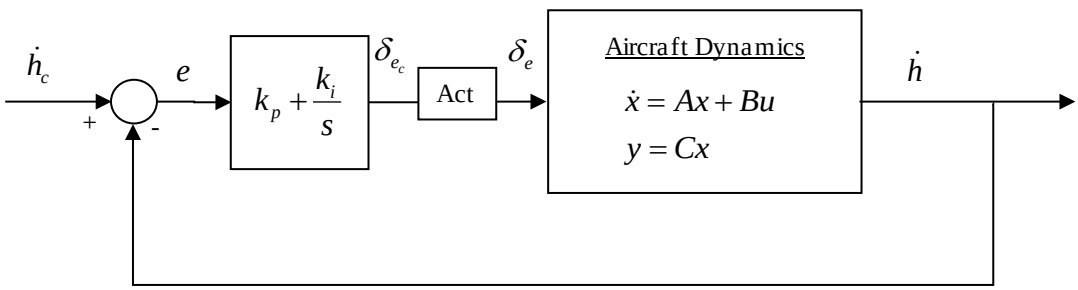

Figure 35. Vertical Speed Controller

The initial vertical speed mode-control law exhibited undesirable, transient behaviors when initialized at very small or very large vertical speeds. To correct the latter problem, a simple proportional-only pitch control law that commanded zero pitch and would activate any time the vertical speed exceeded 2000 fpm. Additionally, the vertical speed controller command was subjected to a shaping function (see figure 36), which limited the rate at which vertical speed command could change.

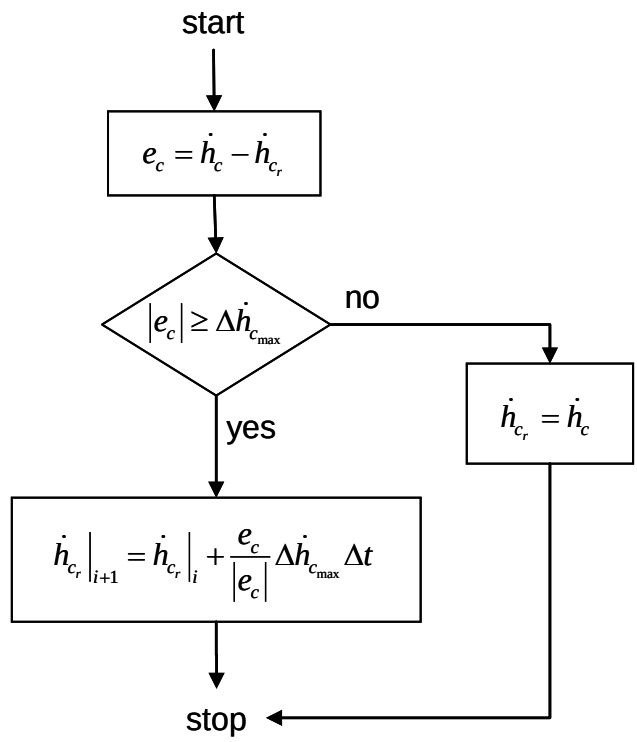

Figure 36. Ramp Shaping Function Used With the Vertical Speed Controller

7.2.1.1 Vertical Speed and Stall.

The vertical speed algorithms worked well when the airspeed placed the aircraft on the front side of the thrust curve where positive speed stability exists. In this region, faster airspeed increases drag and slower airspeed reduces drag, thus pitching for altitude rate works well. In cases in which the aircraft is near maximum L/D or on the slow side of maximum L/D, the induced drag becomes dominant and decreased speed results in increased drag causing speed instability. At such slow airspeeds, the vertical speed algorithm would fail to work properly and, left unattended, would increase pitch until the aircraft stalls. To prevent the autopilot from stalling the aircraft, the algorithm recognized the low speed condition and transitioned the aircraft to FLC mode if such a low speed was attained.

The FLC mode pitches for speed rather than flight path. This algorithm is not sensitive to the speed stability of the aircraft and works equally well on the front and back sides of the curve. When the transition is made, the aircraft maintains the target speed, but will not hold altitude (unless there is sufficient power applied). For the Cessna R182, the chosen transition speed was 70 kts, which is close to the best glide speed (or maximum L/D) for the aircraft.

7.2.2 The FLC Mode.

The FLC mode is a form of airspeed control. This control law consists of a PI compensator in the feed-forward path with speed and an altitude rate loop in the feedback path. The altitude rate

loop is required for system stability, but does not change the commanded airspeed and resulting aircraft rate of climb. The control law is represented in equation 3.

$$\delta_e = \left(k_p + \frac{k_i}{s}\right)\left(V_{IAS_c} - V_{IAS}\right) - k_b \dot{h} \tag{3}$$

The block diagram is shown in figure 37.

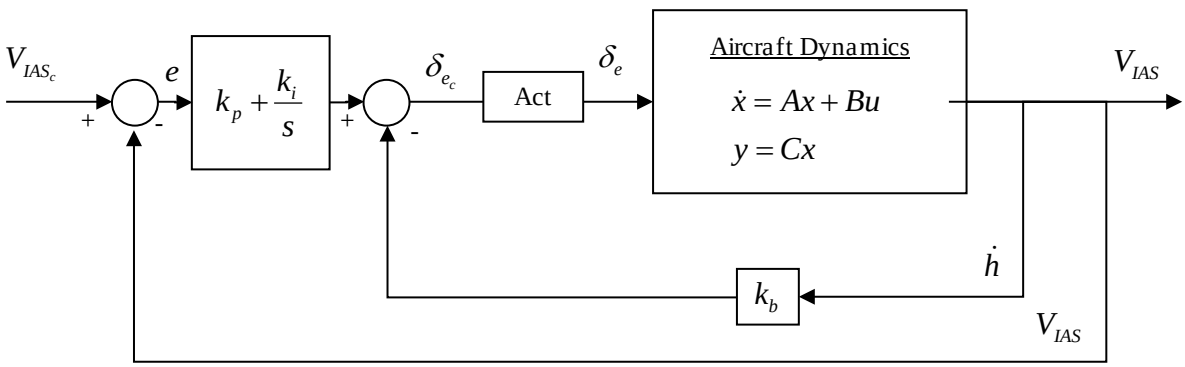

Figure 37. Speed Capture for FLC Mode

This implementation of FLC also includes an input shaper of the same form found for vertical speed in figure 36 to prevent large speed command discontinuities from reaching the controller.

7.2.2.1 Vertical Speed Capture Within FLC.

To prevent undesirable climbs and descents during significant speed changes, vertical speed mode is often temporarily engaged while in FLC mode to prevent altitude changes. Typically, this occurs when an aircraft is commanded to speed up while in a climb or slow down when in a descent. Because FLC mode only knows to capture speed, it is possible for it to descend in a climb to capture the higher speed (similar problem in a descent). To correct this tendency, the condition is identified, and a simple vertical speed controller is activated to bring the aircraft to a level flight condition while it accelerates or decelerates to the commanded speed.

The logic for this operation is shown in figure 38. The terms e_{climb} and e_{IAS} are the errors in altitude and absolute (not ramped) speed error, respectively. The ramped speed target refers to the speed target that comes from the shaping function in equations 4 and 5.

$$e_{climb} = h_c - h \tag{4}$$

$$e_{IAS} = V_{IAS_c} - V_{IAS} \tag{5}$$

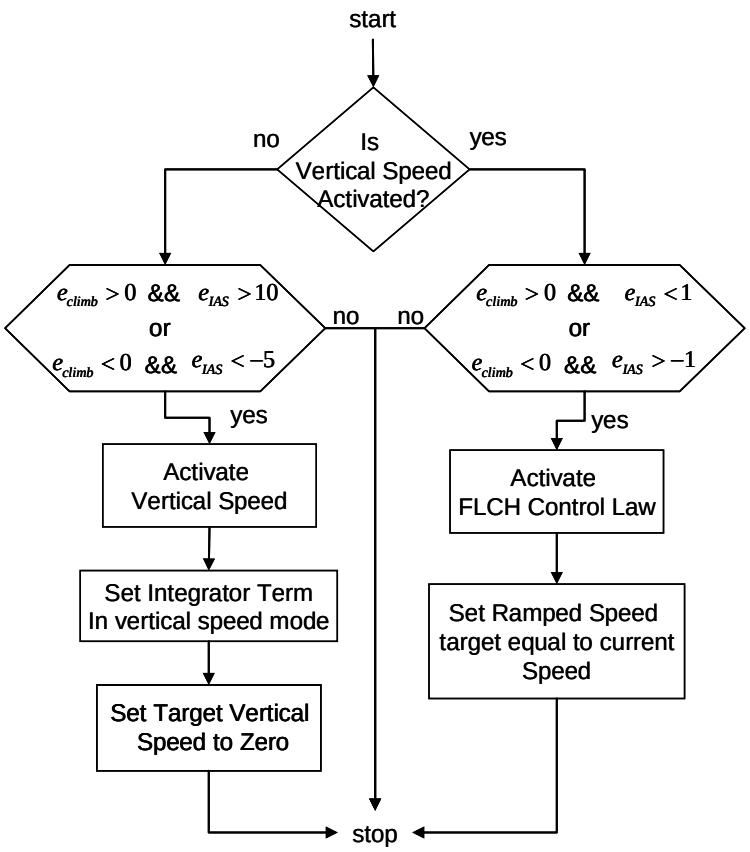

Figure 38. Logic for Engaging Vertical Speed Mode During FLC Mode

Any time vertical speed is engaged, it is important that the integrator is set properly. In this case, the vertical speed integrator is set equal to the FLC integrator to eliminate any transient behavior. Once the proper conditions are set for the FLC mode to be re-engaged, the FLC mode is activated. As part of initialization, the ramped speed input for the shaper is reinitialized by setting it to the current speed.

7.2.2.2 Speed Filtering.

One problem with the FLC mode was that it was particularly sensitive to variations in speed due to turbulence and could yield a rough ride to occupants by aggressively trying to maintain a particular speed. To prevent this, filtering was applied to the airspeed measurement used by the FLC mode. A 0.5-second time constant was used for the filtering.

7.2.3 Altitude Hold and Capture.

Altitude hold commands the aircraft to maintain a specific altitude, but, rather than feedback altitude directly to elevator, altitude error is used to generate a commanded altitude rate signal using a gain, $K_{\dot{h}}$. Equation 6 and figure 39 show the relationship.

$$\dot{h}_c = K_{\dot{h}}\left(h_c - h\right) \tag{6}$$

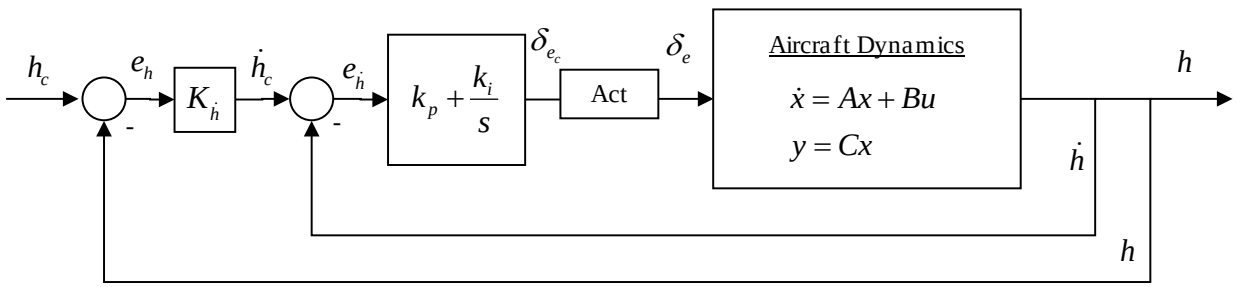

Figure 39. Altitude Hold and Capture

When an aircraft climbs or descends to a new altitude, the climb is either accomplished using vertical speed mode or the FLC mode. In either case, a transition must be made at some point to capture the altitude. To ensure a smooth transition, the altitude hold function is engaged when the product of the altitude error with $K_{\dot{h}}$ equals the current vertical speed. The relation is shown in equation 7.

$$\left|\dot{h}\right| \geq \left|K_{\dot{h}}\left(h_c - h\right)\right| \tag{7}$$

7.2.4 Control Surface Deflections.

Achieving the proper control surface deflections needed to support the position-based autopilot functionality required a special servo control algorithm to drive the control surface to the commanded value. The algorithm is contained within the cs_control object. It is based on a proportional plus integral plus derivative (PID) controller in conjunction with a special shaper to preprocess the commanded control surface position. This shaper is more than a simple ramp in that it estimates the required acceleration and deceleration of the motor as it travels toward the commanded position.

The commanded position from the shaper is fed to a PID controller, which has several special features designed to protect the motors using various limiters. For example, the PID controller can limit the position, the rate, and the acceleration of the motor. If any of these limits is exceeded, the integrator is suspended from operating. The algorithm also generates its own derivative signal and enables the operator to apply filtering as required to reduce the noise of the differentiated signal. The controllers for both elevator and aileron are shown in figure 40.

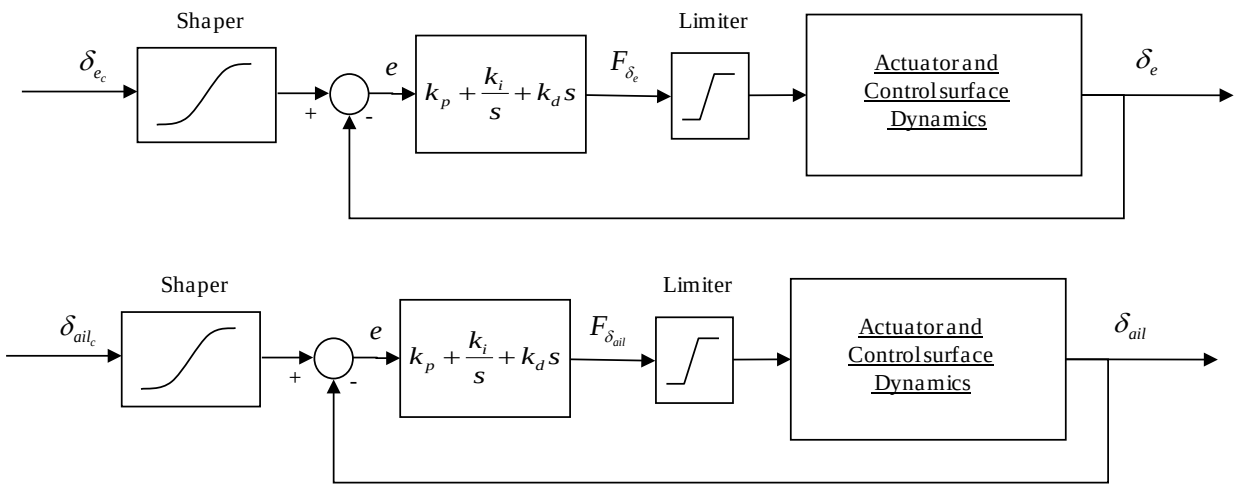

Figure 40. Controller for Commanding Control Surface Deflections

The controller used for controlling output torque of the servos, the PID object, was essentially the same controller with the initial trajectory shaper eliminated.

7.3 STANDARD AUTOPILOT MODES NOT IMPLEMENTED.

Typical full-featured autopilots include the ability to intercept and track flight paths defined by radio navigation aids (e.g., very high frequency (VHF) Omni-directional ranges localizer, and glideslope transmitters) or by other means (e.g., defined three-dimensional trajectories not constrained by particular navaids). These features were not needed in the present project, so they were not implemented as part of the work described in this report.

8. STABILITY AUGMENTATION ALGORITHMS.

The purpose of stability augmentation is to modify the natural dynamics of the aircraft to achieve a more desirable behavior. To implement mild stability augmentation on an aircraft with reversible controls, the torque-based, back-drivable servo actuators were used to provide stabilizing inputs to the system while allowing the pilot to simultaneously move the controls through the entire range of motion. A potential disadvantage of this approach is that changes in the output torques of the servos can degrade the tactile feel of the aircraft, which may be objectionable to pilots. Accordingly, the primary challenge was to design the system to provide adequate augmentation while minimally changing the tactile response.

8.1 LATERAL STABILITY AUGMENTATION.

Lateral stability augmentation was implemented to improve the lateral stability of the aircraft without interfering with its ability to be hand flown by the pilot. In this case, improved stability consisted of the augmented aircraft having a tendency to always return to a wings-level attitude.

The bank angle control law, similar to the one used for the autopilot, was used to add extra lateral stability; however, it had no input shaper to modify the response. Instead, the allowable control

torque applied was limited to a very small level. The reduced control force enabled the pilot to easily override the always-on wing leveler. The wing leveler was only powerful enough to gently displace the ailerons from their equilibrium position. The reduced allowable control force was obtained by changing the actuator controller settings. The basic control law is shown in figure 41.

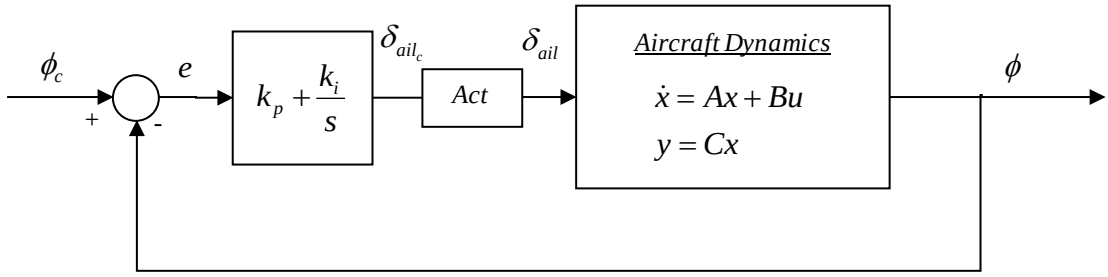

Figure 41. Bank Angle Stability Augmentation

One of the first problems discovered with the system was that the integrator, designed to guarantee zero steady-state error in the autopilot, created a problem for stability augmentation. The reason is that if enabled during long piloted turns, the integrator would wind up to its allowable limit. This would create an undesirable roll bias in the opposite direction when the controls were neutralized. To avoid this problem, the integrator was deactivated when the bank angle exceeded 5°. The proportional control alone was allowed to function, and it was sufficient to right the aircraft to within 5° of level. At that point, the integrator reactivated and the aircraft returned to level flight. The integrator also created some very slight roll oscillations when the aircraft was in level flight. Because of this problem, the integrator was finally turned off, resulting in a small reduction in performance, but a better perceived ride for the occupants.

8.1.1 Tactile Consequences of the Control Law.

Although the basic control law for stability augmentation is straightforward, the tactile consequences of having the control law running in concurrence with the pilot's manual control were more complex. One major problem was that, whereas low control torques were desirable from a piloting tactile perspective, the low control torques were often not enough to move the ailerons sufficiently to right the aircraft. For instance, a torque limit of 5 in.-lb was barely noticeable to the pilot and, most of the time, it was sufficient to right the aircraft. However, in some cases, the natural stiction in the cable-pulley control system could not be overcome using only 5 in.-lb. A 10 in.-lb torque guaranteed good behavior, but created a heavier control feel for the pilot.

The magnitude of the force was not the only consideration in pilot perception of control feel. The choice of servo actuation made a big difference in the tactile feel perceived by the pilot (see figure 42). The servo can be driven either by a torque or a position-based control law, and the outer loop can either be designed to command an aileron torque or an aileron position merely by a change in gain. Either method is satisfactory for stabilization, but the two have distinctly different tactile characteristics from the pilot's point of view.

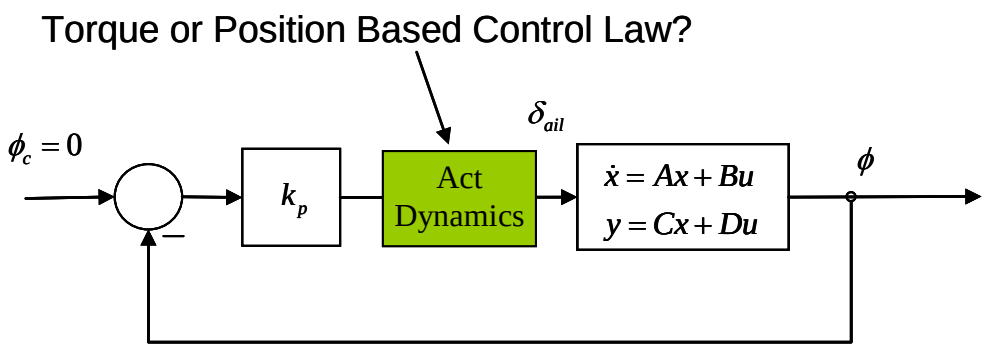

Figure 42. The Type of Actuator Control Law Influences the Tactile Feel

Figure 43 shows the subtle distinction. The position-based controller always applies the maximum allowable torque to achieve a particular aileron displacement, whereas the torque-based controller applies a torque as a function of bank angle. The result is that the position-based control law may feel like a continuous bias to the pilot, but the pilot can feel the torque-based controller ramp up as bank angle is increased.

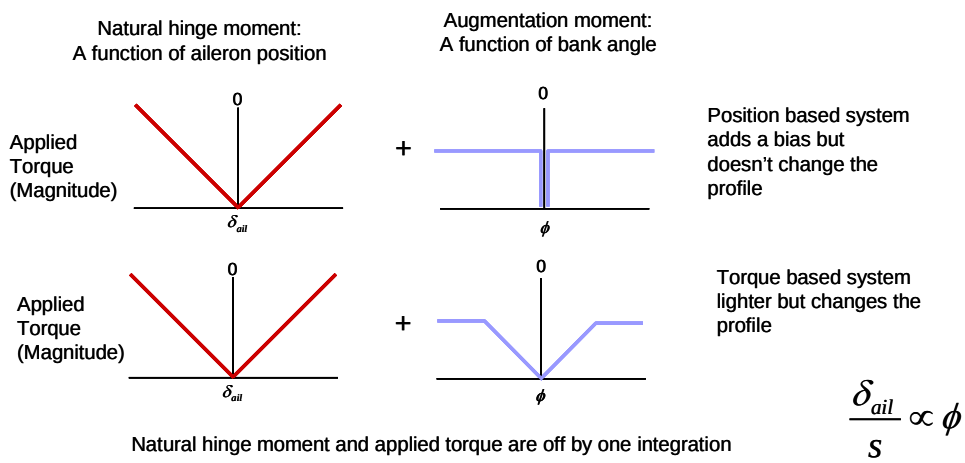

Figure 43. Difference in Tactile Feel Between Torque and Position-Based Control Laws

The natural hinge moment of the aileron is a function of the displacement of the control surface, so the tactile feel of the aileron is such that the stick force increases as more aileron displacement is applied. When the position-based controller is used, this paradigm is preserved, but displaced. The pilot feels heavier controls, but the original tactile relationship does not change. However, when the torque control law is applied, the aileron does not initially feel as heavy, but the pilot can feel the torque increase with bank angle (up to the saturation point), which can be disconcerting. The problem is that the aileron deflection is proportional to roll rate rather than bank angle, so the tactile feel of the controller is off by one integration and is not masked by the normal feel of the aircraft.

The torque-based controller can create lower initial stick forces, but does not mask the controller's action from the pilot, whereas the position-based controller does, but at an expense

of higher torques. The position-based system is superior if the torques can be kept very low. In the Cessna R182, the forces were high enough that the torque-based law was eventually used, even though, the position-based system had been used in the simulator.

8.1.2 Tactile Consequences of Servo Mechanizations.

Regardless of the type of control law used for roll stability augmentation, one phenomenon that was noticed by several pilots had to do with control bumps when the direction of servo-applied torque reversed. The control bumps were thought to be caused mainly from backlash in the servo itself, resulting in some degree of motor/gear-train travel at zero torque, and followed by a small but noticeable control bump in the opposite direction from previously applied torque when backlash in the gear train ended. A shorter gear train with a larger motor would decrease backlash and the associated phenomenon. It is important to note that minimization of backlash is crucial for pilot acceptance in the design of servos to be used for full-time stability augmentation of cable-controlled aircraft.

8.2 LONGITUDINAL STABILITY AUGMENTATION.

The purpose of the longitudinal stability augmentation is to increase the ease of flying the aircraft in pitch. However, unlike the lateral case in which zero bank angle is used as a control objective, there is no obvious design goal for control for longitudinal stability augmentation.

Initially, increased pitch rate damping was considered. However, pitch rate damping generally has the effect of increasing short period damping, rather than effectively damping the phugoid mode, which is the dominant mode for controllability in light aircraft. To change phugoid damping, pitch feedback is required. The problem with pitch feedback in this case shows that, unlike roll, there is no good pitch target that is always appropriate. The required pitch angle varies with aircraft trim and with the phase of flight. The obvious solution for this type of problem is to use a washout filter, in the same way a washout filter is used on yaw dampers to washout the low frequency dynamics of a turn. This was first tried in the simulator, but was determined to have an unusual tactile feel, as the controller would initially provide strong resistance to the pilot, but would gently fade away.

In simulator experiments, pitch feedback appeared to work better. Proportional pitch feedback, using a zero-pitch set point implemented with a control force limiter, achieved the desired stability augmentation results (see figure 44). Because the controller was strictly proportional, the human operator could override the controller with the yoke or the trim. At high-pitch angles, the controller contributed a bias to the control force, which was indistinguishable from normal pitch force. However, the controller was effective at preventing large pitch swings due to an excited phugoid oscillation.

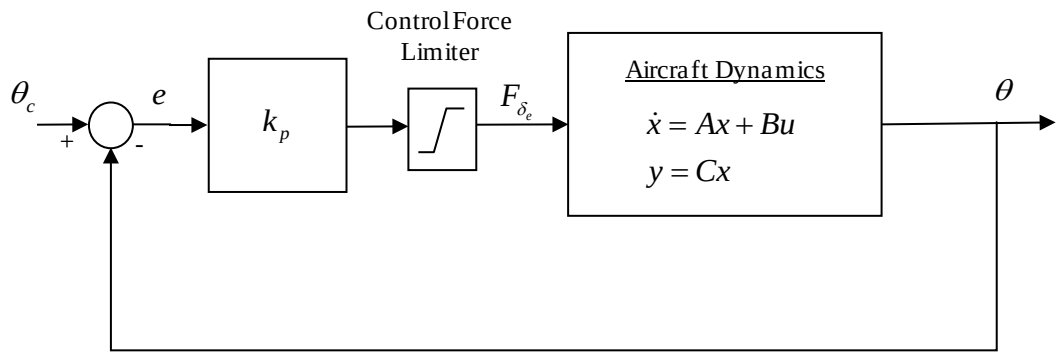

Figure 44. Longitudinal Stability Augmentation Used on the Simulator

In flight, however, the pitch controller felt awkward, especially when sufficient pitch trim was applied. In the simulator, applying trim with the control law in operation had the convenient result of moving the pitch set point. In the aircraft, where more disturbances were present and the pitch trim setting was not available as a measured quantity, the application of the trim against the pitch controller could result in the control law being saturated in one direction, but still be active in the other (see figure 45). Thus, the control law could be biased to the point in which it would not work.

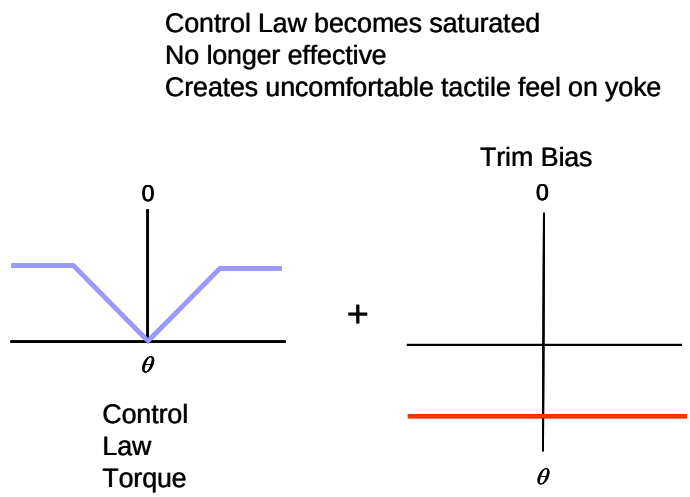

Figure 45. Trim Impact on the Controller

The washout filter proved to be a much better solution for the aircraft and the tactile feel was acceptable to the subject pilots. In addition, the washout filter had the advantage of being completely independent of pitch trim. The formulation of the washout filter is expressed by equations 8 and 9 where θ_c, the target pitch angle, is constantly lagging the actual pitch angle by means of a first order lag.

$$\delta_{e_{Torque}} = k_p\left(\theta_c - \theta\right) \tag{8}$$

$$\theta_c = \left(\frac{1}{\tau s + 1}\right)\theta \tag{9}$$

This formulation of the washout filter is more convenient for the system because the value of θ_c can be changed or held constant in certain instances.

One problem for the washout filter is how it should handle the transition into one of the pitch envelope protection modes. In some cases, the simultaneous operation of stability augmentation and pitch envelope protection could provide a tactile feel of a system-releasing pressure. This was due to the washout filter washing out the contribution of the stability augmentation when it was not expected. To solve this problem, stability augmentation was only allowed to function within the normal operating boundary of approximately ±15°. Outside of this boundary, the θ_c value would be held constant at the saturated boundary value, so that outside of the boundary, the system would always pull back toward the boundary, but not washout. Originally the washout filter was turned off outside the boundary, but this created its own discontinuity, so deliberate saturation was the better solution.

9. ENVELOPE PROTECTION ALGORITHMS.

Envelope protection was designed to activate when the aircraft entered a dangerous condition, alert the pilot to the situation, and intervene to assist in placing the aircraft back into a safe flight condition. Unlike stability augmentation, with which the challenge was to be inconspicuous, the intent with envelope protection was to alert the pilot tactilely and use the servos to right the aircraft.

9.1 LATERAL ENVELOPE PROTECTION.

The purpose of lateral envelope protection is to prevent excessive and presumably unintentional bank angles. Solving this problem appears straightforward: If the aircraft banks beyond a certain point, the controller can simply apply a restoring force using some proportional control law. However, there are three problems with this approach:

1. Torques must be high to be detected.
2. Controls can snap back if the pilot suddenly releases the yoke.
3. Abrupt disengagement of the system can yield a perceived bump in the controls.

The first problem observed was that the torques generally had to be high or the pilot could easily ignore them. In gentle maneuvers in which an overbank condition was entered slowly using only slight aileron displacement, activation of the envelope protection system easily alerted the pilot. However, during more aggressive maneuvering in which aileron stick forces were already high, the pilot could miss the torque input completely. This was partly due to the linear nature of the control law. Figure 46 shows that the ramping nature of the torque increase could be missed.

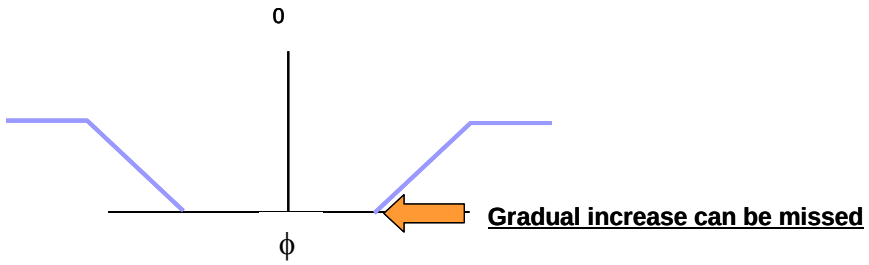

Figure 46. Gradual Torque Increases Can Be Missed

To address this problem, several ideas were proposed and attempted. One was to use a quadratic increase in torque. Because this resulted in instability and unpredictable behavior, this idea was quickly discarded. Another idea was to introduce a hysteresis in the system so that the pilot would be subjected immediately to a non-zero torque. This worked, but was uncomfortable and disconcerting to the pilot. Ultimately, in the simulator, a large gain and a high allowable torque was chosen as the best solution. However, this created additional problems.

During initial simulator tests, even a fairly benign control law moved the aileron control to the extreme opposite position when the pilot released the yoke. In this case, the applied control force was calculated as a simple function of bank angle, not aileron position, and the aircraft could not react fast enough in bank to prevent the controller from moving the yoke to the opposite extreme. Forces high enough to be noticed by the pilot for the purposes of envelope protection were always strong enough to cause this problem. In addition to this problem, once the aircraft started to recover, this primitive controller suddenly turned off, and the air loads on the ailerons abruptly moved them back toward the neutral position.

To prevent this problem, aileron deflection rate was used as a feedback parameter, as shown in figure 47. With the rate term added to the feedback path of the controller, a large damping force was generated any time the ailerons started moving too fast. With sufficient tuning of the gains, a desirable response was achieved.

Another problem encountered was that of a perceived discontinuity (bump) in control forces when the system disengaged. Initially, the system simply disengaged when the bank angle of the aircraft returned to normal limits. However, if the ailerons were in motion at that time, a bump could be felt in the control yoke on disengaging. The solution was to maintain damping for several seconds after the proportional part of the controller ceased operating, gradually tapering the damping term to zero.

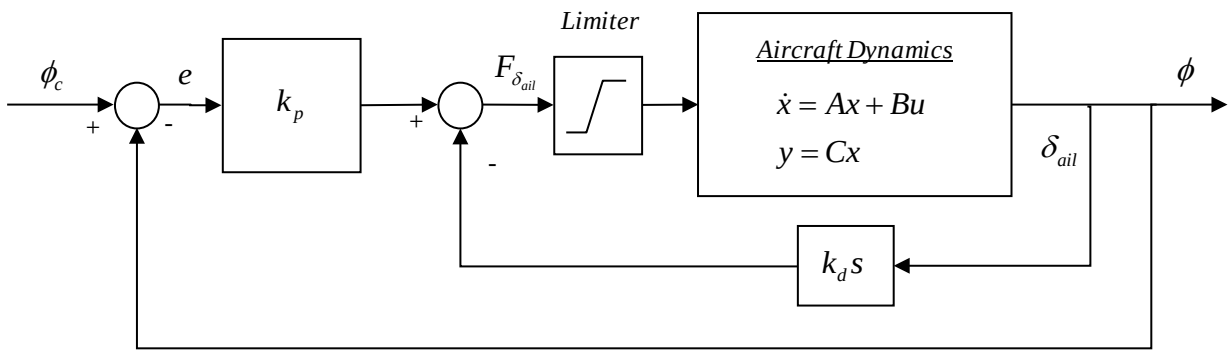

Figure 47. Bank Angle Envelope Control Used in the Simulator

This basic solution, a proportional gain with rate feedback on the control surface position and a soft shutdown, was so successful in the simulator that it became the model for all the other envelope protection modes. However, when the system was moved to the actual aircraft with the flight servos, the control surface rate feedback (the enabling discovery from the simulator) was rendered nearly useless because of servo chatter. The rate feedback had enough noise to cause severe servo chatter; therefore, it had to be greatly reduced, which resulted in the re-emergence of the snap-back problem.

To provide a reasonable alert to the pilot while using lower torque values, hysteresis was reconsidered. In this solution, shown in figure 48, the engagement of the envelope protection was delayed until a sufficient displacement into the region had been achieved, and then all the associated torque was applied at once. To disengage, the torque followed the normal linear path. However, to eliminate the uncomfortable bump, a fast and sufficient first order lag was applied to the signal. This removed the bump, but still provided enough of a discontinuity that the pilot was unlikely to miss it. The soft shutdown routine was maintained.

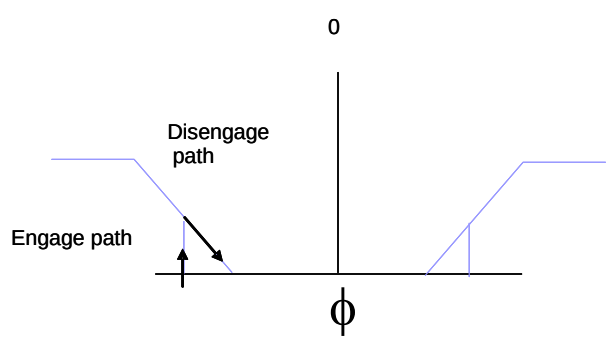

Figure 48. Bank Angle Envelope Control Using Hysteresis

9.2 LONGITUDINAL ENVELOPE PROTECTION.

The longitudinal envelope protection system is designed to protect against the following conditions:

- Stall
- Overpitch
- Overspeed

Each of these conditions involves applying pitch control force to move the aircraft away from a dangerous situation. The initial lessons learned from the development of lateral envelope protection were applied to the longitudinal cases as well. Control surface rate was used in each case to avoid control yoke snap-back tendencies, and damping terms were tapered to zero on disengaging the mode. As with roll, the pitch servo did not tolerate the control surface damping well and had to be greatly reduced. However, the snap-back problem was not as serious in pitch and, therefore, did not present the same concern.

9.2.1 Stall.

Stall protection is one of the most important elements of envelope protection. It is designed to prevent the pilot from stalling the aircraft, which could be catastrophic at low altitude. To prevent a stall in the current system, AoA is measured if in excess of a certain prestall limit and is fed back through a proportional controller to generate a nose-down stick force. Elevator deflection rate feedback is used to prevent any discontinuous yoke movements if a pilot releases the yoke. A force limiter is used to prevent large commanded forces. Figure 49 shows the stall-prevention block diagram.

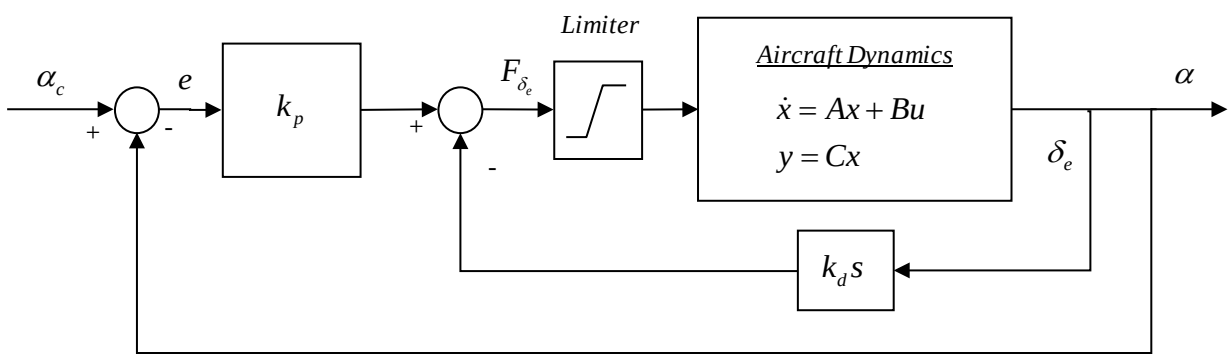

Figure 49. Stall Prevention

Very low-speed flight was one problem encountered in simulation. If the pilot pulled the aircraft into a high-pitch attitude, let the speed drop well below normal stall speed, and then stalled the airplane, the initial force-based controller had the tendency to push the yoke violently full forward because there was little aerodynamic stick force to oppose it. To solve this problem, the force limiter was modified to scale the maximum allowable force as a function of airspeed. In the simulator, this started at approximately 55 kts and reduced to zero by approximately 20 kts. However, this became problematic in the aircraft because the controller tended to release pressure as the aircraft moved deeper into the stall, creating a confusing tactile response for the pilot. Because of this problem, the low-speed force limiter was shut off. In a production system, such a limiter should be reconsidered, but for a much reduced speed range.

9.2.2 Overpitch.

Overpitch protection is activated when the aircraft exceeds a certain pitch bound. In the simulator, the range was 20° in either direction. However, in the aircraft, this was reduced to +18°/-7°. As with roll and stall envelope protection, an initial-pitch envelope protection system was implemented as a force-limited proportional controller with control surface rate feedback to eliminate yoke snap-back tendencies. In the aircraft, the gain had to be reduced. However, as predicted, the problem encountered with overpitch recovery was the tendency to overstress the aircraft when recovering. Several methods were considered as potential solutions, including implementing a force limiter as a function of airspeed. Ultimately, a more formal solution was employed using an inner loop to command g-force directly. In this controller, a PI controller is contained in the inner loop around measured g-forces. The control force limiter and the control surface rate loop are also contained in this loop (see figure 50).

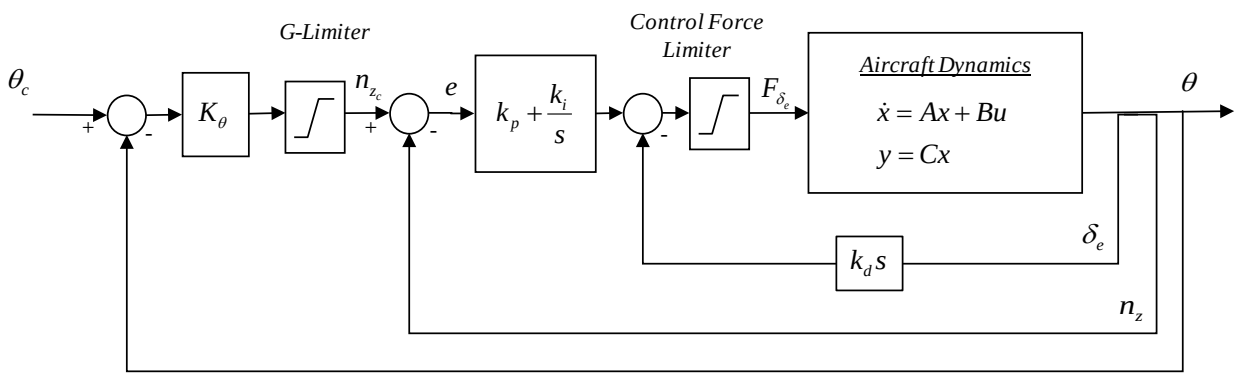

Figure 50. Overpitch Envelope Protection

Once a successful g-controller was functioning, a proportional pitch outer loop was employed to correct for excessive pitch. In the outer loop, a g-limiter was used to ensure that commanded g-forces stayed within a reasonable bound. This solution was maintained in the aircraft. Although the g-limiting greatly reduced tactile sensations available to the pilot through the yoke, it was essential for safety.

9.2.3 Overspeed.

The overspeed control law is designed to prevent the aircraft from exceeding its maximum speed. When the aircraft approaches maximum allowable speed, controls engage to pitch the aircraft up to prevent overspeed. Initial versions of this control law explored in simulation would invariably overstress the airframe, so a g-limiting strategy was employed in similar fashion to that used within the overpitch control. In this controller, a PI controller is contained in the inner loop around measured g-forces. The control force limiter and the control surface rate loop are contained in this loop as well. Indicated airspeed is controlled in the outer loop (see figure 51).

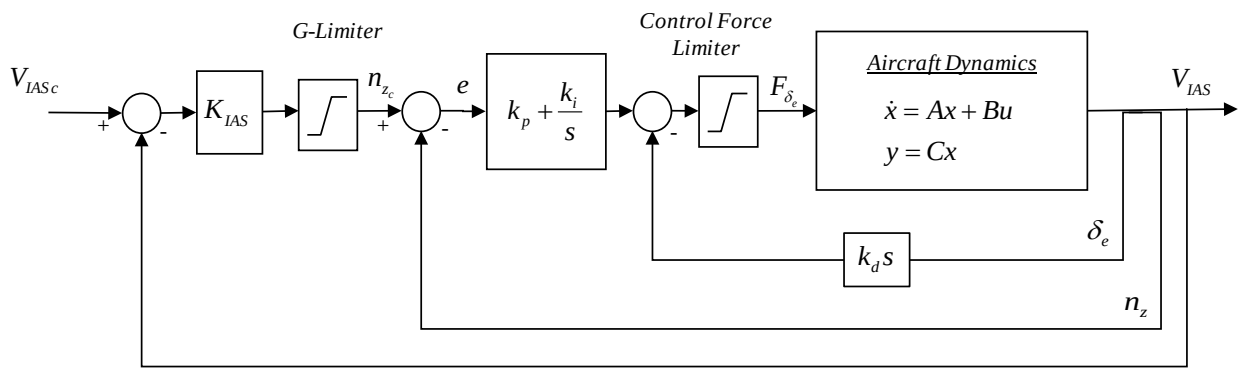

Figure 51. Overspeed Envelope Protection

The problem encountered with this overspeed correction algorithm was the tendency to maintain the maximum g-limit even after the aircraft's nose had been pitched above the horizon. The typical behavior would be for the aircraft to correct the overspeed, but to pitch excessively high. To correct this problem, a modification was made to the g-limiter. The g-limiter was made to reduce the allowable g-loading as the pitch angle became positive. At 5° positive pitch up, the g-loading was reduced to 1g, so the aircraft would tend to pitch to 5° and then wait for the airspeed to bleed off. This solution worked reasonably well in the aircraft and the simulator.

9.3 MODE SWITCHING.

One of the challenges in managing envelope protection features is establishing appropriate mode switching between the various control laws. Generally, mode-switching problems consist of two distinct types:

1. Mode switching between stability augmentation and envelope protection
2. Prioritizing between simultaneous adverse conditions

As a general rule, only one control law should be running at a time. Otherwise, the system behavior may be unpredictable. Therefore, it is necessary prioritize control laws in various situations.

With lateral control, mode-switching concerns are minimal. The stability augmentation system does not interfere with envelope protection because it saturates long before envelope protection is engage; therefore, both modes can run simultaneously.

However, with longitudinal control, the stability augmentation system can interfere with the envelope protection features. As previously discussed, the washout filter had to have its commanded pitch value saturated while envelope protection features were activated.

Simultaneous adverse conditions can exist with longitudinal envelope protection. Particularly, without adequate prioritization, the overpitch algorithm could potentially be activated during either stall or overspeed. For example, an aircraft can overspeed while in an excessive pitch-down attitude and stall while in an excessively high-pitch attitude. To solve this problem, a

control law prioritization was implemented for longitudinal control. If the aircraft experienced multiple adverse longitudinal conditions at once, the envelope protection system addressed them according to the following priority list, in descending order:

1. Stall
2. Overspeed
3. Overpitch

One interesting problem encountered while testing occurred during accelerated stalls. It was possible to stall the aircraft at a very low-pitch angle and during recovery to invoke the low-pitch side of the overpitch algorithm. In this case, a limit cycle between the modes could develop when the aircraft recovered from a stall only to have the overpitch algorithm recover the aircraft back into a stall. To correct this problem, servo actuation by the overpitch algorithm was suppressed when the AoA of the aircraft was greater than 5°. The rationale was that during most underpitch maneuvers, the AoA would be very small, so the presence of a higher AoA might indicate accelerated stall recovery (see figure 52).

Figure 52. Accelerated Stall Can Trigger Underpitch

10. MANUALLY-ENGAGED UNUSUAL ATTITUDE RECOVERY DESIGN.

In addition to the always-on stability augmentation and envelope protection features, an unusual attitude recover function was implemented that required manual engagement by the pilot. The basic design concept for this feature was to simply roll the aircraft to a wings-level condition and then correct the pitch attitude. The initial thought was to use or modify the existing autopilot bank angle and pitch control algorithms to support this function. However, both the roll and pitch control laws needed modification to provide acceptable unusual attitude recovery performance.

10.1 BANK ANGLE CONTROL.

The bank angle system used for the autopilot was far too slow to be adequate for use in unusual attitude recovery because the shaping module within the algorithm commanded a smooth and uniform roll rate. For recovery, the wings needed to be promptly brought to level. To facilitate the appropriate performance, the control law shown in figure 53 was used. The control law is a simple PI bank angle controller with a limiter to prevent excessive aileron commands. In practice, an aileron limit of 15° worked well.

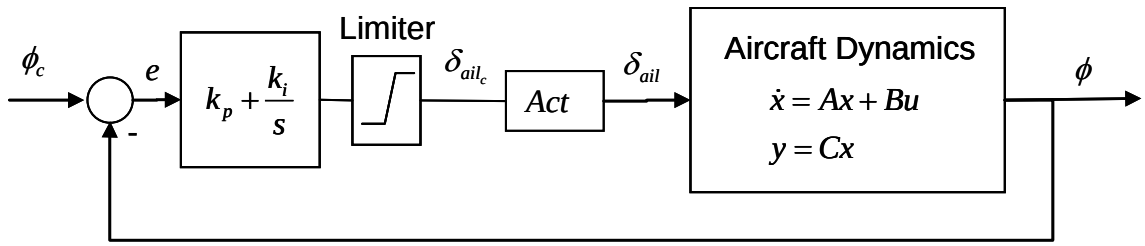

Figure 53. Wing Leveling Algorithm Used for Recovery

10.2 PITCH RECOVERY CONTROL.

The autopilot's vertical speed controller was not appropriate to use for recovery because it was designed to capture a specific vertical speed using fine adjustments to pitch. Therefore, it was not fast or aggressive enough to adequately correct extreme pitch errors. Additionally, it had no g-limiting protection to prevent overstressing the aircraft.

Initially, modifications were made to a controller that used direct pitch feedback to try to achieve a g-limited system without controlling n_z directly. For example, one method was to bound elevator deflection as soon as some maximum n_z boundary was reached. All of these methods resulted in unpredictable and undesirable behavior, usually involving some limit cycling of the system reaching and leaving the n_z boundary. There was no guarantee that the n_z boundary would not be exceeded. These observations quickly led to the conclusion that an explicit n_z loop with a limiter would be more effective.

The resulting control law for pitch recovery is shown in figure 54. The control law has successive loop closures with the inner loop controlling n_z and the outer loop commanding pitch. The outer loop uses a PI controller to calculate a g-loading based on the pitch error.

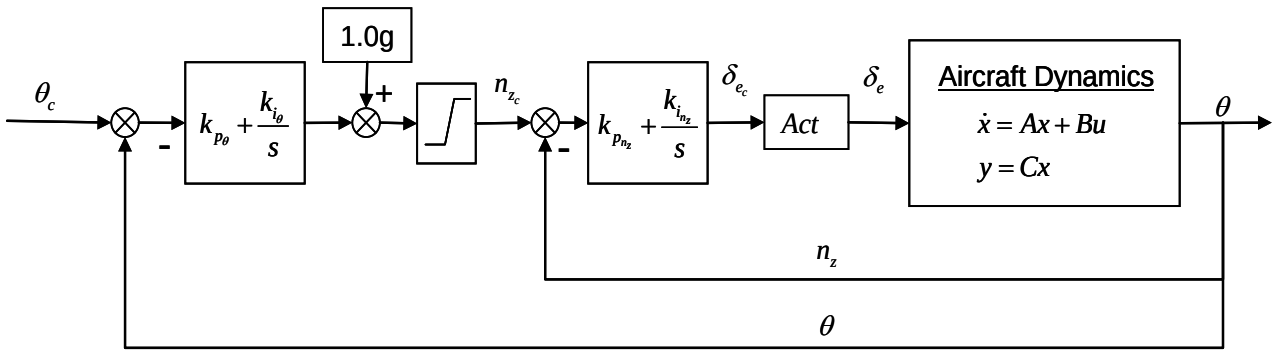

Figure 54. Pitch Control Law Used for Recovery

This g-loading was limited to a maximum limit based on the aircraft's structural capabilities. A bias of 1g was added to ensure a proper 1g condition at a zero pitch angle. The inner loop controller was a PI controller that drove the aircraft to the commanded g-loading from the outer loop.

One concern was that the control law makes use of two integrators. To achieve zero steady-state error in pitch, only one integrator was required. Ultimately, the outer integrator could easily drive the system to the desired pitch and accept n_z errors in the inner loop. The inner loop integrator was added to ensure that the actual g-loading would not exceed the commanded limit. However, this design still proved insufficient to guarantee that the g-loading would not exceed desired limits.

If inner loop gains were chosen to make the control law fast, it was likely that the overshoot in the response would exceed the g-limit regardless of limiting the commanded input. To correct this problem, the dynamics of the inner loop were made slower to ensure that the overshoot was minimized. Although this eliminated any overshoot and created a more pleasing ride, the ability of the control law to capture the target pitch angle was compromised.

In theory, the gains of this control law can be chosen so that the control law with the n_z inner loop can be as effective at tracking pitch as the direct-pitch control law. In the analytical environment, this worked well, but the concern of aggressive inner-loop dynamics made such implementations impractical.

This is a case in which the application of modern control techniques with an appropriately crafted cost function might enable a desired response subject to the constraint of benign inner-loop dynamics. This approach has not been further investigated.

Instead, a second control was implemented for fine tuning the unusual attitude response once the pitch error was reduced. In this control law (figure 55), a PI control strategy was applied directly to the pitch error. Because this control law has no protection from overstressing, it was important that it be applied once the aircraft is in a semi-stable condition.

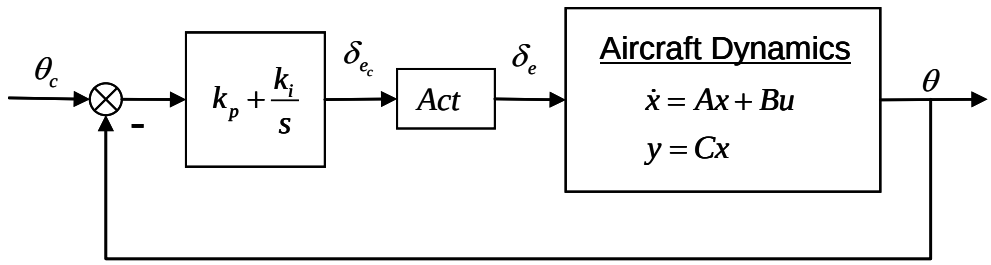

Figure 55. Control Law for Fine Pitch Control

Several parameters are tracked to ensure that the aircraft is in a semi-stable state. These include the bank angle, the pitch angle, and the pitch rate. To transition to the tighter control law, each of these parameters must be within a safe boundary, as shown in figure 56. The aircraft must be close to a level pitch attitude and not pitching at a high rate. Pitch rate must be taken into account to capture the case in which the aircraft has a very high pitch rate as it passes through nominally level pitch attitude. In this case, the pitch rate makes a transition to the tighter control law unsuitable.

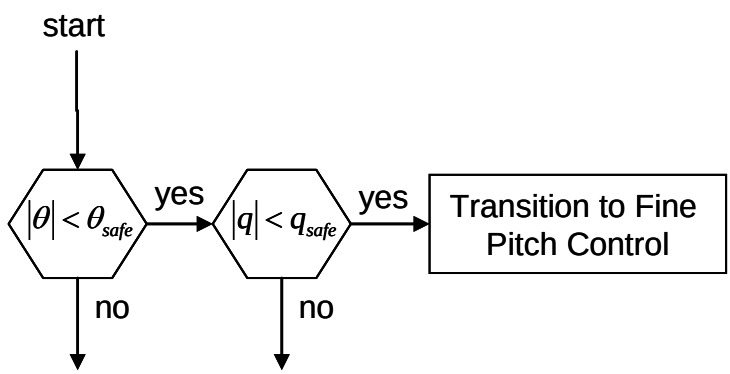

Figure 56. Logic Used to Determine Transition to Fine Pitch Control

10.3 OUTER LOOP LOGIC.

The application order of the roll and pitch control laws and the transition out of recovery mode must be managed by external logic (as shown in figure 57). The basic design premise is that the wings should be rolled level before any pitch control is applied. The roll controller runs continuously, but the pitch controller is permitted to run only when the bank angle is within a safe bound.

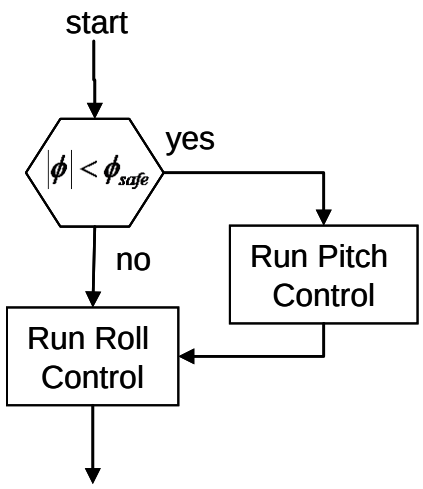

Figure 57. Logic Used to Orchestrate Roll and Pitch Control

When the aircraft is sufficiently stable in both roll and pitch, transition can be made to the nominal autopilot modes; in particular, level mode and vertical speed mode when the commanded vertical speed is zero. The bank angle, pitch angle, and pitch rate must all be within specified transition bounds to allow the transition, as shown in figure 58.

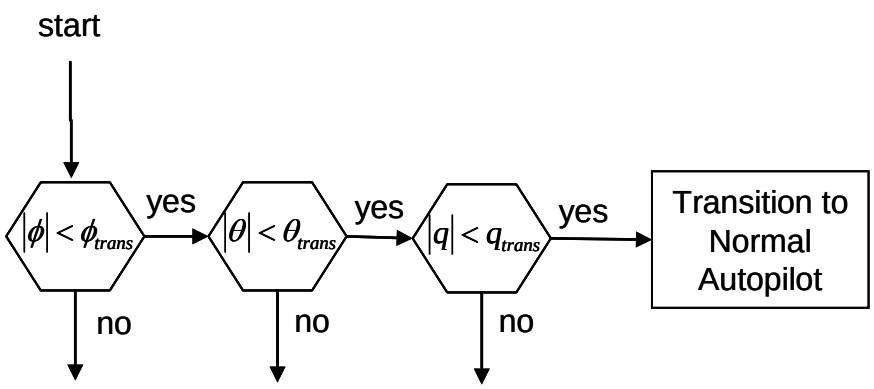

Figure 58. Logic Used to Determine Transition to Autopilot

It is essential to make sure that both roll and pitch are satisfactorily close to zero before making the transition. This was learned through an interesting failure of the original design, which transitioned to the autopilot modes individually without consideration of the state of the other axis. This could cause early and improper transition to the autopilot modes when the unusual attitude was not fully eliminated first. Often, an unusual attitude would start when the aircraft was in a high bank angle, but still in a relatively level pitch attitude.

While the aircraft was in a level pitch attitude, it was transitioning toward a very low pitch attitude. The original logic would evaluate the problem as a roll-only problem and transition to the vertical speed autopilot immediately. Once the nose inevitably dropped, the vertical speed

mode, not able to handle the high pitch change, would exceed the g-limits of the system. Once roll and pitch were coupled in the transition logic, this problem was eliminated.

11. FLIGHT TEST RESULTS.

This section presents quantitative flight test data taken for the autopilot functions, the full-time stability augmentation functions, and the envelope protection functions. Section 12 discusses the flight test results. Section 13 provides recommendations for design of envelope protection systems.

11.1 STANDARD AUTOPILOT FUNCTIONS.

The following standard autopilot functions were implemented: wing leveler, heading capture and hold, vertical speed capture and hold, and flight level change. Flight data from these functions are shown in sections 11.1.1 through 11.1.5.

In figures 59 through 63, the lefthand plots include heading, pitch, roll, and pressure altitude, plus aileron position and servo-applied torque. The righthand plots include indicated airspeed, vertical speed, AoA, and normal acceleration, plus elevator position and servo-applied torque.

11.1.1 Wing Leveler.

Figure 59 shows flight data from engagement of the wing leveler following a roll of approximately 25° to the right. For convenience, vertical speed control was also engaged to maintain zero vertical speed during this period of data collection. The wing leveler is engaged at time 14 seconds and succeeds in recovering to within nominally level flight in approximately 6 seconds. Noisy data for aileron and elevator positions prior to wing leveler engagement are due to those positions being derived from potentiometer measurements prior to engagement and encoder measurements thereafter.

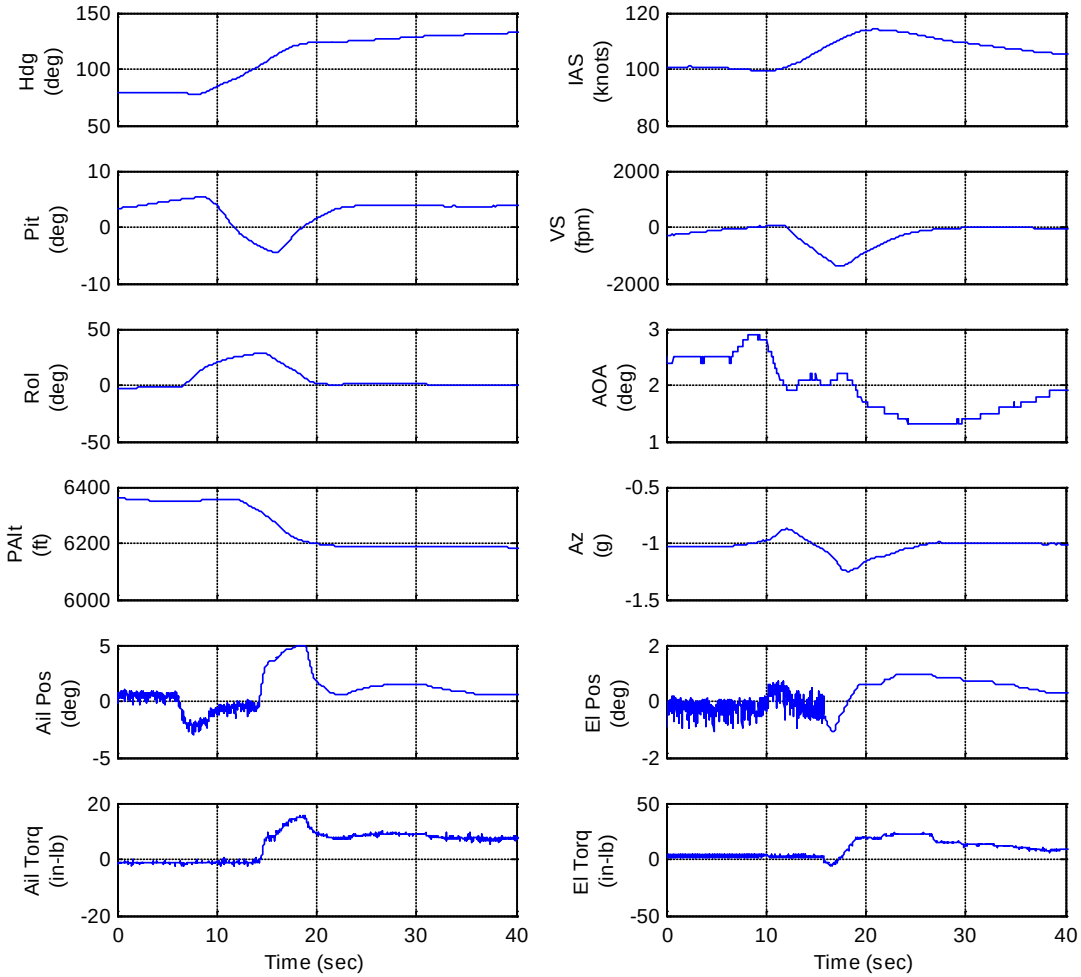

Figure 59. Wing Leveler

11.1.2 Heading Capture and Hold.

Figure 60 shows flight data from a heading capture and hold. Desired heading is shown in the upper lefthand plot as a red trace. It is adjusted from 90° to 360° (or 0°) at time approximately 10 seconds. The aircraft executes a lefthand turn and achieves a nominal northward heading within approximately 30 seconds.

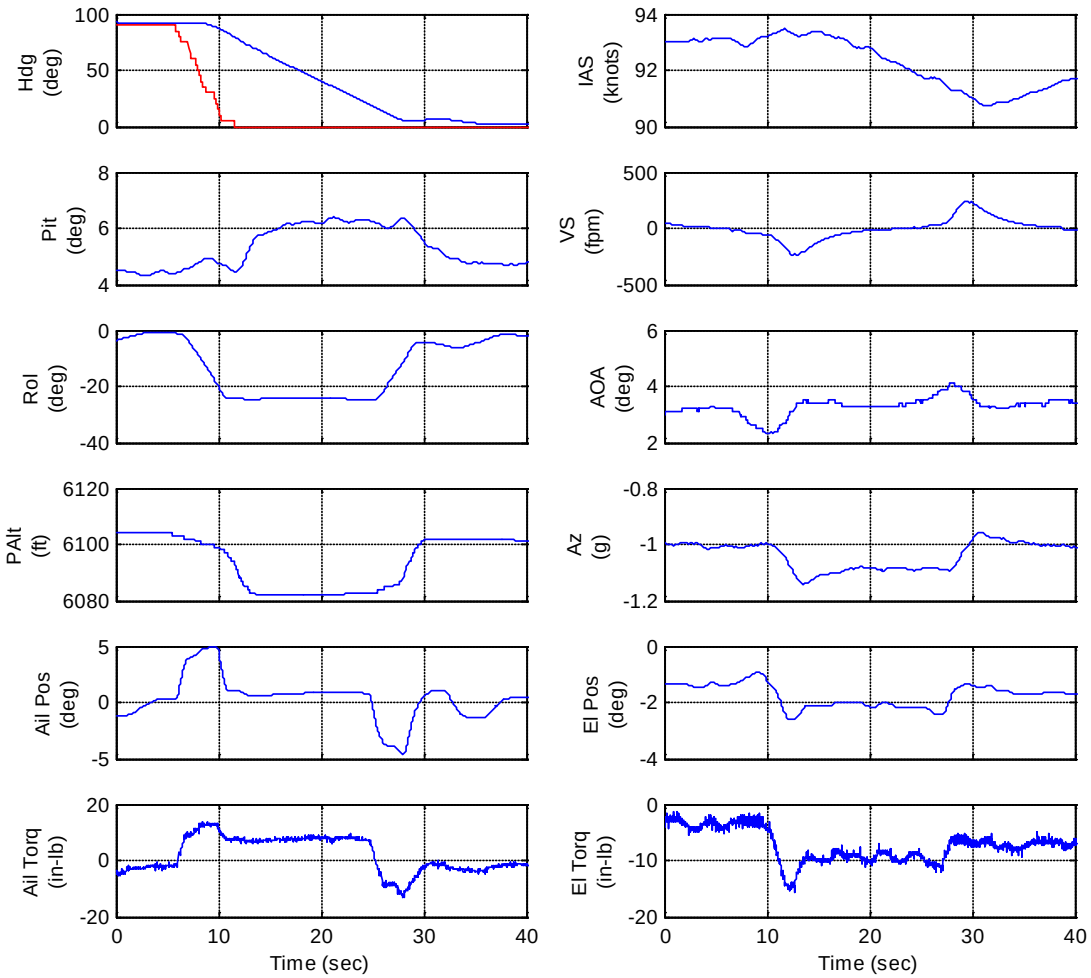

Figure 60. Heading Capture and Hold

11.1.3 Vertical Speed Hold.

Figure 61 shows flight data from a descent at a commanded vertical speed. For convenience, heading hold was engaged during data collection. The descent is initiated at approximately 10 seconds with a commanded rate of 500 fpm. The aircraft descends from 8500 ft mean sea level (MSL) to 7500 ft MSL in approximately 2 minutes. At higher airspeeds, some slow oscillation of the elevator control and resulting vertical speed are observed for undetermined reasons.

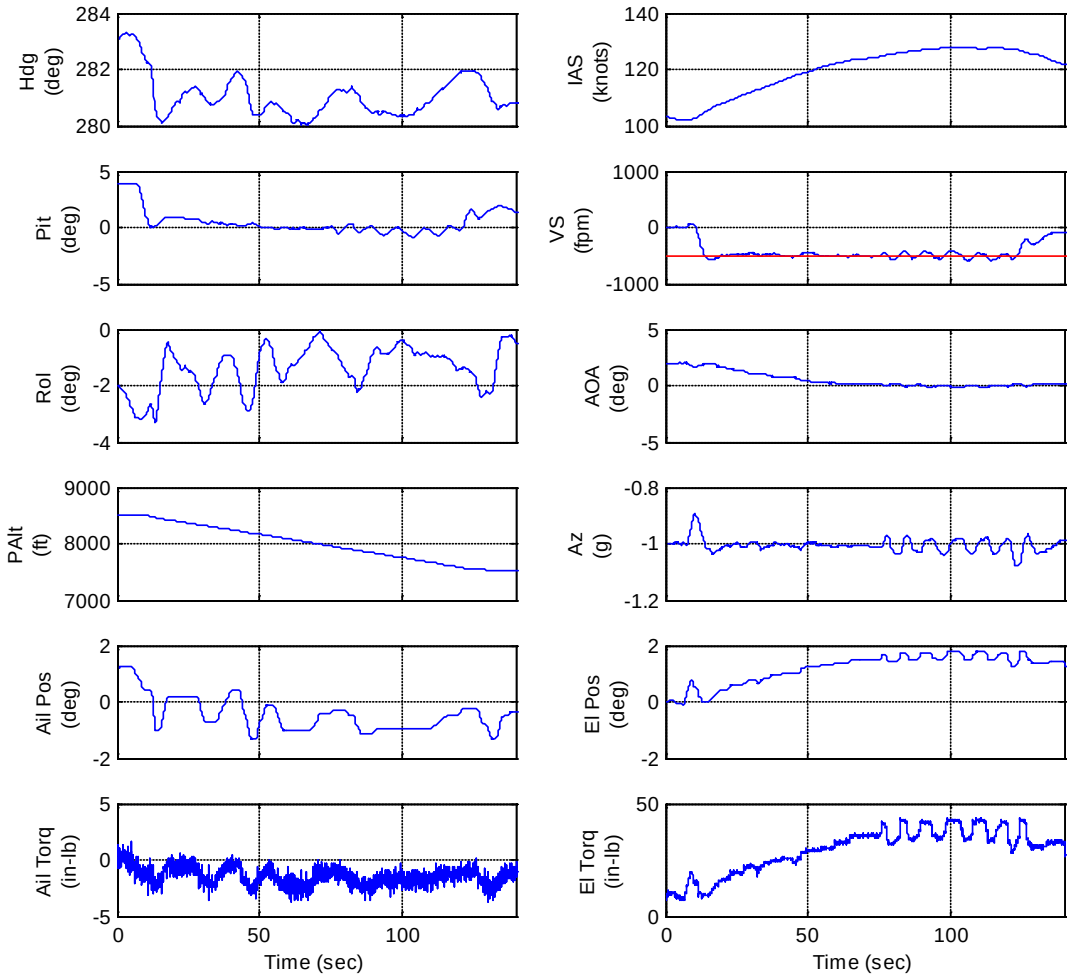

Figure 61. Descent at Commanded Vertical Speed

11.1.4 Flight Level Change.

Figure 62 shows flight data from a commanded flight level change climb (a climb at a specified constant airspeed). For convenience, heading hold was engaged during this period of data collection. The commanded airspeed is 85 knots indicated air speed (IAS), and the climb is initiated from 7500 ft MSL. Airspeed bleeds off until it reaches the commanded value of 85 knots, where it remains for the rest of the climb until the aircraft levels off at 8500 ft MSL.

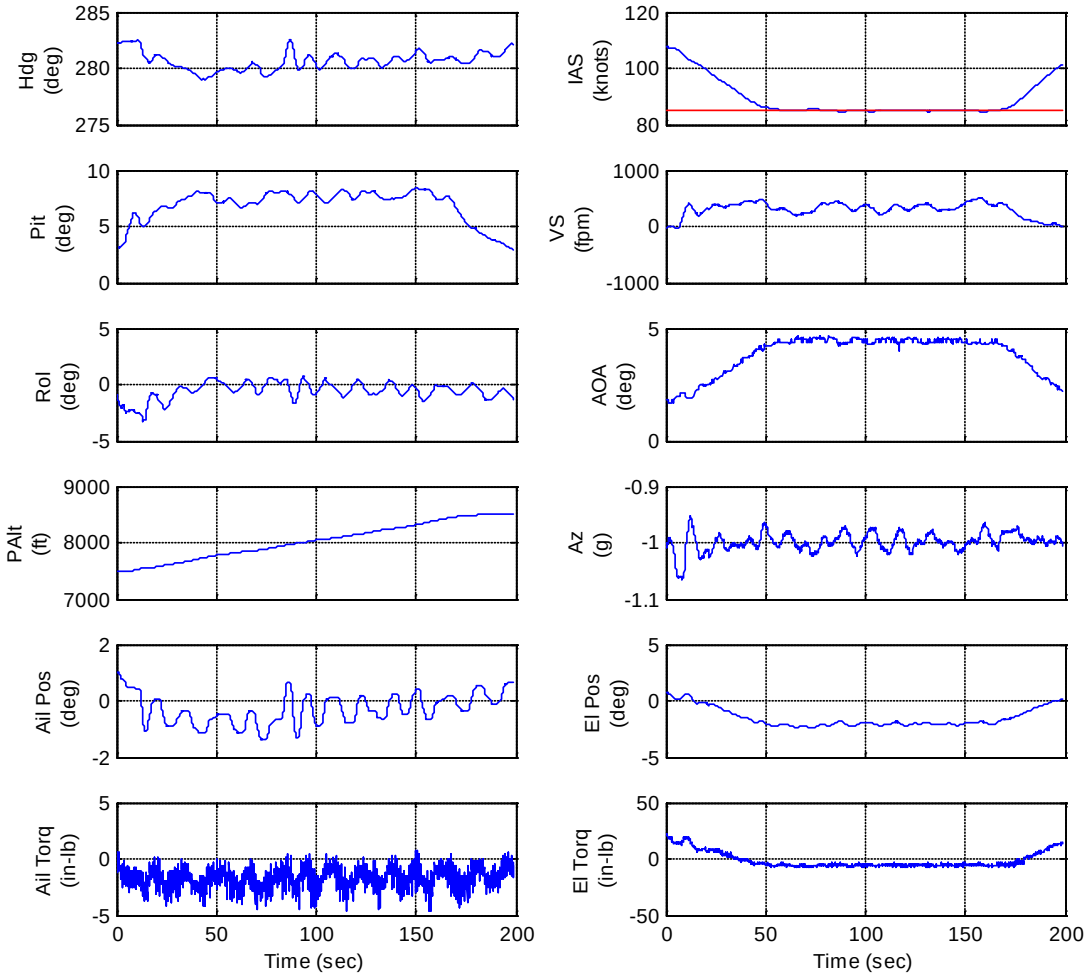

Figure 62. Flight Level Change

11.1.5 Vertical Speed Hold With Automatic Switch to FLC.

Figure 63 shows flight data from an airplane with vertical speed hold with an automatic switch to FLC.

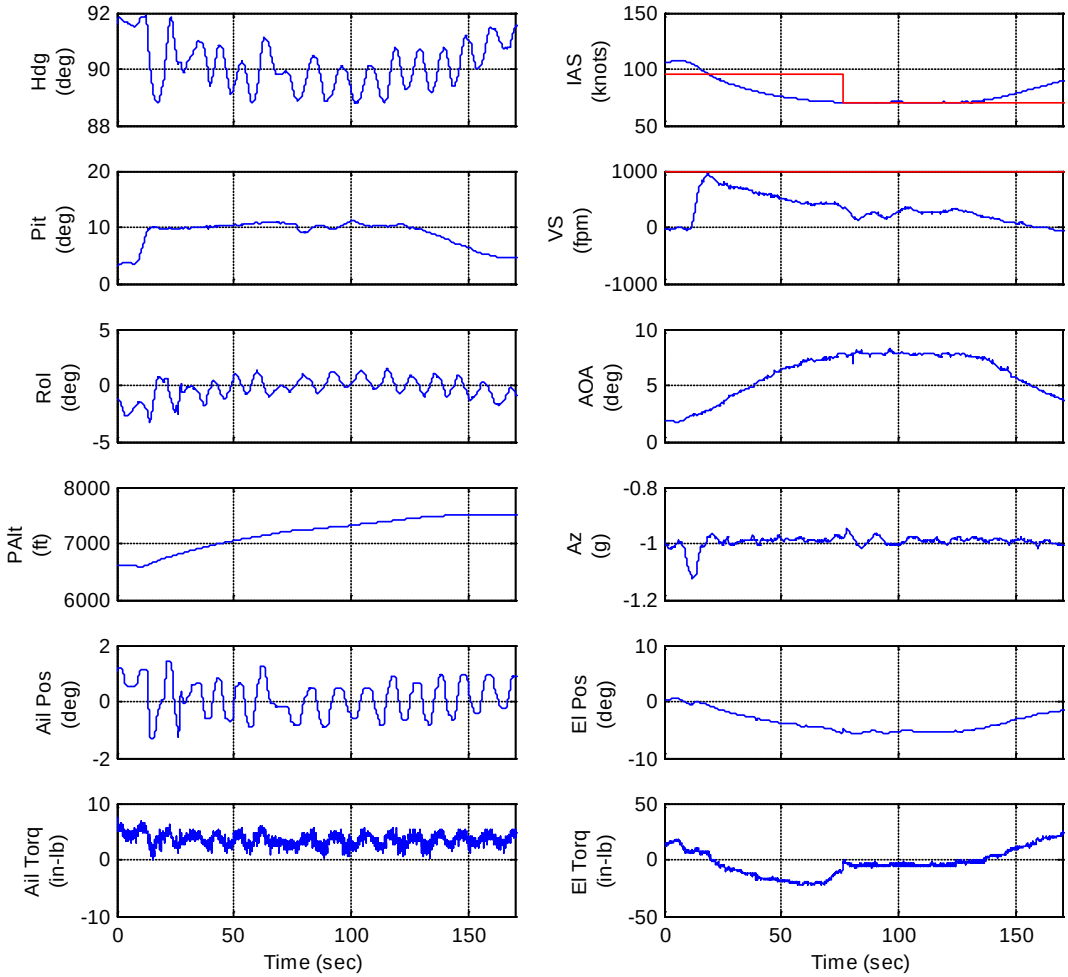

Figure 63. Vertical Speed Hold With Automatic Switch to FLC

To protect the aircraft from slowing to an unacceptably low airspeed during a climb at constant commanded vertical speed, in the event adequate power is unavailable, the autopilot automatically switches to a constant-airspeed climb if a specific airspeed is reached. In this case, the aircraft is commanded to climb at 1,000 fpm starting at time approximately 10 seconds, and the autopilot attempts to achieve this climb rate. However, inadequate power is available to sustain this climb rate, and the airspeed decays until reaching 70 knots IAS at approximately 75 seconds. At this point, the autopilot switches from vertical speed mode to FLC mode and holds the speed constant at 70 knots until the climb is concluded at the commanded new altitude of 7500 ft MSL.

11.2 STABILITY AUGMENTATION.

This section shows flight data from the unaugmented aircraft in lateral and longitudinal modes and the results of stability augmentation features implemented in the flight control system.

In figures 64 through 68, the lefthand plots include heading, pitch, roll, and pressure altitude, plus aileron position and servo-applied torque. The righthand plots include indicated airspeed, vertical speed, AoA, and normal acceleration, plus elevator position and servo-applied torque.

11.2.1 Unaugmented Spiral Mode.

Figure 64 shows flight data for the unaugmented, native airplane after being put into a 35° bank and having controls released by the pilot. The bank angle naturally steepens and exceeds 45° within 20 seconds. Meanwhile, the nose drops and a descent at vertical speed in excess of 2000 fpm rapidly develops. In this example, normal acceleration gradually builds up to approximately 1.6g. This is the unaugmented natural behavior of this certified, fixed-wing airplane in its spiral mode (and an example of the initial sequence that can lead to a typical visual flight rules (VFR)-into-IMC accident).

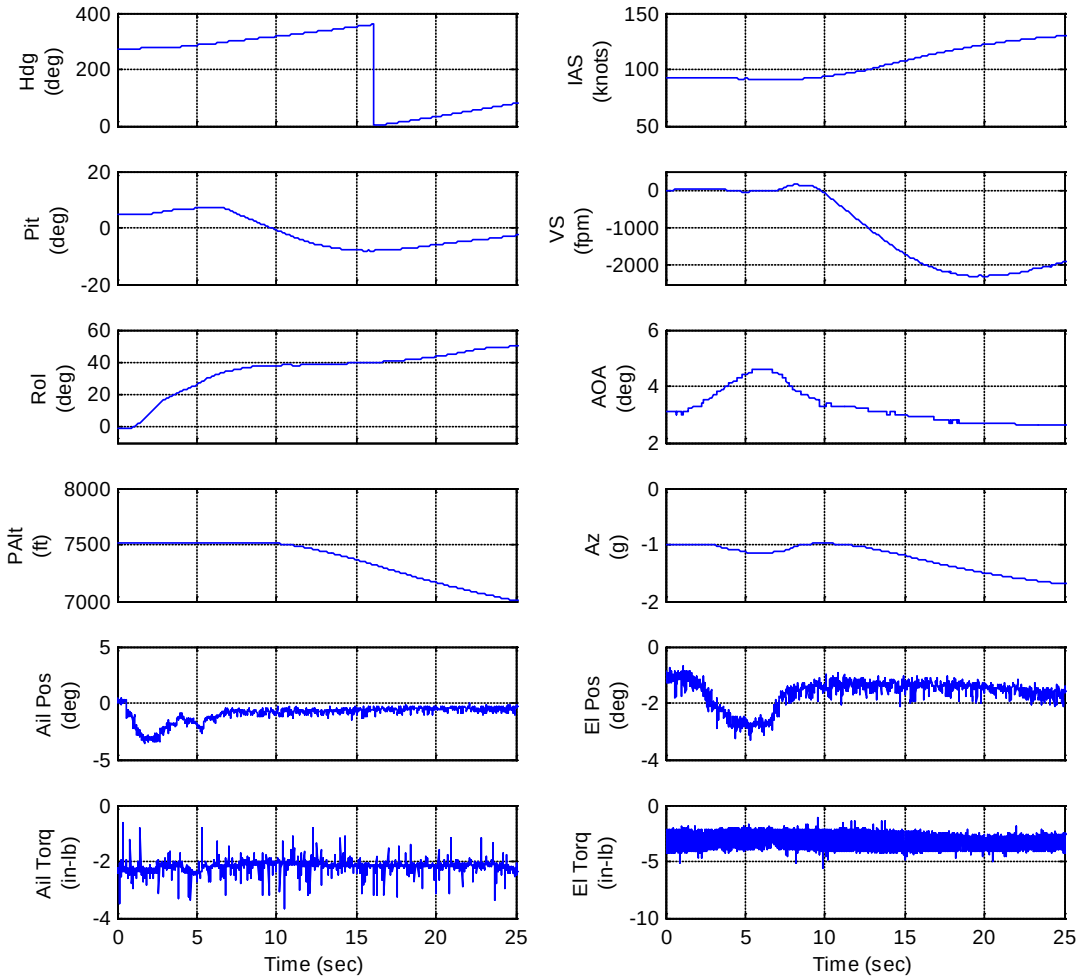

Figure 64. Unaugmented Spiral Mode

11.2.2 Lateral Stability Augmentation.

Figure 65 shows the results of a similar maneuver to that of figure 64, but with lateral stability augmentation enabled. A torque limit of 10 in.-lb is imposed on the aileron servo for lateral stability augmentation, so as not to significantly affect the manual control feel of aileron control for the pilot flying the aircraft. In this example, a bank of 45° is initiated and thereafter the pilot releases the controls. In this example, rather than the bank angle continuing to increase as in the unaugmented case, the lateral stability augmentation system returns the bank angle to near level over the ensuing 15 to 20 seconds.

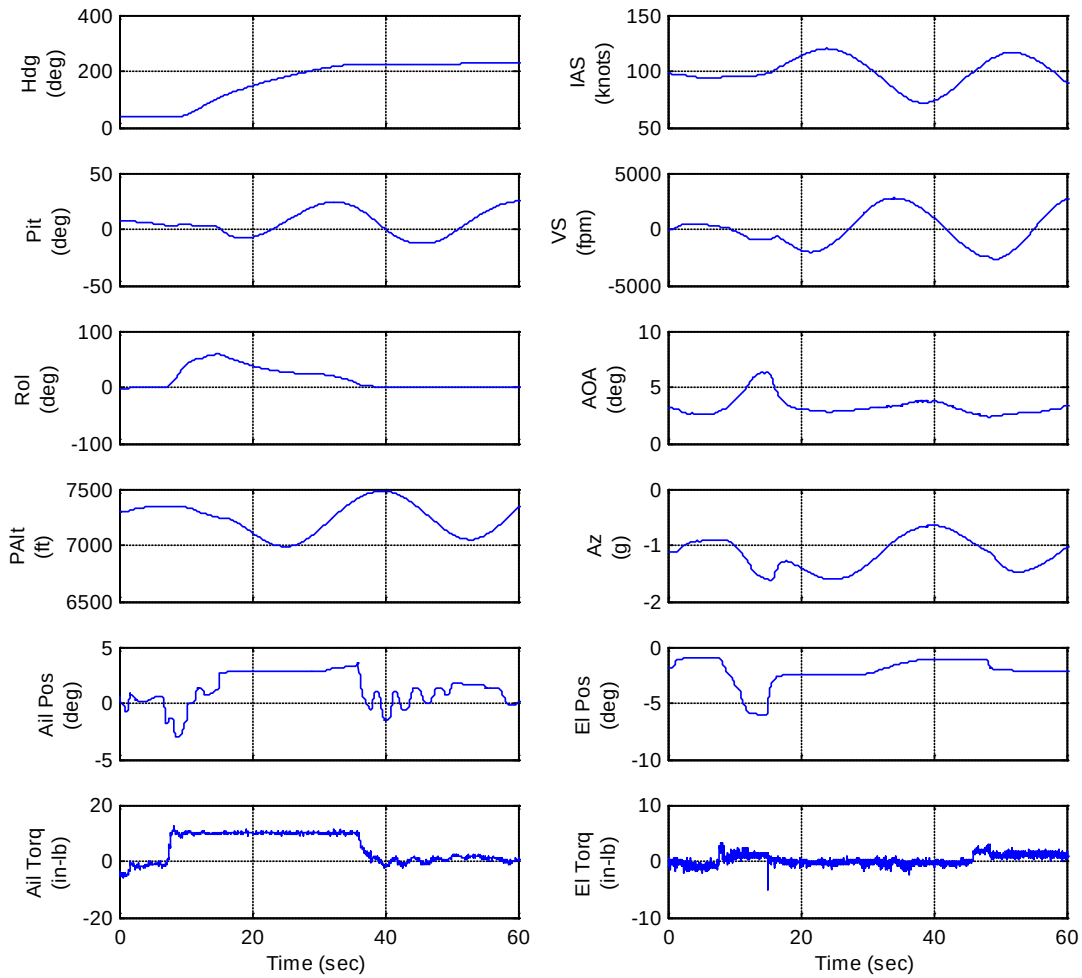

Figure 65. Spiral Entry With Lateral Stability Augmentation On

In this example, a significant vertical speed has developed by the time wings are brought back to level and a robust phugoid mode is exhibited by the aircraft with vertical speeds in excess of ±2000 fpm, both positive and negative. However, the maximum altitude loss from the beginning of the initial bank maneuver is only 300 ft, in contrast to the rapid spiral descent in the augmented case. It is important to note that the phugoid dynamics exhibited would easily terminate with normal pilot inputs on the controls, unlike this hands-off demonstration; thus, there is great potential value in lateral stability augmentation alone.

11.2.3 Unaugmented Phugoid Mode.

Figure 66 shows the natural longitudinal dynamics of the unaugmented aircraft. The aircraft is briskly pitched up at the beginning of the sequence to a pitch angle of 23° and a vertical speed of 2300 fpm, and then the yoke is released. Slight rudder pressure is used as needed to avoid excessive heading change during the ensuing longitudinal motions. As shown in the figure, the natural phugoid mode of the aircraft continues with very little damping. The cycle period is approximately 26 seconds.

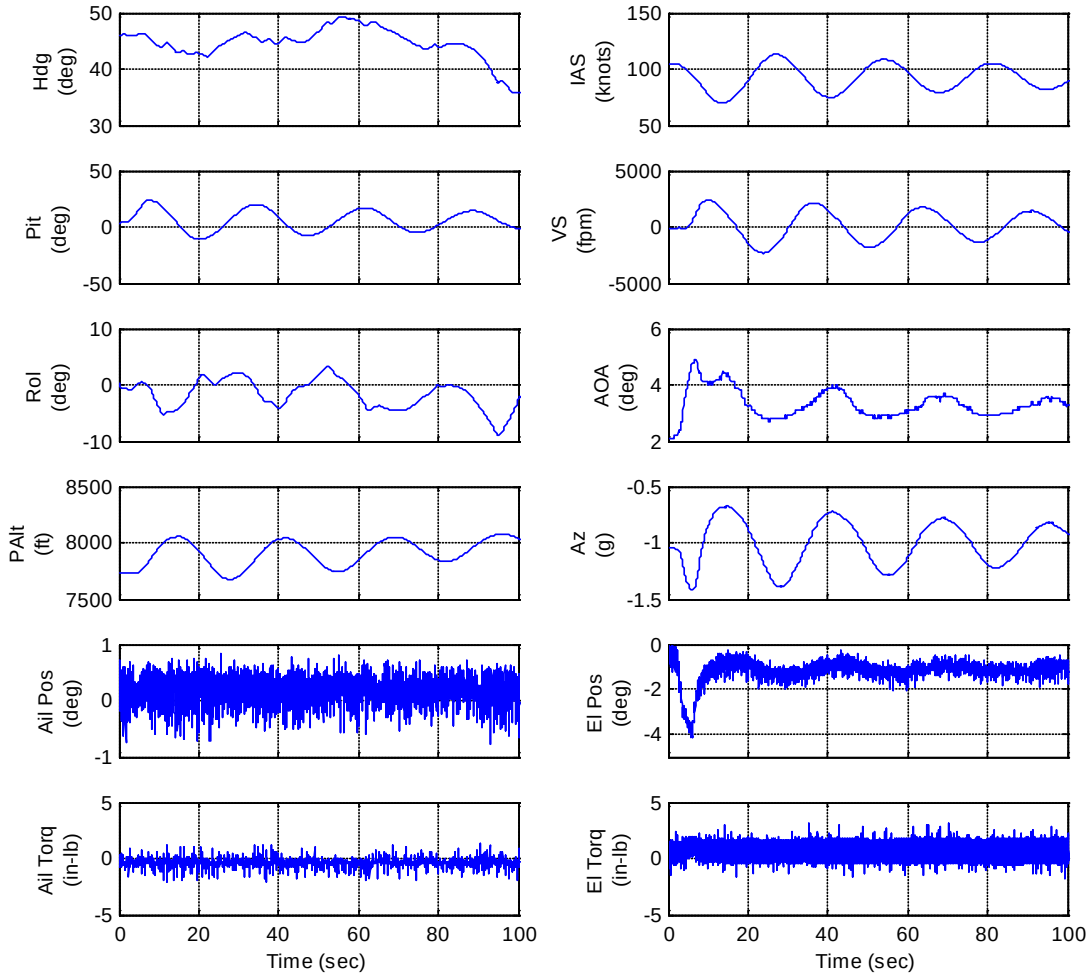

Figure 66. Unaugmented Phugoid Mode

11.2.4 Longitudinal Stability Augmentation.

Figure 67 shows the longitudinal dynamics of the aircraft with longitudinal stability augmentation on. The aircraft is pitched up to a pitch angle slightly more than 10° and approximately 1000 fpm climb rate, then the yoke is released. The stability augmentation algorithms substantially damp the ensuing phugoid motion, which is nearly eliminated within the single cycle shown in these data.

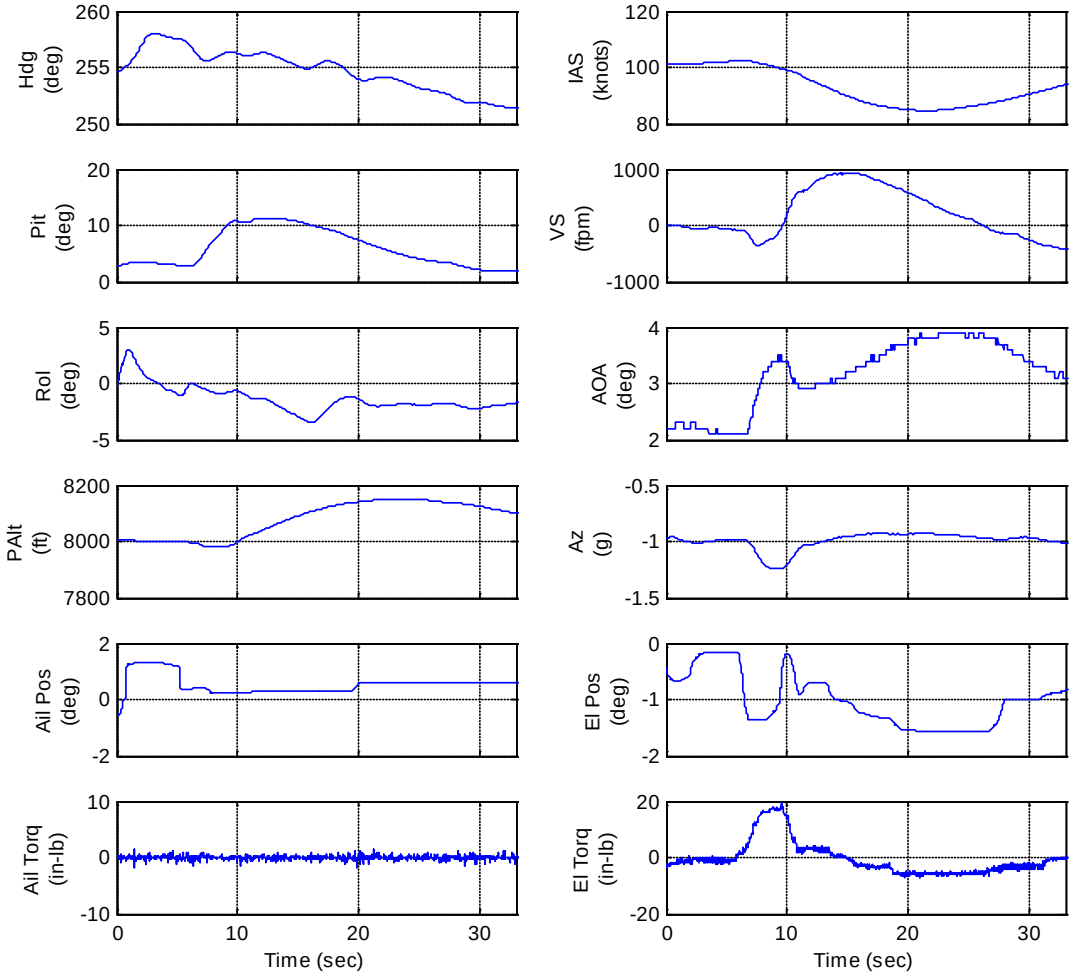

Figure 67. Pitch Up Maneuver With Longitudinal Stability Augmentation

11.2.5 Combined Lateral and Longitudinal Stability Augmentation.

Figure 68 shows the results of a similar maneuver to that of figure 65 (spiral mode entry), but with both lateral and longitudinal stability augmentation enabled. A bank of slightly greater than 35° is initiated and thereafter the pilot releases the controls. In this case, the bank angle recovers to near zero in approximately 10 seconds, and the altitude excursion is limited to less than 100 ft with the phugoid mode well-damped by the presence of the longitudinal stability augmentation.

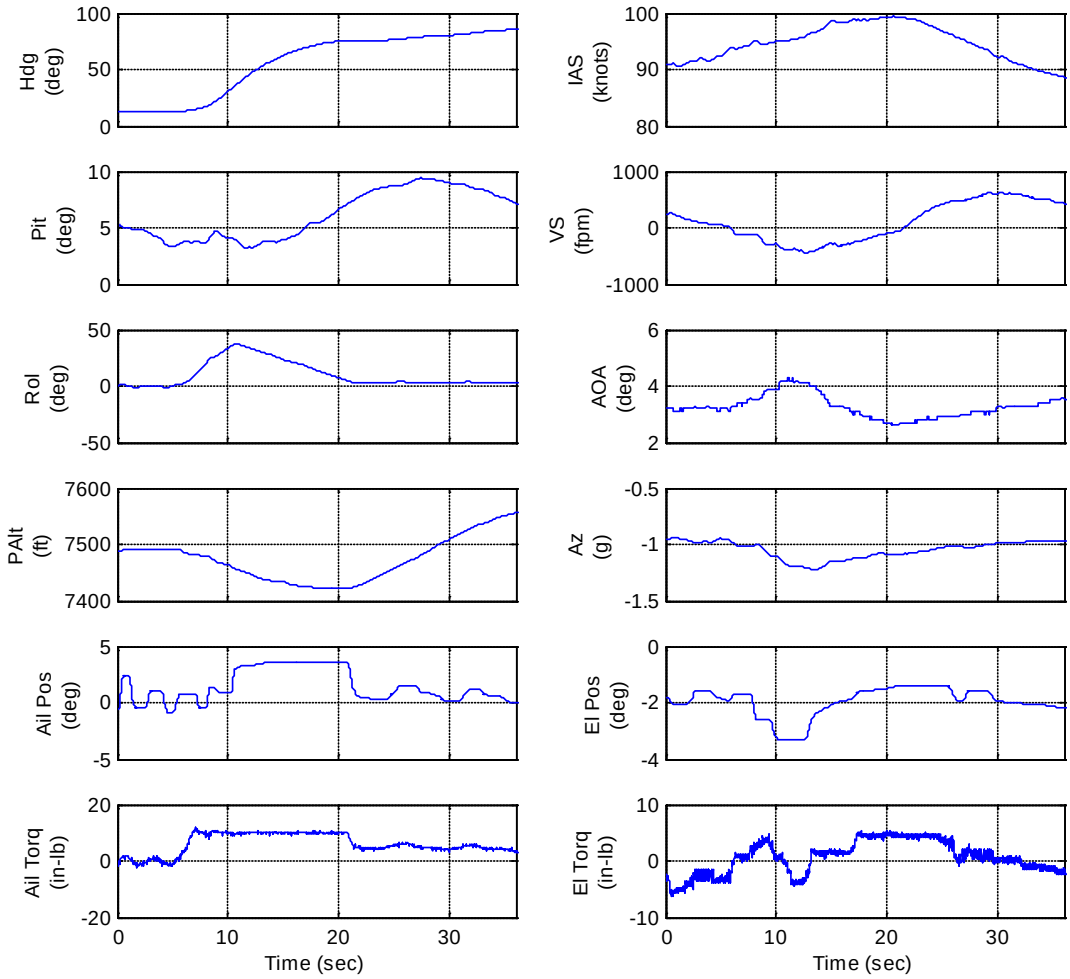

Figure 68. Spiral Entry With Lateral and Longitudinal Stability Augmentation On

The presence of both lateral and longitudinal stability augmentation in this cable-controlled aircraft, with the back-drivable servos limited to 10 in.-lb, did not significantly alter the control feel of the manual controls for the pilot manipulating the yoke. Yet, the aircraft exhibited a natural tendency to return to straight and level flight if the controls were released, unlike the unaugmented aircraft. The conclusion from the pilot's flight was that this type of stability augmentation was both unobtrusive and potentially quite valuable to reduce the risk of LOC accidents due to an inexperienced pilot flying into conditions in which a visual horizon is not available.

11.3 ENVELOPE PROTECTION.

This section shows flight data from the aircraft with automatic envelope protection features enabled. In the cases shown, stability augmentation is also enabled, but, in practice, its limited effects make very little difference to performance during periods when the much more powerful envelope protection algorithms engage.

In figures 69 through 73, the lefthand plots in the figures show heading, pitch, roll, and pressure altitude, plus aileron position and servo-applied torque. The righthand plots show indicated airspeed, vertical speed, AoA, and normal acceleration, plus elevator position and servo-applied torque.

11.3.1 Overbank.

Figure 69 shows flight data from a series of roll maneuvers with envelope protection enabled. (Both lateral and longitudinal stability augmentation are also enabled.) The pilot rolls the aircraft to the right, then to the left, and repeats the sequence, achieving bank angles of approximately 60° in both directions. However, after a bank angle of 40° is exceeded, the envelope protection system issues visual and auditory warnings of the overbanked condition and provides substantial torque on the yoke counter to the existing roll.

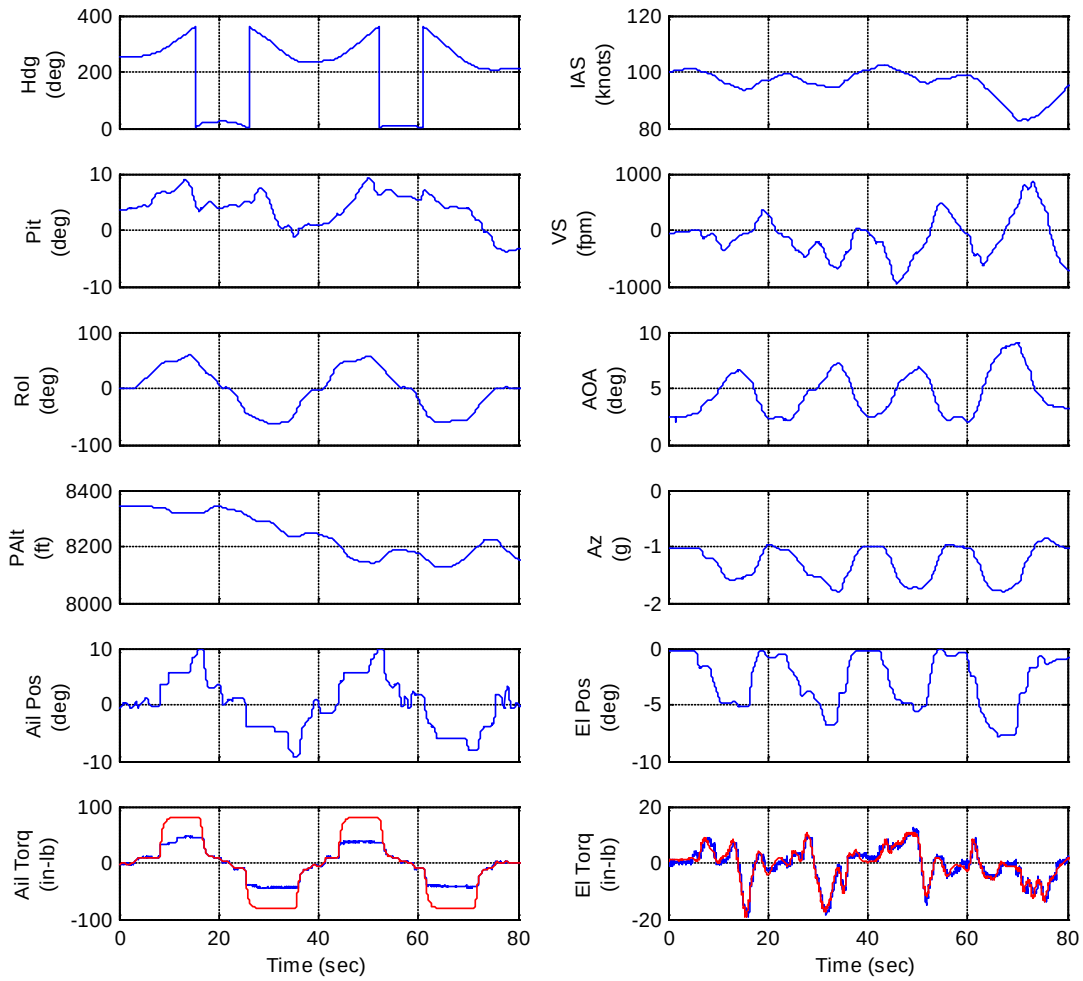

Figure 69. Overbank With Envelope Protection On

The proportional gain and servo-torque limit were chosen in this case to provide a distinctive tactile alert of the overbanked condition to the pilot. The lower-left plot shows that the envelope protection algorithms were commanding a roll torque of 80 in.-lb (red trace), but because of a number of lower-level constraints in the system, the roll torque actually delivered was slightly less than 50 in.-lb (blue trace). Nevertheless, rolling far past 40° to 45° of bank required substantially more effort on the part of the pilot than without the envelope protection system engaged. In practice, the envelope protection system provided a wall of rapidly increasing stiffness that was difficult to push past, and when the pilot relaxed pressure on the yoke, the aircraft rapidly returned to a bank angle of less than 40°.

The envelope protection system, together with torque counter to the overbanked condition, issued visual annunciations (on the PFD as shown in figure 70) and auditory annunciation ("Overbank – Roll Left" or "Overbank – Roll Right" via the intercom system), announcing the overbanked condition. Once bank angle recovered to less than 38°, the overbank protection algorithm turned itself off with an annunciation of "Recovery Complete." Servo command shaping was used to provide a soft taper of applied torque during turnoff to avoid a tactile bump through the yoke.

Overbank protection was quite effective in creating what amounted to a soft wall in roll, beyond which it was quite difficult to push the airplane. After recovering to an angle of bank within the prescribed limit, the presence of lateral stability augmentation gently and gradually recovered the aircraft to straight and level flight with no further inputs from the pilot. If stability augmentation was turned off, the airplane was left at the boundary of the envelope protection overbank engagement in the absence of further pilot control input.

Figure 70. The PFD Annunciation of a Right-Hand Overbank Condition (simultaneous auditory annunciation through intercom is “Overbank – Roll Left”)

11.3.2 Stall.

Figure 71 shows incipient stalls with envelope protection on. The pilot pulls the aircraft into a nose-high attitude and AoA increases as airspeed bleeds off. At time approximately 21 seconds, AoA reaches 15°, and the stall envelope protection algorithm engages with visual and auditory annunciations, imparting a strong, positive elevator torque of approximately 60 in.-lb to push the nose of the aircraft down, thereby decreasing AoA. In this example, the pilot persists in imparting up elevator pressure, and several seconds after the first stall protection sequence completes, a second similar sequence occurs at time approximately 27 seconds.

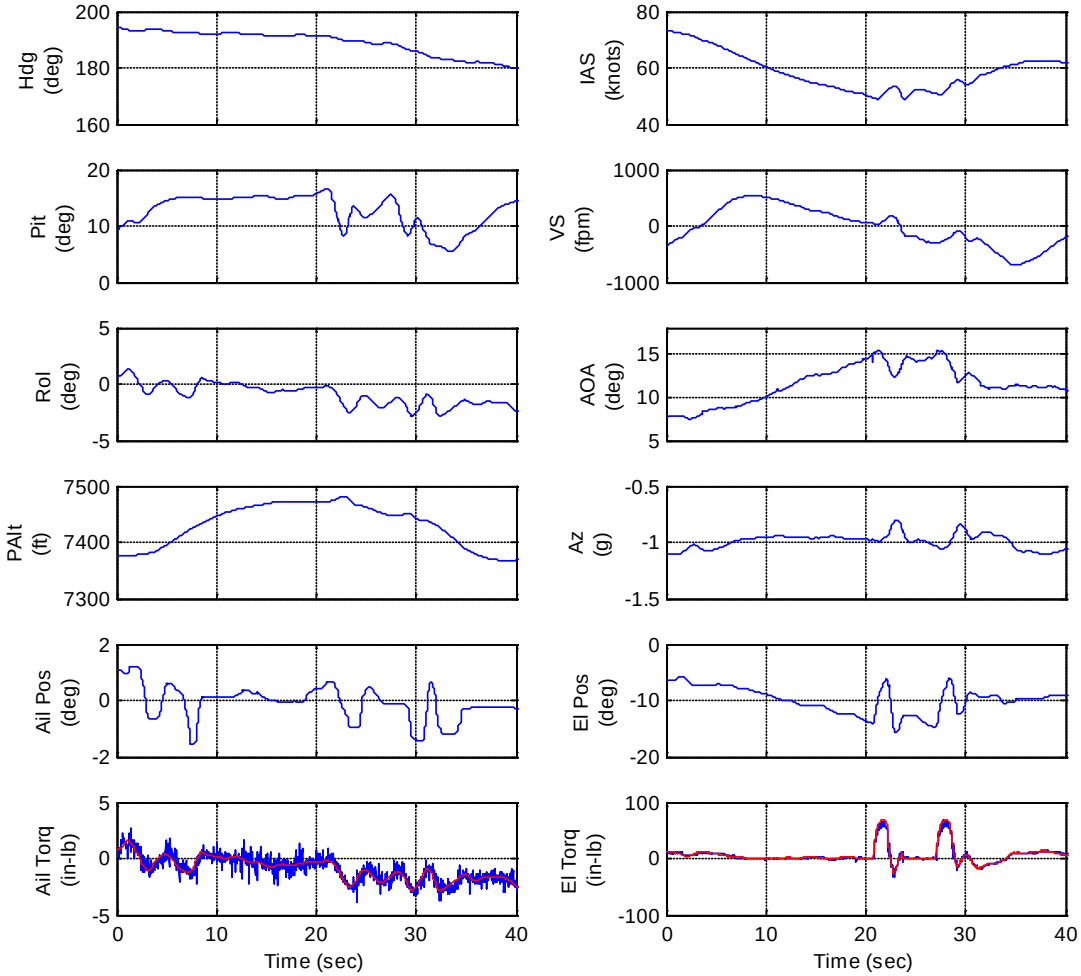

Figure 71. Incipient Stalls With Envelope Protection On

During the engagement of stall envelope protection algorithms, visual and auditory annunciations ("Stall—Pitch Down") as shown in figure 72, were given, the yoke buzzers were turned on, and the elevator servo exerted forward-elevator torque with a limit of 60 in.-lb. of torque. The servo-actuation of the elevator made it extremely difficult to pull the aircraft further into a full stall without considerable, deliberate, and forceful effort on the part of the pilot. Of note, this was true for both low-airspeed wings-level stalls and high-airspeed accelerated stalls with significant bank angles. After the AoA decreased to less than 14°, the envelope-protection algorithm switched off and a "Recovery Complete" annunciation was given.

The tactile sensation of the yoke buzzers was so attention-getting that it was almost impossible to ignore the incipient stall condition, even without reference to the visual warning or the auditory annunciation. This is a critically important attribute of a stall warning system because many inadvertent stalls occur during flight conditions with multiple distracters. A pilot is unlikely to notice visual annunciations at all and could well ignore verbal annunciations during such circumstances; however, tactile warning through the yoke via a high-frequency yoke buzzer, was impossible to ignore. The natural tendency was to relax one's grip on the vibrating yoke, which

is helpful in allowing the AoA to decrease to a safer value. If properly associated with impending stall through pilot training, it is believed that it would become an essential safety feature to prevent inadvertent stalls and could lead to substantial diminution of LOC accidents.

Figure 72. The PFD Annunciation of Incipient Stall (simultaneous auditory annunciation is "Stall—Pitch Down." Note the stall margin indicator is touching the top of the aircraft chevron, indicating AoA equal to critical angle of attack)

11.3.3 Overpitch.

Figure 73 shows a pair of overpitch maneuvers. The pilot pitches the aircraft up manually, and when pitch crosses a threshold of 18°, the envelope protection system issues visual and auditory warnings of overpitch (similar to those shown for stall), and the pitch servo applies torque in a direction that pitches the aircraft back down toward level flight. In this case, the torque applied by the system approaches approximately 80 in.-lb, creating a substantial, but not impenetrable barrier, to further pitch increases by the pilot. Once the pilot begins to relax pressure on the yoke, the aircraft pitches back over toward a level flight attitude. After the pitch recovers to less than 16°, the envelope protection algorithm switches off and warnings cease. A final annunciation of Recovery Complete is issued.

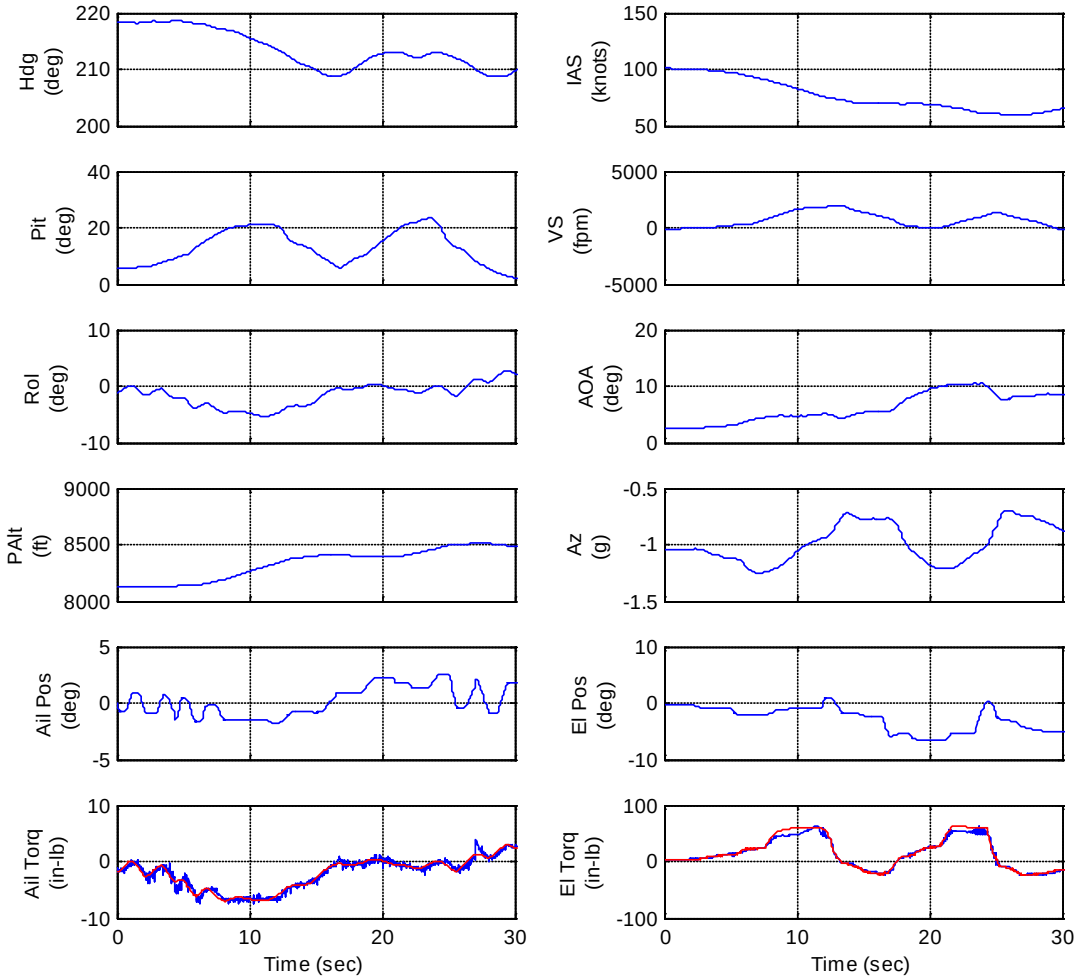

Figure 73. Overpitch With Envelope Protection On

Overpitch protection is also available for negative pitch (data not shown). The threshold in the negative case was set for this particular aircraft at -7°, a limit that was not found to engage during normal flight operations.

During flight tests, the yoke buzzers were enabled to come on during overpitch envelope protection, but this was felt to be unnecessary for these functions. It was judged to be more appropriate to reserve yoke buzzer activation for a single function—that of incipient stall warning.

11.3.4 Overspeed.

Figure 74 shows a combined negative overpitch and overspeed maneuver. The pilot pitches the aircraft down and overpitch envelope protection engages at time approximately 4 seconds as the pitch exceeds -7°. Shortly after, as the aircraft indicated airspeed exceeds 120 knots (very conservatively set for the purpose of these flight tests), overspeed protection engages. In both cases, visual and auditory warnings are issued and torque on the elevator is applied to pull the

aircraft nose upward, reaching a maximum of about 40 in.-lb. As the pilot releases forward pressure on the yoke, the aircraft recovers to level flight. As the envelope protection algorithms switch off, a final annunciation of Recovery Complete is issued. Longitudinal stability augmentation is on in this case, causing a forward elevator torque to be commanded after envelope protection algorithms have switched off, to damp out the ensuing phugoid oscillation.

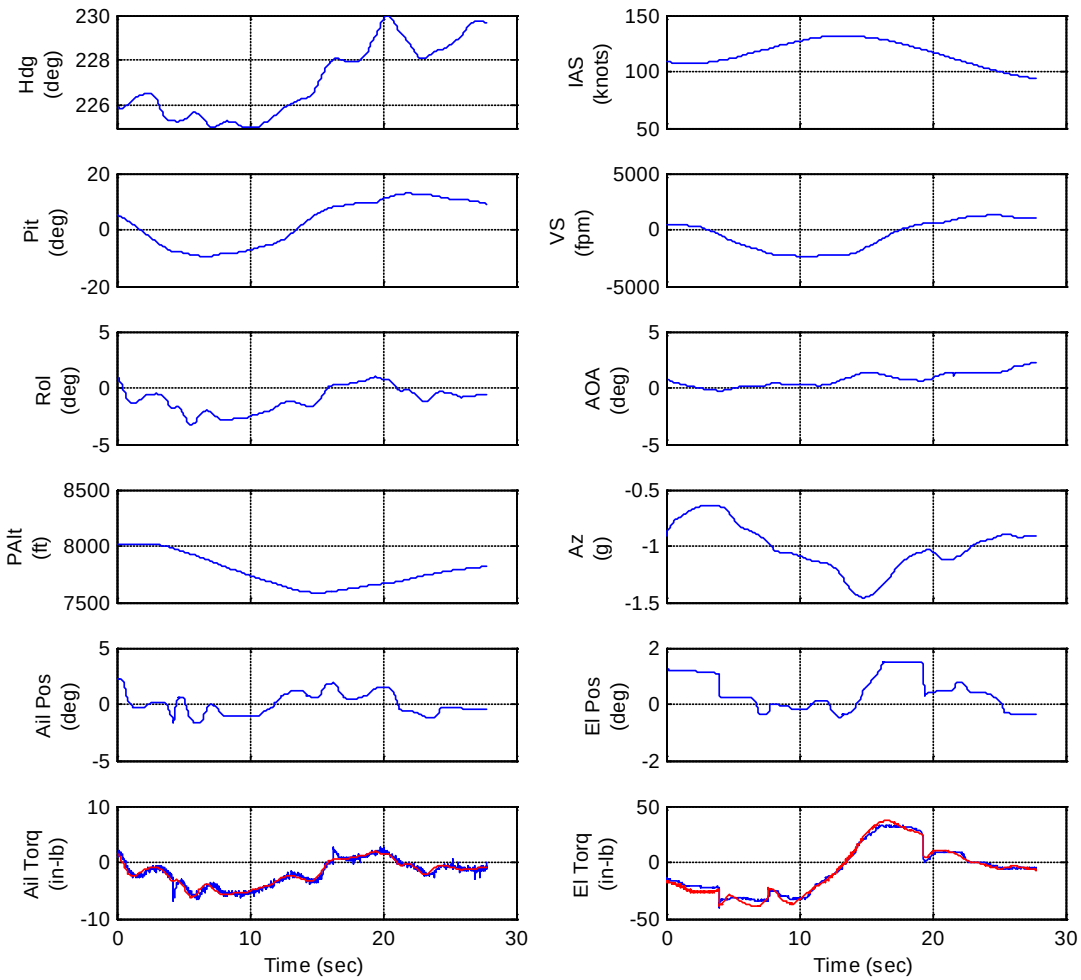

Figure 74. Overspeed With Envelope Protection On

11.4 UNUSUAL ATTITUDE RECOVERY.

In addition to stability augmentation and envelope protection functions, which are always on and automatic, a manually selected unusual attitude recovery function was implemented. This required the pilot to manually engage the recovery sequence by pushing a designated button on the touchscreen mode control panel.

11.4.1 Unusual Attitude Recovery.

An example of a manually-selected unusual attitude recovery sequence is shown in figure 75. The pilot deliberately banks the aircraft to 60°, allowing the nose to fall through, and manually

selects unusual attitude recovery as the pitch attitude passes through -10° at time = 10 seconds. The unusual attitude recovery algorithm first rolls the aircraft level between time = 10 to 15 seconds, then initiates a pullup to achieve nominally level flight by approximately time = 19 seconds. After straight and level flight conditions are reached, the unusual attitude recovery hands off control to the autopilot in wings level/vertical speed zero mode.

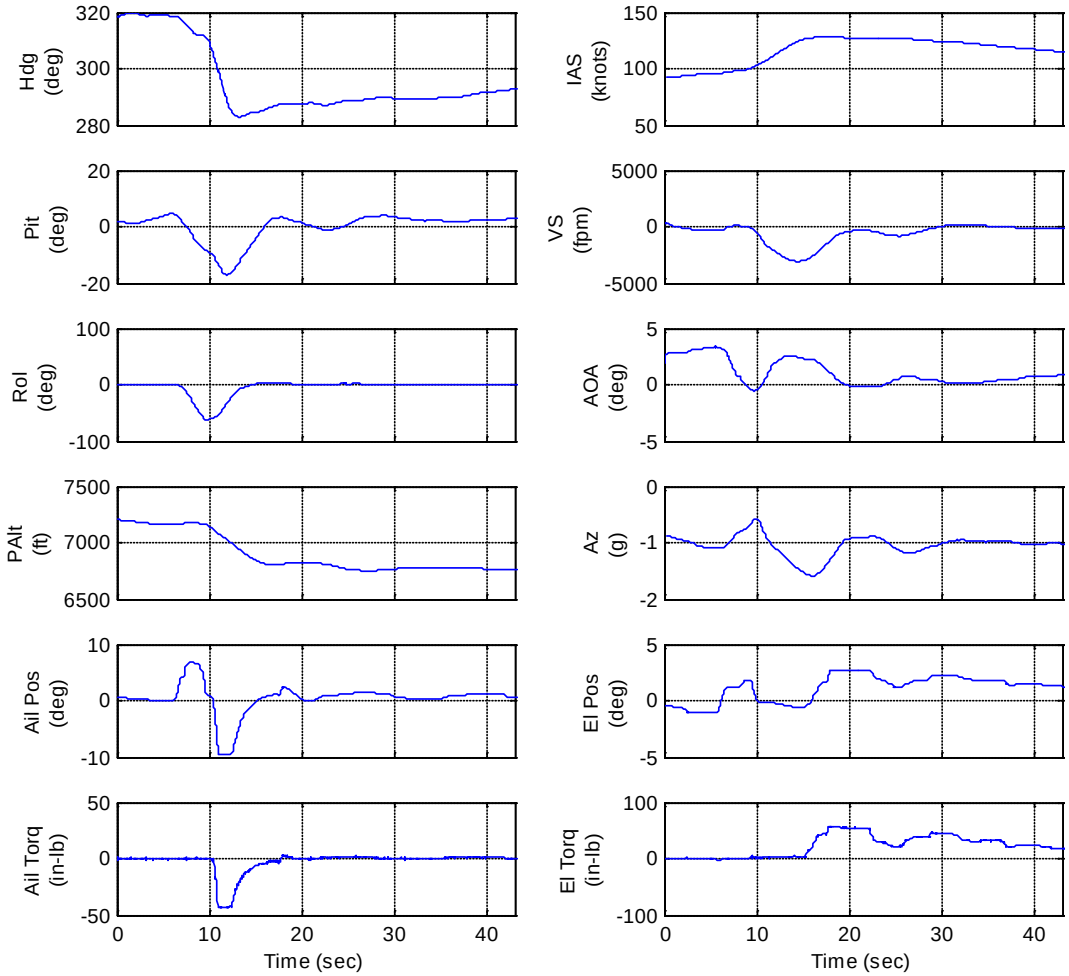

Figure 75. Unusual Attitude Recovery

During the unusual attitude recovery sequence, visual and auditory explanations of what the controller is doing are issued (e.g., rolling left followed by pitching up). At the conclusion of the sequence when straight and level flight has been accomplished, a visual and auditory annunciation of Recovery Complete is issued.

It is important to note that even in this significant unusual attitude case, maximum altitude loss following engagement of the unusual attitude recovery sequence is only approximately 400 ft. Also, the maximum g-load exerted on the airframe in this case is merely 1.6g. All of the longitudinal control modes, including unusual attitude recovery, have g-limiting built in. For the purposes of these flight tests, the limit was set to 2g.

12. DISCUSSION.

This section provides a discussion of the stability augmentation and envelope protection features implemented during this research.

12.1 UTILITY AND RELATIVE IMPORTANCE OF FEATURES.

The two major categories of LOC accidents are dominated by two phenomena: stall and excessive bank. Stall is the initial cause of LOC in a number of common scenarios, including low-and-slow stall-spin accidents at pattern altitude, departure stalls, and accelerated stalls during aggressive maneuvering. Excessive bank leads to LOC accidents associated with continued VFR-into-IMC accidents by pilots not qualified to fly by reference to instruments. Associated with these accidents is pilot disorientation, either prior to, during, or following the excessive banked condition and resulting spiraling dive.

Accordingly, it was found that among all the capabilities implemented in the experimental system, two in particular stood out as extremely valuable: stall protection and overbank protection.

12.2 STALL PROTECTION.

Stall protection, as implemented in the experimental test aircraft, included visual and auditory warnings based on measured aircraft AoA. The final version of the system also included vibratory tactile warning of impending stall in the form of a yoke buzzer. A combination of all of these warnings was particularly effective in gaining pilot attention, providing stall situational awareness to the pilot, and encouraging corrective action in a timely manner. In addition to the warnings, a stall margin display on the PFD was found to be generally useful for continuous pilot awareness of AoA status (see figure 22).

Stall envelope protection also included deliberate forward pressure on the yoke, provided by the envelope protection servos. Because the yoke forces were already so high close to stall in this particular aircraft, the additional force provided by the envelope protection system was not perceived by the pilot as a warning. Instead, rather than alerting the pilot to the impending stall condition, the additional forward pressure functioned to make it much more difficult for the pilot to pull all the way through to an actual stall.

The combination of the visual, auditory, and tactile alerts with the forward pressure on the yoke made it impossible to stall the airplane without a very deliberate, forceful, and decisive action on the part of the pilot. As a consequence, it is anticipated that such a system would virtually eliminate inadvertent stalls and the accidents that result from them.

In particular, the tactile sensation of the yoke buzzers was so attention-getting that it would have been almost impossible to ignore the incipient stall condition, even without reference to the visual warning or the auditory annunciation. This is a critically important attribute of a stall warning system because many inadvertent stalls occur during flight conditions with multiple distracters, and a pilot is unlikely to notice visual annunciations and could ignore verbal

annunciations during such circumstances. However, tactile warning through the yoke via a high-frequency yoke buzzer was impossible to ignore. If properly associated with impending stall through pilot training, it is believed that it would become an essential safety feature to prevent inadvertent stalls and could lead to substantial diminution of LOC accidents.

Although not tested, even an AoA awareness and stall warning system including only some subset of the visual, auditory, and tactile warnings was determined to be potentially advantageous. Such an information and warning system would not need to include autopilot servo functions and, while not providing forward yoke pressure during an incipient stall, would still serve to alert the pilot sufficiently to make an inadvertent stall highly unlikely.

12.3 ROLL STABILITY AUGMENTATION/OVERBANK PROTECTION.

The natural dynamics of fixed-wing aircraft include the spiral mode, in which an aircraft placed at a moderate angle of bank with no further control inputs diverges toward greater bank angles and a significant spiral dive develops. This has been the cause of innumerable VFR-into-IMC accidents in which a non-instrument-rated pilot lost outside visual reference and was unable to keep the aircraft wings level. A simple modification of the aircraft dynamic characteristics to eliminate spiral instability would likely eliminate such accidents.

Accordingly, roll stability augmentation (as implemented in this research, mechanized in such a way that it is always on and does not adversely affect the manual control feel of the aircraft), was determined to be of extraordinary value. The aircraft could be manually controlled with ease, with very little change to its natural characteristics, because of the deliberate low torque limits placed on the control system for stability augmentation and the back-drivable nature of the servos. However, once the pilot released pressure on the controls, regardless of the angle of bank, the aircraft had a natural tendency to return to straight and level flight on its own. The contrast between the natural unaugmented airplane, which would diverge into a spiral dive with descent rates greater than 2,000 fpm in ten seconds or less, and the augmented airplane, which would return to a sedate straight-and-level flight condition after being released, was striking.

Alone, the roll stability augmentation system is of great value and its implementation in the fleet should be encouraged.

The addition of overbank envelope protection, wherein visual and auditory warnings are displayed past a certain bank angle and servo action to lessen the bank of the airplane occurs, is also of value. In this case, because of lighter roll control forces in the unaugmented airplane, the resulting control forces exerted by the servo on the yoke are quite apparent to the pilot when the envelope protection bank-angle limit is exceeded.

Both roll stability augmentation alone and roll stability augmentation in combination with roll envelope protection are valuable additions that would stand to enhance the safety of the fleet. It is likely that VFR-into-IMC accidents, in particular, would be greatly reduced by such additions.

12.4 OTHER FEATURES.

In addition to those mentioned in section 12.3, the other stability augmentation and envelope protection features implemented were longitudinal stability augmentation (to dampen the phugoid mode), overpitch protection, and overspeed protection. These features were somewhat useful for particular situations, but overall were of limited practical value in comparison to the extremely valuable stall protection and lateral stability augmentation/overbank protection features. It may be convenient to implement these additional features in particular systems, but their presence or absence is not considered to be of great importance in the vast majority of typical flight scenarios that lead to LOC.

13. RECOMMENDATIONS REGARDING FUTURE DESIGNS AND CERTIFICATION STANDARDS.

13.1 KEY FUNCTIONAL CAPABILITIES.

Dominant causes of LOC accidents in GA are aerodynamic stall and loss of lateral control due to pilot disorientation in the absence of a visual horizon. Practical retrofittable means to combat LOC accidents in cable-controlled GA aircraft were developed and flight tested during this research.

It was found that the inclusion of AoA awareness aids based on measured AoA to be both practical and of great value for a typical GA aircraft. AoA awareness may be furnished by visual, auditory, and tactile means, the latter being extraordinarily valuable in alerting the pilot to incipient stall in conditions with high levels of distraction.

Active envelope protection against imminent stall, including visual, auditory, and tactile annunciations, together with servo engagement to prevent inadvertent exceedance of critical AoA, could prevent stall-induced LOC accidents in a variety of flight conditions. Such a system can be made compatible with existing cable-controlled aircraft using appropriately back-drivable, torque-limited servos and inexpensive, modern sensing systems now commonly available.

Lateral stability augmentation via an always-on, torque-limited controller that does not adversely affect manual control feel of the aircraft, has potentially great value in reducing the incidence of VFR-into-IMC LOC accidents. The addition of more forceful lateral envelope protection using higher torque limits for overbank conditions is a practical and potentially effective addition to lateral stability augmentation.

In general, the technology to make AoA awareness, stability augmentation, and envelope protection systems at an affordable cost for light GA aircraft is now available. Encouraging retrofit of the existing fleet and inclusion of such systems on a forward-fit basis for new GA aircraft has the potential to substantially decrease the future incidence of GA LOC accidents.

13.2 PHILOSOPHICAL CONSIDERATIONS.

For a given set of desired functional capabilities in any envelope protection system, there are many possible mechanizations. For instance, different types of servos might be used, different formulations of control laws might be applied, and different styles of information presentation to the pilot might be employed.

This section does not attempt to discriminate or draw conclusions on the particular means by which systems should be mechanized. Such considerations will be at the designer's discretion, depending on tools and technologies available at the time, all of which are rapidly changing within all the technical subdisciplines applicable to flight control systems.

The remainder of this section instead focuses on performance aspects of envelope-protection systems that form the basis, collectively, for judging a resulting system to be acceptable. The intent is to establish, from a performance standpoint, what key aspects of a light-aircraft envelope-protection system should be considered for minimum performance specifications and, in turn, as standards for certification.

13.3 HIGH-LEVEL DESIGN PRINCIPLES.

In any envelope-protection system, the following key principles should be adhered to:

- Automation must always be subordinate to the human pilot.
    - The pilot should be able to override the system at all times.
    - The pilot should be able to fully inactivate the system if so desired.
- The system mode of operation should be apparent to the pilot.
    - The operational state of the system should be displayed in an obvious manner at all times.
    - Changes in operational mode of the system should be displayed and audibly annunciated.
- The system should be failsafe and failures should be made obvious to the pilot.
    - Failures of system components should not compromise the ability of the pilot to manually control the aircraft.
    - Failures of system components should not endanger the structural integrity of the aircraft.
    - Whenever detectable, failures of the system should be annunciated to the pilot.

- Pilot-in-the-Loop features must work well with or without pilot inputs on the controls.

  - The magnitude of forces imparted by the system and felt at the yoke or sidestick must, in reversible-control aircraft, be a subordinate design goal to acceptable response of the aircraft, both with and without pilot inputs.

  - The system should not unduly interfere with the normal control feel of the aircraft within its inner-flight envelope, where inner refers to that portion of the envelope within some defined vicinity of nominal straight and level flight.

- Informing the pilot can include multiple sensory modes.

  - Visual annunciation is important, but often ineffective in circumstances in which the pilot's attention is focused outside the cockpit.

  - Auditory annunciation is better with spoken words rather than nonspecific tones.

  - Tactile forces applied through the yoke or sidestick are helpful, but can be nonintuitive.

  - Tactile vibrations applied through the yoke or sidestick are very attention-grabbing, but nonspecific, and should be reserved for a single circumstance (e.g., impending stall).

The authors of this report recommend the adoption of the above key high-level design principles as guidance for certification of envelope protection systems in light aircraft.

13.4 DESIRABLE DESIGN ATTRIBUTES.

From recent flight experience in the development of a prototype envelope protection system, the following aspects of good design have been developed. These are advisory in nature and should not necessarily become minimum performance specifications for envelope protection systems. However, they can serve as elements of guidance for the system designer and for the certification authorities.

13.4.1 Servo Design.

Future servo designs may evolve from the present typical motor and gear-train technology. For the purposes of present and future designs, the following capabilities for servos used in cable-controlled aircraft are desirable:

- Servos used to provide envelope protection functions in a cable-controlled aircraft should be functionally back-drivable. Functional back-drivability means that with the servo engaged and operating, the pilot can freely manipulate the controls and move them

throughout their normal range of motion without undue interference from the activated servo, even if the servo is applying torque to the system.

- Servos in the system should not interfere with normal manipulation of the controls when the servo is disengaged or powered off. Multiple means of accomplishing this are possible; examples include the presence of a dropout gear and the capacity to easily back-drive the unpowered servo because of its inherent design attributes.

- A means to mechanically disconnect the servo from the cable-control system if the servo is internally jammed in a fixed position, through use of a shear pin, slip clutch, or similar frangible or slippable link, is essential. If no such mechanism is provided, a functionally equivalent capability must be demonstrated to ensure that the controls cannot be compromised by an internally jammed servo.

- The servo should include an unambiguous indication of whether it is engaged or disengaged from the cable-control system. The control laws must, in general, take this status into account for proper initialization and avoidance of undesirable transient behavior when engaging.

- Minimization of backlash is important to avoid subjective tactile bumps in a pilot-in-the-loop system. Generally, this is more easily achieved through the use of a larger motor and a shorter gear train for a given desired output torque capability.

13.4.2 Lateral Protection.

Lateral envelope protection may be viewed in two typical modes of operation. First, lateral stability augmentation serves to implement a greater tendency for the aircraft to return to wings-level flight after being rolled to nonzero bank angles.

Second, lateral envelope protection actively alerts the pilot to bank angles in excess of some limit and actively applies significant torques to the controls to roll the aircraft back to within that limit.

13.4.2.1 Lateral Stability Augmentation.

Full-time, always-on-by-default lateral stability augmentation to eliminate roll divergence, in and of itself, is an extremely valuable capability. In the context of eliminating LOC accidents, this capability alone could significantly reduce the incidence of fatal VFR-into-IMC events.

For lateral stability augmentation, the following good design principles apply:

- To be unobtrusive to the pilot, control forces added to the system by stability augmentation systems should be as light as possible, while still ensuring an adequate positive roll stability for the aircraft. Optimally, the pilot should find it difficult to notice that the system is active at all. The manual control of the aircraft should feel much like that of a natural unaugmented airplane during maneuvering flight, but if the pilot removes

hands from the yoke, the airplane should gradually return to wings-level flight rather than diverging into a spiral.

- The lateral stability augmentation should achieve positive roll stability for the aircraft.

- Stability augmentation should not adversely affect the flight dynamics of the aircraft anywhere within the aircraft's normal flight envelope.

- The design should avoid perceptible force discontinuities or bumps on the control yoke or stick, as these are viewed very negatively by pilots.

13.4.2.2 Lateral Envelope Protection.

For lateral envelope protection, the following are good design principles:

- The value of bank angle past which envelope protection activates should be chosen to avoid interference with normal maneuvering of the aircraft in typical flight scenarios.

- Activation of envelope protection should be accompanied by both visual and auditory warnings. These warnings should indicate, to the extent practicable, what is wrong and what should be done to fix it. An example auditory warning would be "Overbank… Roll Right" or "Overbank… Roll Left." An example visual alert would be a curved arrow on the PFD showing the direction for rolling out of the excessive bank.

- Forces on the yoke opposite the direction of excessive bank should increase rapidly as the bank angle limit is passed. These forces should not be so great as to make it physically impossible to push the aircraft past them, but should be large enough that it is obvious that the control system is attempting to right the aircraft.

- If the pilot decides to let go of the yoke after envelope protection intervention has commenced, the control system should avoid excessive snapback of the yoke. One way to implement this is to add a control-surface deflection-rate dependent damping term to the envelope protection control law.

- To avoid repeated limit-cycle-like entrances and exits from roll envelope protection, it is desirable to turn off the roll envelope protection function at a somewhat smaller bank angle than where it is triggered for turn-on. For example, a reasonable turn-on bank angle for a light aircraft is 40° with a turnoff of 38°.

- A more attractive aircraft response is gained through the combination of lateral envelope protection with lateral stability augmentation than with lateral envelope protection alone.

13.4.3 Longitudinal Protection.

Longitudinal protections include stability augmentation (which serves to damp longitudinal modes, such as the phugoid mode) and longitudinal envelope protection (which addresses overpitch, overspeed, and incipient stall conditions).

13.4.3.1 Longitudinal Stability Augmentation.

For longitudinal stability augmentation, the following good design principles apply:

- It is not essential to fundamentally alter the longitudinal dynamics of a fixed-wing aircraft in a stability-augmentation/envelope protection system. The longitudinal stability augmentation, if implemented, may enhance the quality of the overall system, but is not an obligatory feature.

- It is important not to interfere with the pilot's ability to freely maneuver the aircraft in the pitch plane (e.g., by selecting a different pitch attitude through manual pressure on the yoke or adjusting the pitch trim).

- As in lateral stability augmentation, it is important that any stability augmentation feature not adversely affect aircraft dynamics in any portion of the normal flight envelope of the aircraft.

13.4.3.2 Longitudinal Envelope Protection.

Longitudinal envelope protection is the most complex of the envelope protection challenges for practical implementation on a light aircraft. The following good design principles apply:

- Because multiple simultaneous exceedances of longitudinal limits are possible, a clear prioritization must be established for envelope protections. The recommended priority in order of highest to lowest is (1) stall avoidance, (2) overpitch avoidance, and (3) overspeed avoidance.

- All longitudinal maneuvering must obey g-limits to avoid structural damage. Implicitly, g-limits impose an additional superseding constraint on all envelope protection interventions.

13.4.3.2.1 Stall Protection.

- Stall protection is the most vital longitudinal envelope protection function. To be effective, AoA information is essential as a control algorithm input. Measured AoA rather than estimated is essential, unless an estimation method can be proven equivalent in quality to measured AoA under all conditions (typical error less than 0.5°).

- The AoA information should also be displayed to the pilot so a visual representation of stall margin is available.

- When the AoA approaches critical AoA, both visual and auditory annunciations should be given, stating what is wrong and how it should be fixed. An example auditory message is "Stall, stall−push down." An example visual display is a prominent downward arrow appearing on the PFD display.

- Active stall protection features should not activate until stall is imminent (e.g., within 1.0° of critical AoA, not 3.0° or greater as is typical with stall warning horns).

- Yoke forces during stall envelope protection should include sufficient pressure that the pilot must make a substantial maximum-performance pull to overcome them. Given that the vast majority of LOC accidents involve a wing stall initially, this is a key design principle. Nevertheless, the force exerted on the yoke to push the nose over should not be so great that the pilot would be incapable of pulling the aircraft past the limit into a stall if so desired.

- Tactile vibration in the yoke or stick is extremely effective as a stall alert.

13.4.3.2.2 Overpitch/Overspeed Protection.

- Pitch less than a negative limit or greater than a positive limit should trigger visual and auditory annunciations of what is wrong and what should be done to fix it. For negative overpitch, an example auditory annunciation is "Pitch too low−pitch up," with a prominent arrow pointing upward on the PFD. For positive overpitch, an example is "Pitch too high−pitch down," with a prominent arrow pointing downward on the PFD.

- As usual, g-limits must be applied to avoid over-g during envelope protection intervention.

13.4.4 Unusual Attitude Recovery.

Unusual attitude recovery is a manually selected feature that will bring the airplane back to straight and level flight after selection. The following are good design principles for unusual attitude recover:

- As with all protection features, g-limiting is an inherent constraint on unusual attitude recovery.

- For the vast majority of unusual attitudes, it is appropriate to level wings first, then pitch the nose to a near-level pitch attitude. For extreme nose-high starting attitudes, it is appropriate to establish or maintain a nonzero bank angle to allow the nose to fall toward the horizon first, then to roll wings level, and finally to finish pitching to a near-level pitch attitude. The latter approach need not be implemented in order to have a worthwhile unusual attitude recovery system, but it constitutes a more advanced treatment of a narrow set of nose-high initial conditions.

- Unusual attitude recovery mode should annunciate, both visually and via auditory annunciation, the entrance into and exit from the mode.

- Subjectively, aircraft occupants react negatively to a too-rapid change in g-loading rapid. Rate of change of g-loading should be limited to no greater than approximately 0.5g per second to avoid startling or causing undue discomfort to the aircraft occupants during unusual attitude recovery.

- In unusual attitude recovery, detailed in-progress annunciations such as rolling left/right and pitching up/down are potentially helpful but not essential. Such annunciations have potential value in reassuring a panic-stricken pilot that the system is not broken and is doing what it should do.

13.4.5 Tactile Feedback.

- Use of a yoke buzzer is a very effective way to get the pilot's attention. It is a much more noticeable method of alerting the pilot that something is wrong, rather than pushing back on the yoke with a very low-bandwidth force. It is particularly effective as a means of alerting the pilot to impending stall.

- Because tactile vibration is a nonspecific warning and must be associated with a particular hazard through training, use of a tactile buzzer as a general warning for more than a single type of warning is not desirable.

13.4.6 Additional Considerations.

- For all envelope protection functions, a Recovery Complete annunciation is potentially helpful, but not judged to be essential.

- Lateral envelope protection is valuable with or without longitudinal envelope protection. However, a full suite of longitudinal envelope protection features generally require some form of lateral envelope protection to be practical. An exception to this general rule would be a simple single-feature stall protection system.

- Protection features are still quite valuable in the absence of the ability to change power settings. Urging the pilot to change power settings may be appropriate under certain circumstances, but direct control of power settings is not a requirement for a useful envelope protection system.

14. REFERENCES.

1. Krey, N.C., "2007 Nall Report, Accident Trends and Factors for 2006," AOPA Air Safety Foundation, 2007.

2. Duerksen, N., “Fuzzy Logic Adaptive Decoupled Flight Controls for General Aviation Airplanes,” Doctoral Thesis, Wichita State University, Spring 1996.

3. Wilson, J. and Peters, M., “General Aviation Envelope Protection Feasibility Study,” FAA report DOT/FAR/AR-11/9, June 2011.

4. Wilson, J. and Peters, M., “General Aviation Accident Prevention – Basic Envelope Protection, Phase II: Simulator Design, Envelope Protection Algorithms and Initial Simulator Findings,” FAA report DOT/FAA/TC-12/15, October 2012.

APPENDIX A—FLIGHT CONTROL SOFTWARE DESCRIPTION

A.1 HIGH-LEVEL SOFTWARE ARCHITECTURE.

Figure A-1 shows the high-level object diagram for the flight control (FCON) code.

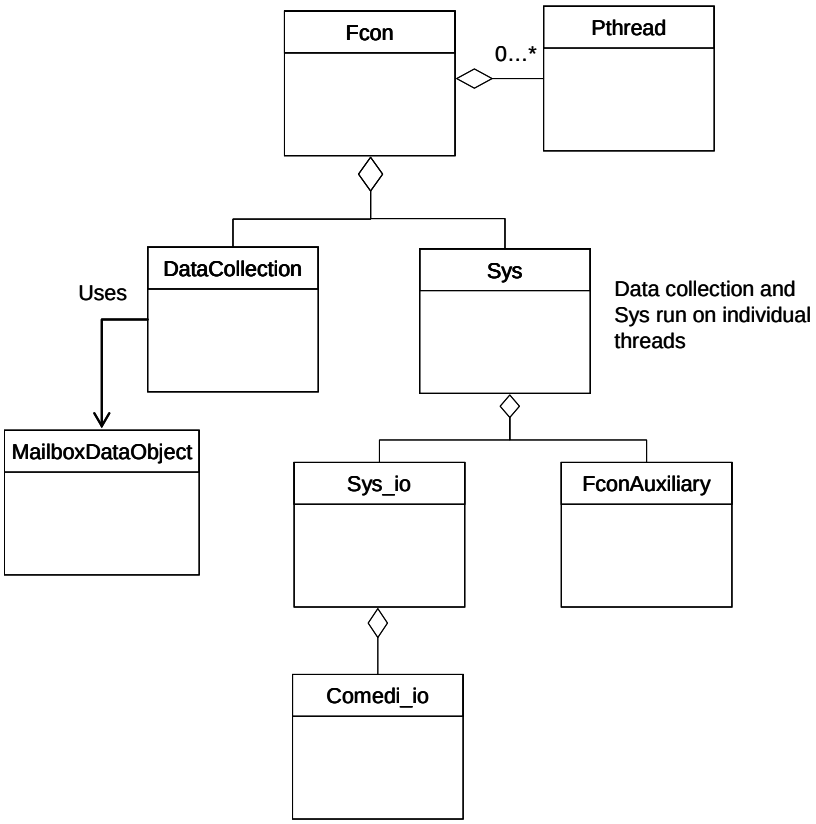

Figure A-1. High-Level FCON Architecture

A.1.1 THE FCON.

The main object for the code is the FCON object. The FCON is based on a generic framework that is slightly modified each time it is used to support whatever processes are required. The code starts the process by setting up the real-time environment and then spawning the required threads. In the case of FCON, two threads are required: the system thread and the data collection thread. The system thread runs all functions for the flight control system with the exception of data collection. Because data collection must write to a file, real-time operation cannot be guaranteed, so it is given its own thread. The FCON ensures that a thread shuts down appropriately, which is particularly important when external devices (i.e., servos) are commanding torques. Improper shutdown could result in nonzero torques being commanded after shutdown.

The threads used in the system are Pthreads, or Portable Operating System Interface (POSIX) threads. The POSIX is a family of standards specified by the Institute of Electrical and

Electronic Engineers for maintaining compatibility between operating systems. The POSIX defines the application programming interface, along with command line shells and utility interfaces, for software compatibility with variants of UNIX® and other operating systems.

A.1.2 THE SYS.

The sys object (short for System) controls all the main flight control processes. At a high level, it manages all of the data input/output (I/O), the servo actuation, and the auxiliary functions. It is at the sys level that the code splits into two main sections:

- Hardware management
- Autopilot and data communications

Hardware management encompasses code that drives the servos and operates the National Instruments data acquisition board, and flight control runs the autopilot and all standard data transfer protocols (serial and User Datagram Protocol (UDP)). This design split has more to do with the evolution of the code rather than any driving rationale. The hardware management code was mature and functioning at a much earlier date, so it was kept distinct and intact from the newer flight control code.

Figure A-2 shows the location of the hardware management code. The sys object is mostly part of the hardware management code and contains the state machines that drive the servos. The sys object also has a sys_io object (System I/O) that manages the communication with the data acquisition card. To facilitate communications with the board, the sys_io object makes use of a series of subroutines based on the COMEDI libraries, which are contained in the Comedi_io object.

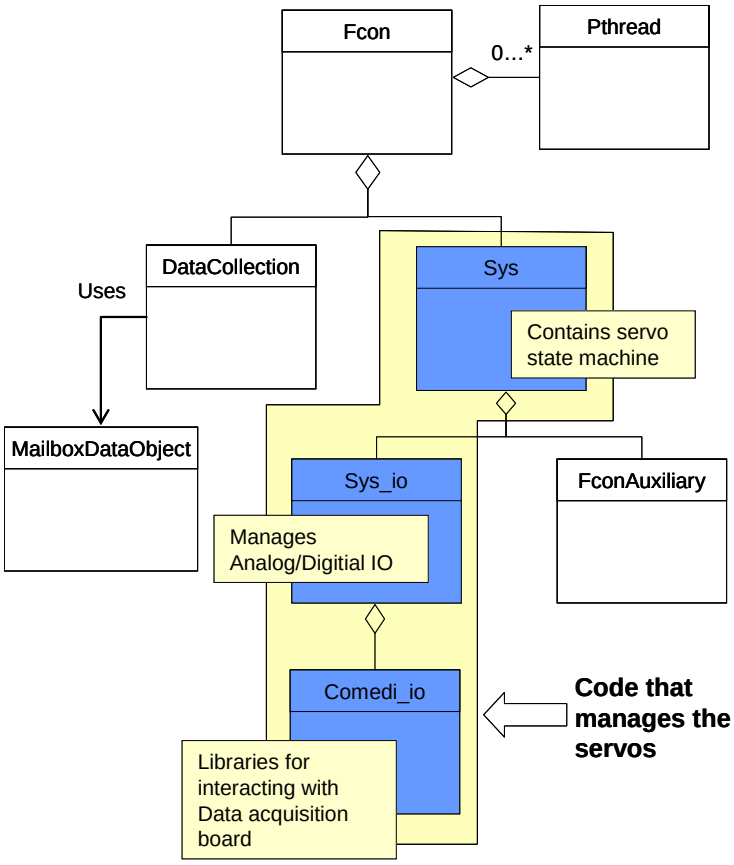

Figure A-2. Hardware-Management Components of the Code

Figure A-3 shows the autopilot and data communication components, which include the sys object and FconAuxiliary. In the sys object, the main system update loop is used to properly sequence the operations that take place within FconAuxiliary, which includes all the flight control functions. The sys object also manages all data flow between FconAuxiliary and the hardware functions.

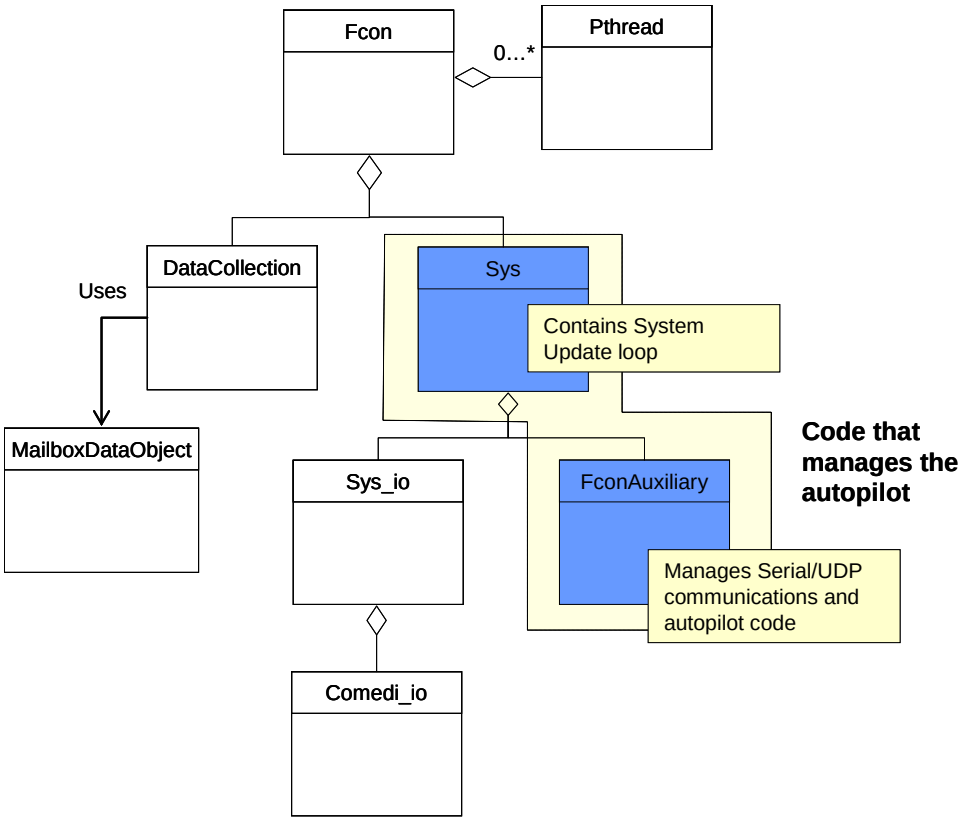

Figure A-3. Autopilot and Communication Code Components

A.1.2.1 Servo State Machine Design.

The sys object is the home for the two identical state machines that govern the operation of the servos. The state machines are based on a simple event-based, nonhierarchical state machine that enables the code to control the state transitions based on an event matrix. The code structure makes the state machine easily configurable to different systems. Because the code is written in C, which doesn't support event-driven programming explicitly, the event-driven nature of the code has to be emulated with the liberal use of enumerated types.

The general structure of the state machine is shown in figure A-4. The state machine has four fundamental states for the servo and numerous events that can be passed to the state machine. The four states are Idle, Home, Servo and Fault.

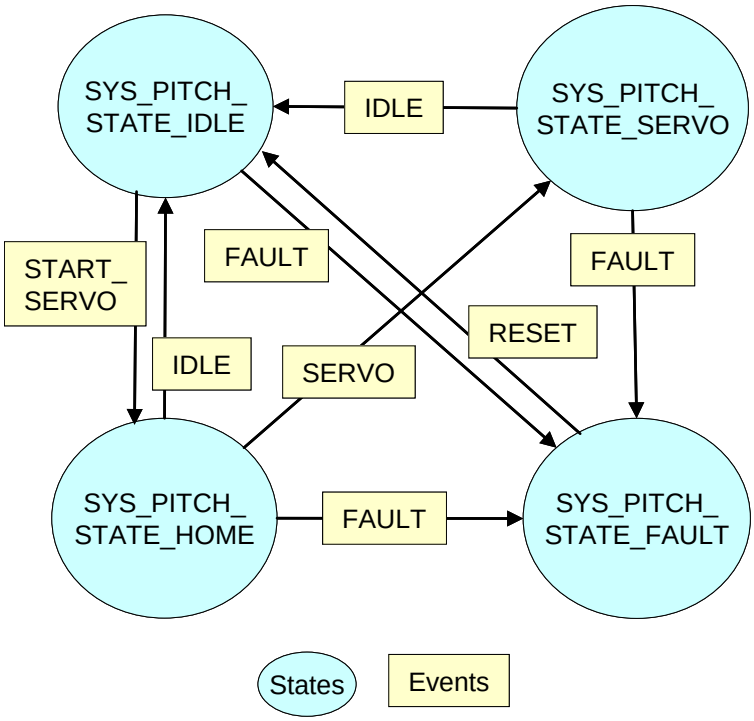

Figure A-4. Servo State Machine Model (Pitch)

- Idle—The servo starts in the idle state in which the servos are on, but not engaged. The dropout gears are not engaged.

- Home—In the home state, initial servo configurations are established. Most importantly, an initial set point for the encoder is established by measuring the servo position as recorded by the potentiometer. The state engages the dropout gear and waits until the engage-indication switch signifies a locked dropout gear. To encourage engagement, the home algorithm gently oscillates the servo motor.

- Servo—Once the homing process is complete, the home state throws an event to move the system to the servo state. In the servo state, the servos respond to torque commands sent to the motor drives.

- Fault—The system is continually checked for faults. If a fault is detected, an event is thrown that transitions the system to the fault state from any other state. To transition out of the fault state, a reset event must be issued, which sends the servo back to the idle state. If the fault has not been corrected, the system will immediately re-fault.

There are five primary failures that trigger a servo fault, as shown in figure A-5.

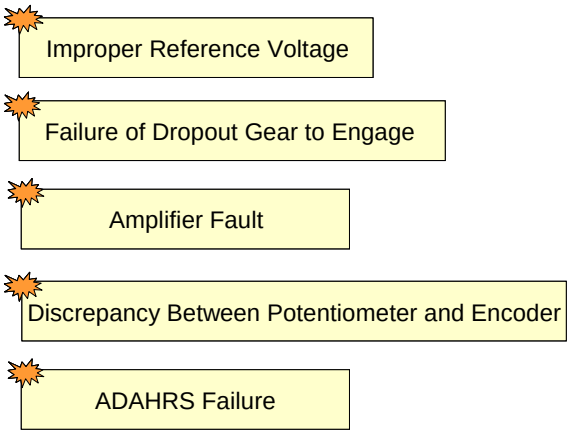

Figure A-5. Faults Detected by the Servo Code

The data acquisition card has a reference voltage that must be maintained so that certain sensed analog signals are properly scaled (e.g., servo potentiometers). If the reference voltage is wrong, measurements will be wrong, potentially resulting in improper function. Under these circumstances, the servos are faulted. If, at any time, the dropout gear engagement indicator switch fails to indicate gear engagement, the servo is faulted. If the drive amplifier indicates a fault, the servos are faulted. The servo position is measured both by a potentiometer and an encoder. The potentiometer is much noisier than the encoder, so the encoder is the preferred measurement; however, if a large discrepancy appears between the servo potentiometer measurement and the encoder measurement, it indicates a problem with servo position. In this case, the servo is faulted. Finally, the servo is faulted if the Air Data Attitude and Heading Reference System (ADAHRS) system fails.

A.1.3 DATA COLLECTION.

The data collection object is designed to write simple ascii data files for data analysis. Because writing such files requires system calls, it cannot be included in the main real-time loop. The data collection object is given a reference to a MailboxDataObject, which is an object within FconAuxiliary that collects data in a separate structure and provides thread-safe access to the data. The MailboxDataObject also contains a variable, which the DataCollection reads to determine when it should collect data.

The FconAuxiliary object is a container for all the nonhardware-related functions of the flight control system.

A.2 Autopilot and Data Communications Code.

The FconAuxiliary object is a container for all the nonhardware-related functions of the flight control system. It is an inconvenient name, reflecting more the software evolution than its function. The FconAuxiliary functions were developed separately from the hardware code. When the code bases were joined, it was done with as little overlap as possible.

Figure A-6 shows the various components. These include the MailboxDataObject, the EvAutopilot, UDPCom, UDPToSimcon, and the SerialComManager.

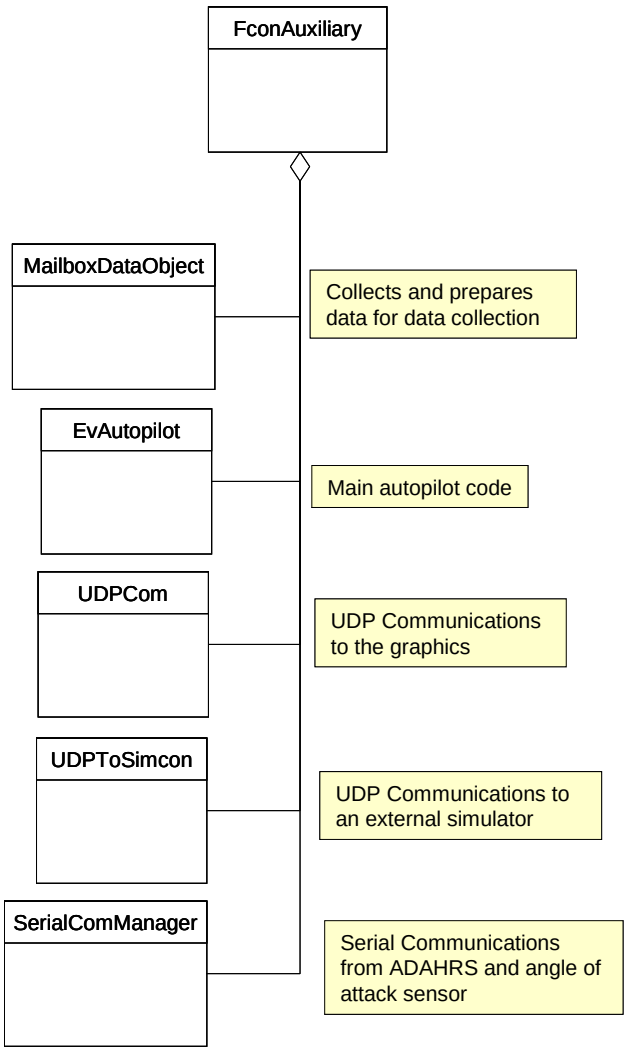

Figure A-6. The Fcon Auxiliary Components

A.2.1 MAILBOXDATAOBJECT.

The MailboxDataObject collects the data from various locations in the code and makes a local copy in several separate structures. It then makes these structures available for reading by the data collection object. It uses a thread-safe architecture to make sure that a structure is always available for reading, while ensuring that the main thread never has to wait for the data collection thread to complete a write of the data. The MailboxDataObject also obtains the data collection status from the autopilot, where the operator can indicate whether data collection is on or off. This status variable is stored in the mailbox object to indicate to the data collection object whether or not data should be collected.

A.2.2 THE UDPCom AND UDPToSimcon.

The UDPCom object is responsible for sending UDP messages to the graphics computer to support the data for the primary fight display (PFD) and to support data to and from the mode control panel (MCP) (see figure A-7). UDPCom creates the appropriate messages and then uses several instances of a generic UDP messaging object, udp_data, to send and receive data from the other computer. The PFD is designed to receive a specific message, which is parsed and created by the PfdData object. The MCP receives an entire structure, contained within the DisplayDataBus. The DisplayDataBus is a member of the EvAutopilot and UDPCom makes a copy of it to send to the MCP. The MCP then returns a modified copy of the DisplayDataBus, which is in turn routed back the EvAutopilot code.

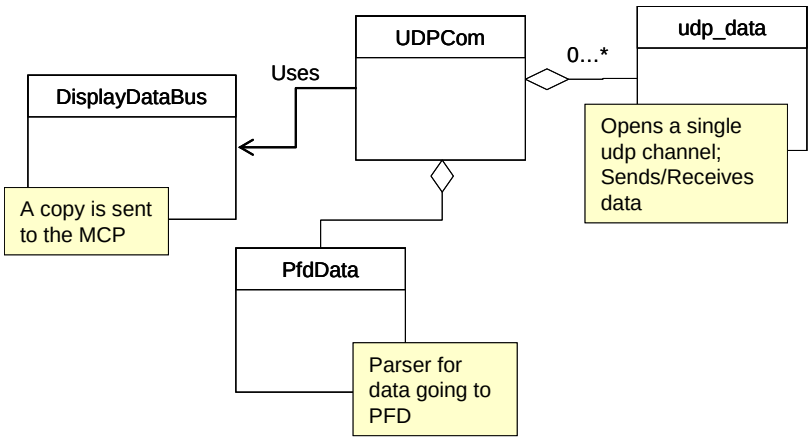

Figure A-7. The UDPCom Internal Structure

The UDPToSimcon object was a late addition to the code, which sends a UDP message with control surface-positions. This was part of the hardware-in-the-loop simulation capability that was developed so that flight control changes could be tested on the ground in a simulator before flight in the aircraft. The original simulator code, Simcon, had been modified to emulate the ADAHRS output and to receive control surface position inputs to enable this testing.

A.2.3 SerialComManager.

The SerialComManager (see figure A-8) managed the serial messages that were received from the ADAHRS. The SerialComManager facilitated the retrieval of data and then performed error checking on the data to ensure that the data were correct. It could run in a dual ADAHRS mode, in which signal comparators would check the agreement between the ADAHRS and fail the system if a discrepancy was detected; however, this was not used during the flight test program because of the unavailability of an additional serial port for the second ADAHRS output. In single ADAHRS mode, the manager would fail the system if any message failed to be received. The SerialComManager had one main object, the message handler, for collecting the data. The message handler would open the individual channels using multiple instances of the SerialCom object, which in turn would pass the encoded data stream to the message handler.

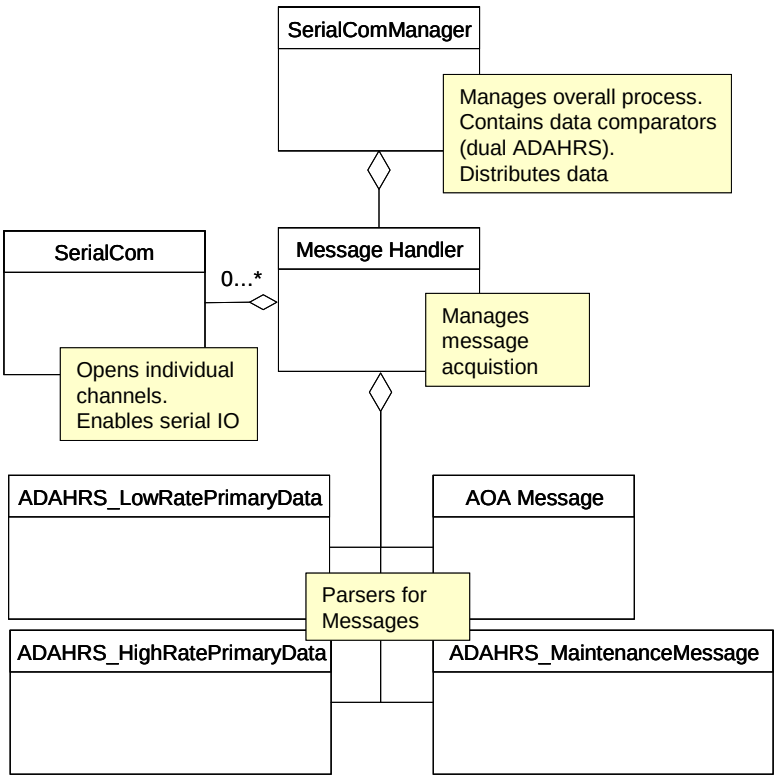

Figure A-8. SerialComManager Internal Structure

The message handler had several parsers for decoding the messages and populating the various data structures. The message handler had a parser for each message that it was to receive. To collect all the desired data from the ADAHRS, three different messages were collected and one message was collected from the AoA Sensor, which included AoA information and Global Positioning System (GPS) position, velocity, and time. The default high-rate message from the ADAHRS had the primary air data and attitude information required; however, to get angular rates and accelerations, a separate high-rate maintenance message had to be read and, to obtain outside air temperature, a third, low-rate message had to be read as well.

A.2.4 EvAutopilot.

The EvAutopilot is the high level object containing the actual autopilot code. The rest of the flight control code can be considered support for the autopilot code. Section A.3 describes EvAutopilot in detail.

A.3 Autopilot and Envelope Protection Code.

The autopilot and envelope protection functions of the code are contained within the EvAutopilot object. Figure A-9 shows the internal object hierarchy for the EvAutopilot. The EvAutopilot object contains two main internal objects: the EvAutopilotExecutive and the DisplayDataBus. The executive is the object that contains the state machines for the autopilot and essentially runs the autopilot. The DisplayDataBus is used primarily for communication with the MCP.

Functions that reside explicitly within the EvAutopilot manage the operator inputs to control the various modes of the autopilot. This consists of evaluating the button presses sensed on the MCP, commanding the appropriate mode changes, and preparing the appropriate response to go back to the MCP. To do this, the EvAutopilot exchanges copies of the DisplayDataBus with the MCP through the provided UDP interface. Additional functions within the EvAutopilot object include the calculations of control surface rates and pitch trim requirements.

A.3.1 EvAutopilotExecutive.

The EvAutopilotExecutive is responsible for orchestrating the majority of the autopilot functions. It responds to commands from the EvAutopilot and transitions state as required. The state machines to manage the lateral and longitudinal autopilot reside explicitly within the executive. The individual autopilot modes (states) are contained within their own objects. The executive also has two different servo torque controller objects, cs_control and PID, which are used with the various autopilot modes, depending on the modes' output.

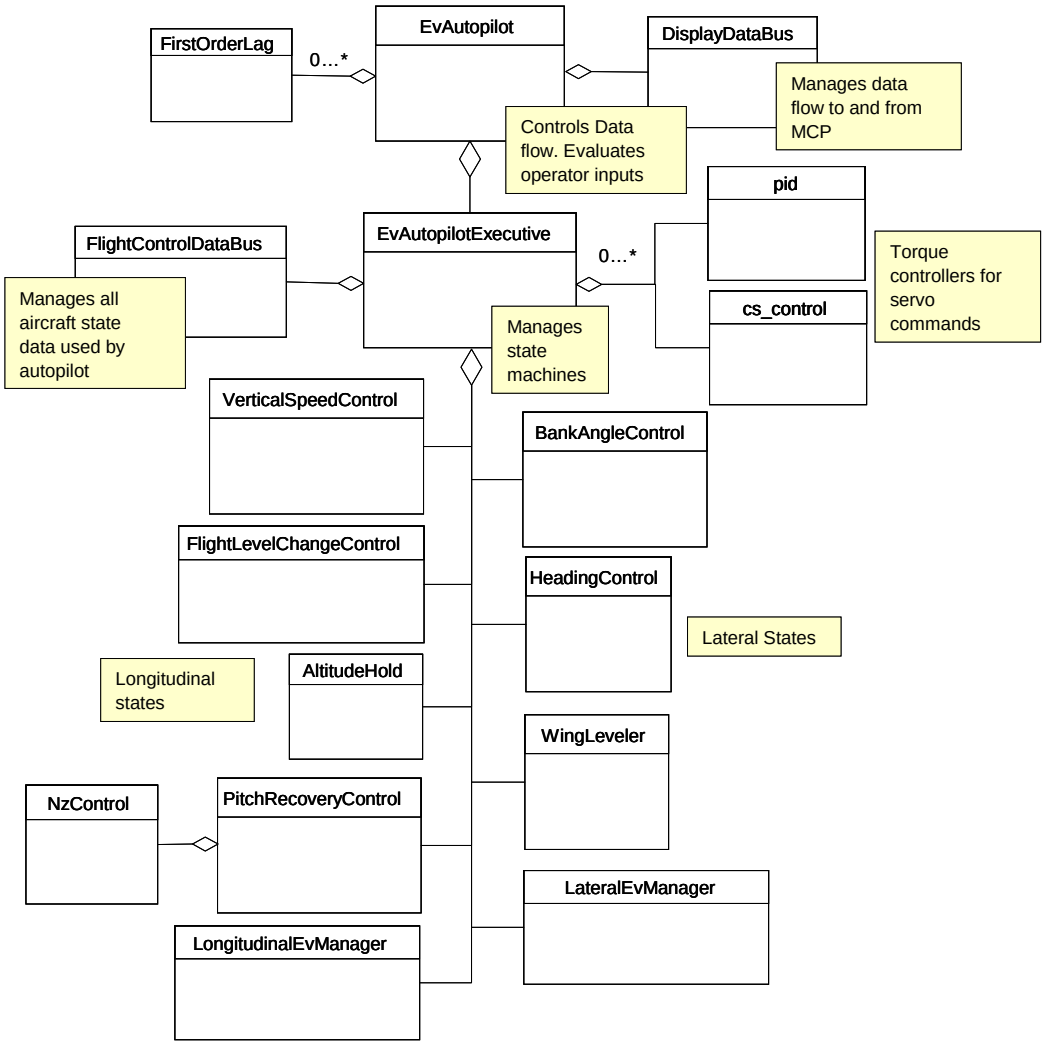

Figure A-9. Internal Object Diagram for the EvAutopilot

A.3.1.1 State Machines.

The state machines within the autopilot are less sophisticated than the ones used for the servo control because there is no need to restrict the transition from one state to another. In the autopilot, any state can transition to another state with the exception that a lateral mode must be engaged before any longitudinal mode can be engaged. This protective measure is done to ensure that the aircraft is always in a wings-level condition before any pitch control is affected. Figure A-10 shows the modes and their function. The envelope protection features are considered to be individual modes within the autopilot hierarchy in which the LongitudinalEvManager encompasses all longitudinal envelope protection functions and the LateralEvManager does the same for lateral envelope protection functions.

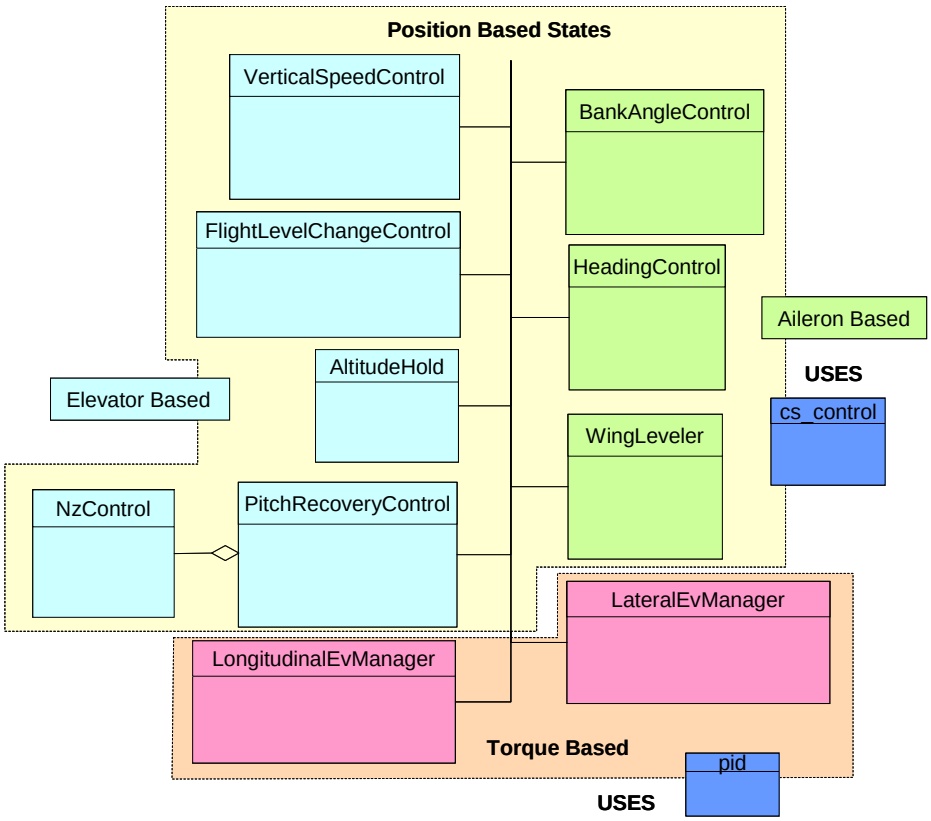

Figure A-10. Autopilot States and Their Functions

The autopilot modes are classified as position based or torque based, depending on whether they command a control surface position or a torque directly. All the strictly autopilot modes (as opposed to envelope protection) are position based, whereas the envelope protection modes are torque based.

A.3.1.2 Torque Controllers.

There are two torque controllers implemented in the autopilot: cs_control and pid. The cs_control object contains a control law for commanding control surface position through torque

actuation. The executive instantiates two instances of cs_control, one for the aileron and one for the elevator. The output from the various position-based control laws is converted to servo torque commands using the cs_control objects.

The pid object is used to ensure that the commanded torque from the torque-based control laws is what is actually measured at the servo output sprocket. The inclusion of the pid controller was a modification. Originally, the commanded torques were applied to the servo directly (open loop). However, in certain instances, especially high-torque scenarios, there could be a large discrepancy between the commanded and the measured output torque, so a feedback-control law was added. The executive instantiates two instances of the pid object, one for the roll servo and one for the pitch servo.

A.3.1.3 Output Saturation.

One of the necessary protections within the autopilot is to ensure that the integrators do not end up in the presence of output saturation. Saturation can be difficult to detect because it likely occurs downstream of the control laws. To provide this protection, the executive measures the commanded output torque compared with the maximum allowable torques within the system. If saturation is detected, the executive posts the saturation state to a variable in the flight control databus. Every control law thereafter reads the saturation state and suspends any internal integrators as required.

A.3.1.4 Autopilot Frame Update Suspension.

When the autopilot is initially engaged, the autopilot state machine initializes the appropriate mode of operation and the mode starts running. In parallel, the servo state machine initializes the servos. It is possible for the autopilot to start running frames before the servos completely engage, which can cause a large step input to the servos when they do engage. In some cases, this can be violent. To prevent this from happening, the servo status is passed to the autopilot on each frame of operation, and if the servo is offline for any reason, the autopilot suspends operation of its internal frame until the servo is engaged. The autopilot is still on and can change state, but it will not run the control laws or pass a command to the servos.

In some cases, this suspension created problems for troubleshooting the code when it was not attached to the servos, so during development, the suspension feature itself needed to be disabled. Here, the risk is that the suspension feature would not be re-enabled when the system was flight tested. To prevent this from occurring, a check of the software for this problem was added to the overall aircraft checklist. Eventually the software had its own checklist to ensure that it was ready for flight.

A.3.1.5 Flight Control Databus.

The flight control databus is an object that the autopilot uses to distribute information between its various objects. It resides within the executive, but most of the autopilot objects are given a reference to the databus.

A.3.2 LongitudinalEvManager.

The LongitudinalEvManager handles the functions of both stability augmentation and envelope protection. Figure A-11 shows the internal structure of the LongitudinalEvManager. The manager contains the stability augmentation functions and the envelope protection functions in separate objects. The longitudinal envelope protection functions are further broken down into their fundamental function, pitch envelope protection, stall envelope protection, and overspeed envelope protection.

A formal-state machine that transitions between the stability augmentation and the envelope protection does not exist. Each can be activated separately and can both run concurrently. The envelope protection functions are managed by a simple state machine that activates an envelope protection mode at the appropriate condition. The envelope protection functions cannot operate concurrently, so a precedence of operation is established if conditions exist to activate more than one mode at a time.

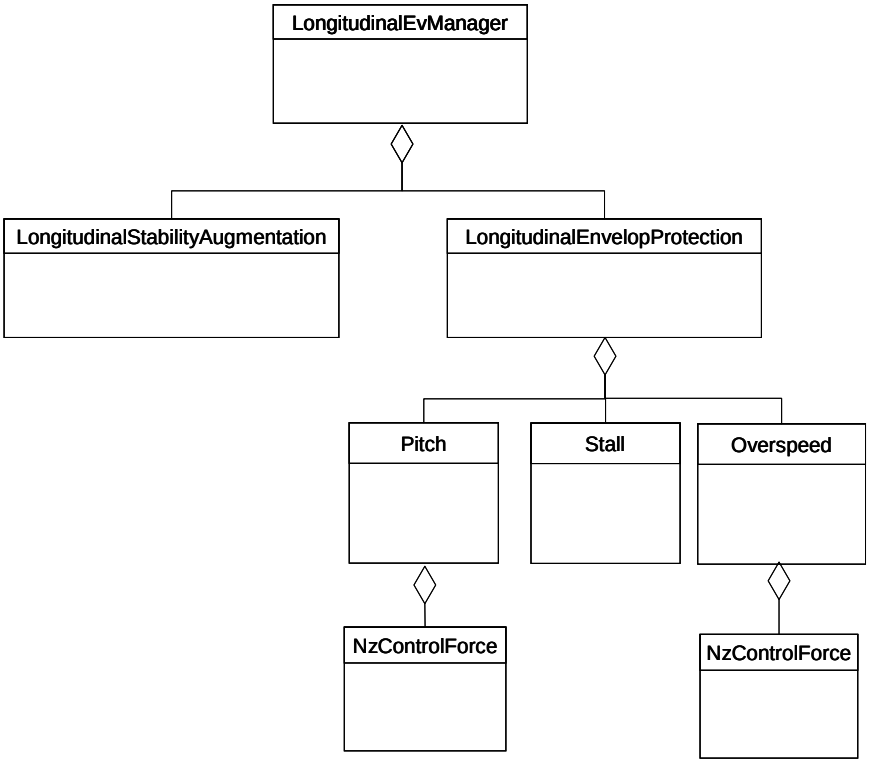

Figure A-11. Internal Structure of the LongitudinalEvManager

A.3.2.1 LateralEvManager.

The LateralEvManager contains objects to support the lateral stability augmentation and the lateral envelope protection functions. Figure A-12 shows the internal structure of the LateralEvManager. A formal state machine that transitions between the stability augmentation and the envelope protection does not exist. Each can be activated separately and can both run

concurrently. Anytime lateral envelope protection is activated, the stability augmentation functions are saturated.

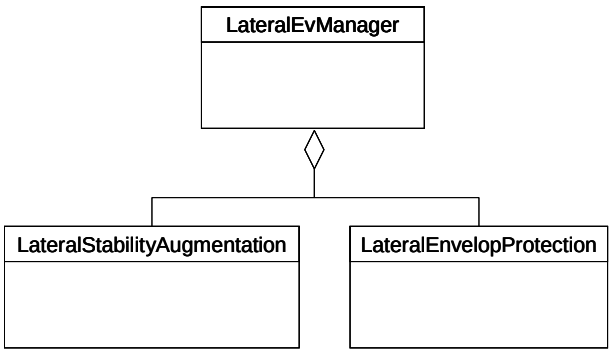

Figure A-12. Internal Structure of the LateralEvManager

APPENDIX B—DERIVATION OF AIRCRAFT EQUATIONS OF MOTION

This section provides a theoretical foundation for the aircraft equations of motion (EOMs) that are used in the aircraft simulation. The foundation will start with the definition of reference frames. Once the reference frames have been defined, the EOMs for the full 6-degree-of-freedom (6-DOF) model are discussed.

B.1 DEFINITION OF BODY FRAME AND INERTIAL FRAME.

The two major reference frames used in the derivation of the aircraft EOMs are the aircraft body fixed-reference frame (denoted with a *b* subscript) and the inertially fixed frame (denoted with an *i* subscript). The aircraft body frame's origin is fixed at the aircraft's center of gravity. The body frame has its $\hat{x}_b$ axis aligned with the nose of the aircraft so that the aircraft's nose points in the positive $\hat{x}_b$ direction. The positive $\hat{y}_b$ direction points out along the aircraft's starboard wing. The $\hat{z}_b$ axis points down to complete a right-handed coordinate frame. Figure B-1 shows the body fixed-reference frame.

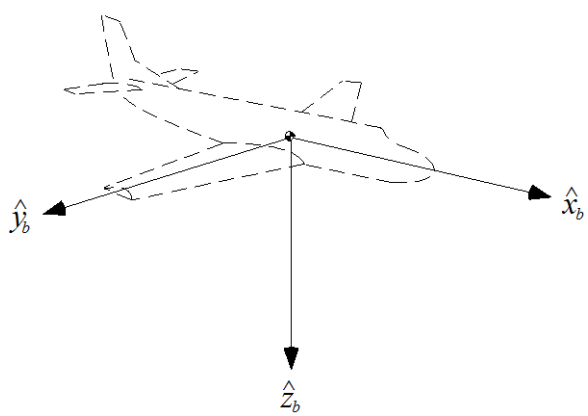

Figure B-1. The Body Fixed-Reference Frame Aligned With an Aircraft

The inertially referenced frame is fixed on a point on the earth's surface and is aligned so that the positive $\hat{x}_i$ axis points in the true north direction and the positive $\hat{y}_i$ axis points in the true east direction. The $\hat{z}_i$ axis points down and is normal to the surface of the earth. The body reference frame can assume any orientation with respect to the inertial frame. Figure B-2 illustrates the relationship between the body and inertial reference frames.

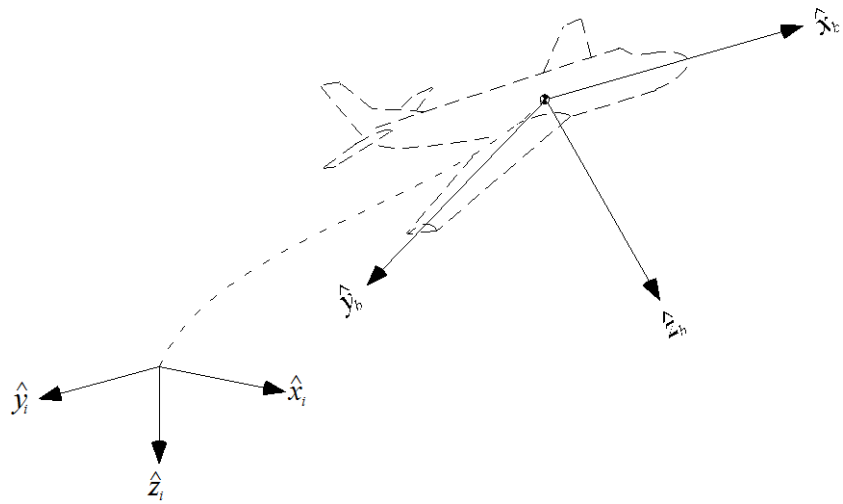

Figure B-2. The Relationship Between Body and Inertial Reference Frames

The orientation of the body frame with respect to the inertial frame is usually described by an Euler angle (3-2-1) sequence of rotations. The ordering of the rotations is critical to the orientation of the body frame. It is difficult to visualize the actual sequence of rotations in a single drawing, so the sequence is illustrated with three separate drawings. Figure B-3 shows the Euler sequence of rotations, which is used to quantify the aircraft's orientation.

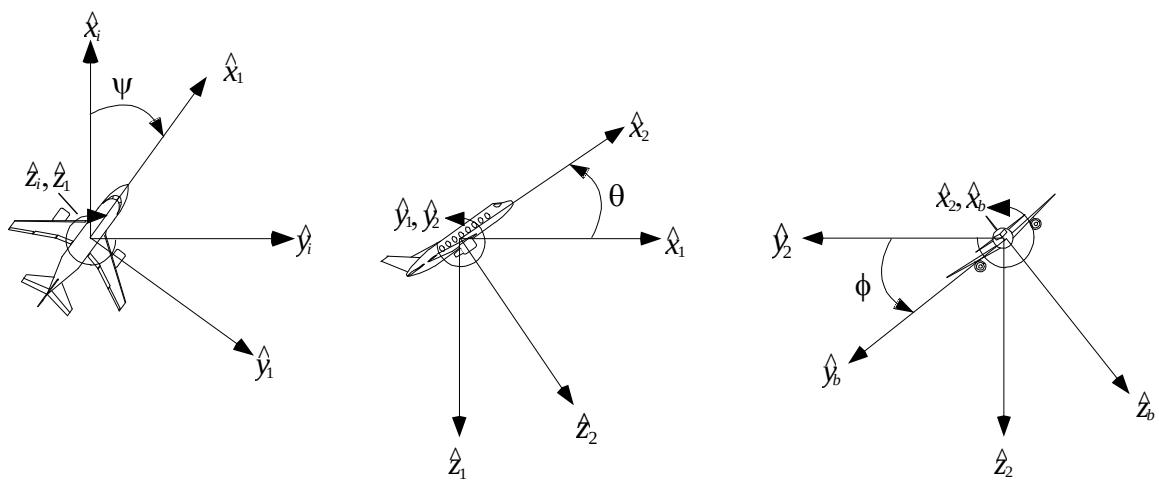

Figure B-3. The 3-2-1 Euler Sequence of Rotations Used to Quantify the Aircraft's Orientation

The first rotation is through the angle ψ about the $\hat{z}_i$ axis to an intermediate reference frame, which is arbitrarily denoted with a 1 subscript. The second rotation is through the angle θ about the $\hat{y}_1$ axis to another intermediate reference frame, which is denoted with a 2 subscript. The final rotation is through the angle ϕ about the $\hat{x}_1$ axis to the body frame. The angles ψ, θ, and ϕ are referred to as the heading, pitch, and roll angles, respectively.

The conversion between the inertial frame and the body frame of the aircraft is accomplished using direction cosine matrices. The first cosine matrix establishes the relationship between the inertial frame and the first intermediate reference frame. Equations B-1, B-2, and B-3 quantify the relationship between the individual rotations. The nomenclature C_θ and S_θ is simplified notation for cosθ and sinθ. This is done for all trigonometric manipulations to simplify the ultimate expression. From the rotation sequence shown in figure B-3, one can write the following direction cosine matrices shown in equations B-1 through B-3.

$$\begin{bmatrix} \hat{x}_1 \\ \hat{y}_1 \\ \hat{z}_1 \end{bmatrix} = \begin{bmatrix} C_\psi & S_\psi & 0 \\ -S_\psi & C_\psi & 0 \\ 0 & 0 & 1 \end{bmatrix} \begin{bmatrix} \hat{x}_i \\ \hat{y}_i \\ \hat{z}_i \end{bmatrix} \tag{B-1}$$

$$\begin{bmatrix} \hat{x}_2 \\ \hat{y}_2 \\ \hat{z}_2 \end{bmatrix} = \begin{bmatrix} C_\theta & 0 & -S_\theta \\ 0 & 1 & 0 \\ S_\theta & 0 & C_\theta \end{bmatrix} \begin{bmatrix} \hat{x}_1 \\ \hat{y}_1 \\ \hat{z}_1 \end{bmatrix} \tag{B-2}$$

$$\begin{bmatrix} \hat{x}_b \\ \hat{y}_b \\ \hat{z}_b \end{bmatrix} = \begin{bmatrix} 1 & 0 & 0 \\ 0 & C_\phi & S_\phi \\ 0 & -S_\phi & C_\phi \end{bmatrix} \begin{bmatrix} \hat{x}_2 \\ \hat{y}_2 \\ \hat{z}_2 \end{bmatrix} \tag{B-3}$$

The product of these three-direction cosine matrices results in the complete conversion between the inertial frame and the body frame, as shown in equation B-5:

$$\begin{bmatrix} \hat{x}_b \\ \hat{y}_b \\ \hat{z}_b \end{bmatrix} = \begin{bmatrix} 1 & 0 & 0 \\ 0 & C_\phi & S_\phi \\ 0 & -S_\phi & C_\phi \end{bmatrix} \begin{bmatrix} C_\phi & 0 & -S_\theta \\ 0 & 1 & 0 \\ S_\theta & 0 & C_\theta \end{bmatrix} \begin{bmatrix} C_\psi & S_\psi & 0 \\ -S_\psi & C_\psi & 0 \\ 0 & 0 & 1 \end{bmatrix} \begin{bmatrix} \hat{x}_i \\ \hat{y}_i \\ \hat{z}_i \end{bmatrix} \tag{B-4}$$

$$\begin{bmatrix} \hat{x}_b \\ \hat{y}_b \\ \hat{z}_b \end{bmatrix} = \begin{bmatrix} C_\theta C_\psi & C_\theta S_\psi & -S_\theta \\ -C_\phi S_\psi + S_\phi S_\theta C_\psi & C_\phi C_\psi + S_\phi S_\theta S_\psi & S_\phi C_\theta \\ S_\phi S_\psi + C_\phi S_\theta C_\psi & -S_\phi C_\psi + C_\phi S_\theta S_\psi & C_\phi C_\theta \end{bmatrix} \begin{bmatrix} \hat{x}_i \\ \hat{y}_i \\ \hat{z}_i \end{bmatrix} \tag{B-5}$$

The inverse of equation B-5 is shown in equation B-6:

$$\begin{bmatrix} \hat{x}_i \\ \hat{y}_i \\ \hat{z}_i \end{bmatrix} = \begin{bmatrix} C_\theta C_\psi & -C_\phi S_\psi + S_\phi S_\theta C_\psi & S_\phi S_\psi + C_\phi S_\theta C_\psi \\ C_\theta S_\psi & C_\phi C_\psi + S_\phi S_\theta S_\psi & -S_\phi C_\psi + C_\phi S_\theta S_\psi \\ -S_\theta & S_\phi C_\theta & C_\phi C_\theta \end{bmatrix} \begin{bmatrix} \hat{x}_b \\ \hat{y}_b \\ \hat{z}_b \end{bmatrix} \tag{B-6}$$

B.2 FLIGHT MECHANICS NOMENCLATURE.

Next, certain flight mechanics nomenclature must be defined. This nomenclature consists of the various linear and angular velocities associated with the motion of the aircraft as well as the forces and moment that are applied. Figure B-4 provides an illustration of the nomenclature as it applies to the aircraft.

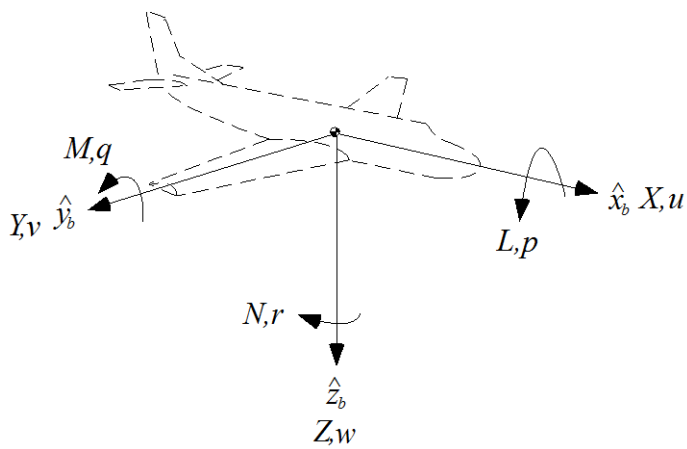

Figure B-4. The Forces, Moments, Velocity Components, and Angular Rates of an Aircraft

Table B-1 summarizes the nomenclature definition so that the mathematical symbols can be associated with the proper terminology. It is important to note that the term L is used to notate the rolling moment. Further along in the text, L is also be used for lift. This is an unfortunate consequence of the merging of two engineering disciplines, dynamics and control, and aerodynamics. To avoid confusion, this document notates the rolling moment using $\overline{L}$ instead of L, which is reserved for lift.

Table B-1. Definition of Flight Mechanics Nomenclature

	Roll Axis $\hat{x}_b$	Pitch Axis $\hat{y}_b$	Yaw Axis $\hat{z}_b$
Angular Rates	p	q	r
Velocity Components	u	v	w
Aerodynamic Force Components	X	Y	Z
Aerodynamic Moment Components	$\overline{L}$	M	N
Moments of Inertia	I_x	I_y	I_z
Products of Inertia	I_{yz}	I_{xz}	I_{xy}

It is important to note that the forces defined in table B-1 are aligned with the body frame. These forces do not directly coincide with the more commonly known aerodynamic forces of lift and drag, which are defined with respect to the wind frame and are discussed in section B.3.

B.3 WIND AND STABILITY REFERENCE FRAMES.

To resolve the relationship between the commonly known aerodynamic forces of lift and drag and the body forces of the 6-DOF model, two additional reference frames need to be derived: the stability frame and the wind frame. These reference frames characterize the relationship of the angle of attack (AoA), α, and the side-slip angle, β, to the body frame velocities. These aerodynamic angles are defined by means of coordinate rotations. The first rotation, about the $\hat{y}_b$ axis, defines the stability axis and the angle is the AoA, α. With no sideslip, α is the angle between the aircraft $\hat{x}_b$ axis and the aircraft velocity vector relative to the surrounding air mass. The AoA is positive if the rotation about the $\hat{y}_b$ axis is negative. This backwards definition is the unfortunate result of merging the disciplines of aerodynamics and classical kinematics.

The second rotation leads to the wind axis, and the sideslip angle is between the stability axis and the wind axis. An aircraft has sideslip if its velocity vector relative to the air mass is not in the plane defined by $\hat{x}_b$-$\hat{z}_b$. The rotation is about the *z*-axis of the stability axis, $\hat{z}_{st}$, and β is defined as positive if the rotation about the $\hat{z}_{st}$ axis is positive. The wind frame's *x*-axis, $\hat{x}_w$, is aligned with the aircraft's velocity vector, which is the vector sum of the body frame velocities, $\vec{V} = u\hat{x}_b + v\hat{y}_b + w\hat{z}_b$. The other axes, $\hat{y}_w$ and $\hat{z}_w$, are orthogonal to $\hat{x}_w$ and to each other. Figure B-5 shows the orientation of the *x*-axes of the stability and wind coordinate systems with respect to the body frame:

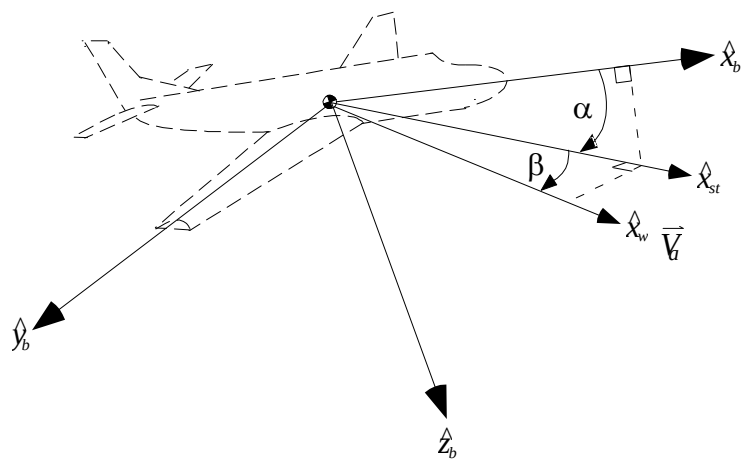

Figure B-5. The Stability and Wind Coordinate Systems

Equations B-7 through B-9 show the direction cosine matrices, which define the transformations between the coordinate frames:

$$\begin{bmatrix} \hat{x}_{st} \\ \hat{y}_{st} \\ \hat{z}_{st} \end{bmatrix} = \begin{bmatrix} C_\alpha & 0 & S_\alpha \\ 0 & 1 & 0 \\ -S_\alpha & 0 & C_\alpha \end{bmatrix} \begin{bmatrix} \hat{x}_b \\ \hat{y}_b \\ \hat{z}_b \end{bmatrix} \tag{B-7}$$

$$\begin{bmatrix} \hat{x}_w \\ \hat{y}_w \\ \hat{z}_w \end{bmatrix} = \begin{bmatrix} C_\beta & S_\beta & 0 \\ -S_\beta & C_\beta & 0 \\ 0 & 0 & 1 \end{bmatrix} \begin{bmatrix} \hat{x}_{st} \\ \hat{y}_{st} \\ \hat{z}_{st} \end{bmatrix} \tag{B-8}$$

$$\begin{bmatrix} \hat{x}_w \\ \hat{y}_w \\ \hat{z}_w \end{bmatrix} = \begin{bmatrix} C_\beta C_\alpha & S_\beta & C_\beta S_\alpha \\ -S_\beta C_\alpha & C_\beta & -S_\beta S_\alpha \\ -S_\alpha & 0 & C_\alpha \end{bmatrix} \begin{bmatrix} \hat{x}_b \\ \hat{y}_b \\ \hat{z}_b \end{bmatrix} \tag{B-9}$$

Using the direction cosine matrices, expressions can be derived for the angles α and β, starting with the definition of true airspeed. The true airspeed of an aircraft, V_a, is defined as the magnitude of the velocity along the $\hat{x}_w$ axis relative to the air mass surrounding the aircraft. By definition, this velocity is the only component of velocity in the wind axis (i.e., the total aircraft velocity is aligned with the $\hat{x}_w$ axis). Written in equation form, $\vec{V} = V_a \hat{x}_w$. Using the inverse of the direction cosine matrix in equation B-9, the body frame velocities can be defined in terms of the true airspeed and the angles α and β.

$$\begin{bmatrix} u\hat{x}_b \\ v\hat{y}_b \\ w\hat{z}_b \end{bmatrix} = \begin{bmatrix} C_\beta C_\alpha & -S_\beta C_\alpha & -S_\alpha \\ S_\beta & C_\beta & 0 \\ C_\beta S_\alpha & -S_\beta S_\alpha & C_\alpha \end{bmatrix} \begin{bmatrix} V_a \hat{x}_w \\ 0 \\ 0 \end{bmatrix} \tag{B-10}$$

The three resulting scalar equations are shown below in equations B-11 through B-13.

$$u = V_a C_\beta C_\alpha \tag{B-11}$$

$$v = V_a S_\beta \tag{B-12}$$

$$w = V_a C_\beta S_\alpha \tag{B-13}$$

Rearranging equation B-12 gives an expression for sideslip:

$$\beta = \sin^{-1} \frac{v}{V_a} \tag{B-14}$$

Taking the quotient of *w/u*, an expression for AoA can be derived, as shown in equations B-15 and B-16.

$$\frac{w}{u} = \frac{V_a C_\beta S_\alpha}{V_a C_\beta C_\alpha} = - = \tan\alpha \tag{B-15}$$

$$\alpha = \tan^{-1}\frac{w}{u} \approx \frac{w}{u} \tag{B-16}$$

Assuming that the AoA is small, it can be approximated as just the ratio *w/u*. Often, this expression is used to substitute α for *w*.

Using the wind reference frame, the relationship can be resolved between the commonly known aerodynamic forces of lift, drag, and thrust (*L*, *D*, and *T*, respectively) and the body forces of the 6-DOF model. It can be seen from the direction cosine matrix 9 that, if the aerodynamic forces are modeled on an aircraft in terms of lift, drag, and thrust, equations B-17 through B-21 are expressions for *X*, *Y*, and *Z* forces in the body frame. The aircraft weight is not included because it is not an aerodynamic force:

$$\sum F_a = T\hat{x}_b - L\hat{z}_w - D\hat{x}_w \tag{B-17}$$

$$\begin{bmatrix} X\hat{x}_b \\ Y\hat{y}_b \\ Z\hat{z}_b \end{bmatrix} = \begin{bmatrix} C_\beta C_\alpha & -S_\beta C_\alpha & -S_\alpha \\ S_\beta & C_\beta & 0 \\ C_\beta S_\alpha & -S_\beta S_\alpha & C_\alpha \end{bmatrix} \begin{bmatrix} -D\hat{x}_w \\ 0\hat{y}_w \\ -L\hat{z}_w \end{bmatrix} + \begin{bmatrix} T\hat{x}_b \\ 0\hat{y}_b \\ 0\hat{z}_b \end{bmatrix} \tag{B-18}$$

$$X = T - DC_\beta C_\alpha + LS_\alpha \tag{B-19}$$

$$Y = DS_\beta \tag{B-20}$$

$$Z = -DC_\beta S_\alpha - LC_\alpha \tag{B-21}$$

The flight-path angle, γ_a, is the angle that the $\hat{x}_w$ axis makes with the *x-y* plane of the inertial frame (horizontal). This angle characterizes the vertical flight path of the aircraft and is formally defined in equation B-22.

$$\gamma_a = \sin^{-1}\left(C_\alpha C_\beta S_\theta - \left(S_\phi S_\beta + C_\phi S_\alpha C_\beta\right)C_\theta\right) \tag{B-22}$$

The *a* subscript on the flight-path angle denotes that it is an aerodynamic flight-path angle, meaning it is the aircraft's flight-path angle relative to the air mass. The aircraft's flight-path angle relative to the ground is generally different because of the influence of winds.

Equation B-22 shows that if both α and β are zero, the Euler angle θ reduces to γ_a.

B.4 SIX DEGREE-OF-FREEDOM EQUATIONS OF MOTION.

Once the reference frames and nomenclature are defined, the derivation of the EOMs is straightforward. The linear EOMs are derived by summing the forces to the time rate of change of linear momentum (mass x acceleration). The acceleration of the aircraft's velocity is determined using the basic kinematic equation, which states that the total acceleration of the aircraft with respect to the inertial frame is equal to the derivative of the velocity vector with respect to the body frame plus the cross product of the angular velocity between the inertial and body frames and the velocity vector. The basic kinematic equation is shown in equation B-23:

$$\vec{a} = \frac{{}^{i}\vec{V}}{dt} = \frac{{}^{b}\vec{V}}{dt} + {}^{i}\vec{\omega}^{b} \times \vec{V} \tag{B-23}$$

where

- $\vec{a}$ is the acceleration of the aircraft with respect to the inertial frame.
- $\frac{{}^{i}\vec{V}}{dt}$ is the time derivative of the velocity vector with respect to the inertial frame.
- $\frac{{}^{b}\vec{V}}{dt}$ is the derivative of the velocity vector with respect to the body frame.
- ${}^{i}\vec{\omega}^{b}$ is the angular velocity: ${}^{i}\vec{\omega}^{b} = p\hat{x}_b + q\hat{y}_b + r\hat{z}_b$.
- $\vec{V}$ is the velocity vector: $\vec{V} = u\hat{x}_b + v\hat{y}_b + w\hat{z}_b$.

The expression for the aircraft's acceleration is shown in equation B-24 and simplified in equation B-25.

$$\frac{{}^{i}\vec{V}}{dt} = \dot{u}\hat{x}_b + \dot{v}\hat{y}_b + \dot{w}\hat{z}_b + \left(p\hat{x}_b + q\hat{y}_b + r\hat{z}_b\right) \times \left(u\hat{x}_b + v\hat{y}_b + w\hat{z}_b\right) \tag{B-24}$$

$$\frac{{}^{i}\vec{V}}{dt} = \left(\dot{u} + qw - rv\right)\hat{x}_b + \left(\dot{v} + ru - pw\right)\hat{y}_b + \left(\dot{w} + pv - qu\right)\hat{z}_b \tag{B-25}$$

To complete the EOMs, the acceleration terms must equate to the applied forces according to Newton's second law ($F=ma$). Table B-1 summarizes the aerodynamic forces applied to the aircraft; however, the aircraft weight must also be considered. The aircraft's weight always acts downward in the $\hat{z}_i$ direction. Using the direction cosine matrix, the aircraft's weight (mg) can be represented in body frame coordinates, as shown in equation B-26:

$$mg\hat{z}_i = mgS_\theta\hat{x}_b + mgC_\theta S_\phi\hat{y}_b + mgC_\theta C_\phi\hat{z}_b \tag{B-26}$$

where

- m is the aircraft's mass and g is the gravitational acceleration.

Summing the forces and equating the force terms yields the final expression, as shown in equation B-27:

$$\begin{aligned}&\left(X - mgS_\theta\right)\hat{x}_b + \left(Y + mgC_\theta S_\phi\right)\hat{y}_b + \left(Z + mgC_\theta S_\phi\right)\hat{z}_b \\ &= m\left(\dot{u} + qw - rv\right)\hat{x}_b + m\left(\dot{v} + ru - pw\right)\hat{y}_b + m\left(\dot{w} + pv - qu\right)\hat{z}_b\end{aligned} \tag{B-27}$$

Equation B-27 can be broken down into its individual components to yield the three force EOMs, as shown in equations B-28 through B-30.

$$X - mgS_\theta = m\left(\dot{u} + qw - rv\right) \tag{B-28}$$

$$Y + mgC_\theta S_\phi = m\left(\dot{v} + ru - pw\right) \tag{B-29}$$

$$Z + mgC_\theta C_\phi = m\left(\dot{w} + pv - qu\right) \tag{B-30}$$

The moment equations are equal to the time rate of change of angular momentum. The angular momentum of the aircraft is equal to the inertia matrix multiplied by the angular velocities. The expression for angular momentum is shown in equation B-31, in which the symbol H is used to denote the angular momentum:

$$\begin{bmatrix} H_x \\ H_y \\ H_z \end{bmatrix} = \begin{bmatrix} I_x & 0 & -I_{xz} \\ 0 & I_y & 0 \\ -I_{zx} & 0 & I_z \end{bmatrix} \begin{bmatrix} p\hat{x}_b \\ q\hat{y}_b \\ r\hat{z}_b \end{bmatrix} \tag{B-31}$$

Because aircraft are symmetric, two products of inertia, I_{yz} and I_{xy}, are zero, and therefore are eliminated from the angular momentum expression. Equation B-31 can be expanded to three scalar equations, as shown in equations B-32 through B-34.

$$H_x = I_x p\hat{x}_b - I_{xz} r\hat{z}_b \tag{B-32}$$

$$H_y = I_y q\hat{y}_b \tag{B-33}$$

$$H_z = -I_{zx} p\hat{x}_b + I_z r\hat{z}_b \tag{B-34}$$

The time rate of change of each of these expressions is calculated using the basic kinematic equation of the form shown in equation B-35.

$$\frac{{}^i d\vec{H}}{dt} = \frac{{}^b d\vec{H}}{dt} + {}^i\omega^b \times \vec{H} \tag{B-35}$$

When the kinematic expressions are summed to their respective moments, the three moment equations are derived. They are shown in equations B-36 through B-38. For convenience, table B-2 summarizes the fundamental kinematic and dynamic EOMs:

$$\overline{L} = I_x \dot{p} - I_{xz}(\dot{r} + pq) + qr\left(I_z - I_y\right) \tag{B-36}$$

$$M = I_y \dot{q} + rp\left(I_x - I_z\right) + I_{xz}\left(p^2 - r^2\right) \tag{B-37}$$

$$N = -I_{xz}\dot{p} + I_z \dot{r} + pq\left(I_y - I_x\right) + I_{xz} qr \tag{B-38}$$

Table B-2. Summary of Kinematic and Dynamic Equations of Motion

Grouping	Equations
Force equations	$X - mgS_\theta = m\left(\dot{u} + qw - rv\right)$ (B-28) $Y + mgC_\theta S_\phi = m\left(\dot{v} + ru - pw\right)$ (B-29) $Z + mgC_\theta C_\phi = m\left(\dot{w} + pv - qu\right)$ (B-30)
Moment equations	$L = I_x \dot{p} - I_{xz}(\dot{r} + pq) + qr\left(I_z - I_y\right)$ (B-36) $M = I_y \dot{q} + rp\left(I_x - I_z\right) + I_{xz}\left(p^2 - r^2\right)$ (B-37) $N = -I_{xz}\dot{p} + I_z \dot{r} + pq\left(I_y - I_x\right) + I_{xz} qr$ (B-38)
Body angular velocities in terms of Euler angles and Euler rates	$p = \dot{\phi} - \dot{\psi} S_\theta$ (B-39) $q = \dot{\theta} C_\phi + \dot{\psi} C_\theta S_\phi$ (B-40) $r = \dot{\psi} C_\theta C_\phi - \theta S_\phi$ (B-41)
Euler rates in terms of Euler angles and body angular velocities	$\dot{\theta} = qC_\phi - rS_\phi \; \dot{\theta} = qC_\phi - rS_\phi$ (B-42) $\dot{\phi} = p + qS_\phi T_\theta + rC_\phi T_\theta$ (B-43) $\dot{\psi} = \left(qS_\phi + rC_\theta\right)\sec\theta$ (B-44)

APPENDIX C—LINEAR FORCE MODEL

The linear force model is largely derived from the classical stability and control derivatives defined for fixed wing aircraft. The model presented here uses classical derivatives for most of the rate terms, but uses a more sophisticated buildup for lift and drag.

There are three forces and three moments that need to be considered. The expressions for force are determined first. Equations C-1 through C-3 define the static force information:

$$X = T - DC_\beta C_\alpha - Y_w S_\beta C_\alpha + LS_\alpha \tag{C-1}$$

$$Y = -DS_\beta + Y_w C_\beta \tag{C-2}$$

$$Z = -DC_\beta S_\alpha - Y_w S_\beta S_\alpha - LC_\alpha \tag{C-3}$$

The forces on the aircraft can be modeled in terms of lift, drag, side-force, and thrust. The lift of the aircraft can be simply represented in terms of the wing reference area, the dynamic pressure, and the lift coefficient:

$$L = qS_w C_L \tag{C-4}$$

The dynamic pressure is defined as follows:

$$q = \frac{1}{2}\rho V_a^{\,2} \tag{C-5}$$

where the true airspeed, V_a, is defined as $V_a = \sqrt{u^2 + V^2 + w^2}$. The lift coefficient is then defined in terms of the many terms that comprise it. The rate terms are nondimensionalized differently than the static terms. Therefore, an additional factor of $\bar{c}/2u$ appears where required. A description of each derivative is given in table C-1.

$$C_L = C_{L_0} + C_{L_u} u + C_{L_\alpha} \alpha + \frac{\bar{c}}{2u} C_{L_{\dot\alpha}} \dot\alpha + \frac{\bar{c}}{2u} C_{L_q} q + C_{L_{\delta e}} \delta_e \tag{C-6}$$

Table C-1. Summary of Lift Coefficient Derivatives

Derivative	Description
C_{L_0}	The lift coefficient at zero degrees AoA. This derivative represents the effects of a cambered wing.
C_{L_u}	The change in lift coefficient with changes in speed. Usually zero for low-mach numbers.
C_{L_α}	The change in the lift coefficient with respect to changes in the AoA. Closely related to the lift curve slope of the wing.
$C_{L_{\dot{\alpha}}}$	The change in lift coefficient with respect to $\dot{\alpha}$ due to the aircraft plunging up and down.
C_{L_q}	The change in lift coefficient with respect to pitch rate. Note that there is a difference between $\dot{\alpha}$ and q.
$C_{L_{\delta e}}$	The change in lift coefficient with respect to changes in the elevator deflection.

Similarly, the drag can be computed as shown in equation C-7. The drag coefficient can be calculated as shown in equation C-8, which is a simple parabolic drag polar:

$$D = qS_w C_D \tag{C-7}$$

$$C_D = C_{D_0} + KC_L{}^2 \tag{C-8}$$

The side force on the aircraft is represented in equation C-9 with the side force coefficient, C_Y, being represented by equation C-10. The derivatives are defined in table C-2:

$$Y_w = qS_w C_Y \tag{C-9}$$

$$C_Y = C_{y\beta}\beta + \frac{b_w}{2u_o} C_{y_p} p + \frac{b_w}{2u_o} C_{y_r} r + C_{y\delta_a}\delta_r \tag{C-10}$$

Table C-2. Stability and Control Derivatives for the Side-Force Equation

Derivative	Definition
$C_{y\beta}$	Variation of side-force with sideslip angle.
C_{y_p}	Variation of side-force with roll rate.
C_{y_r}	Variation of side-force with yaw rate.
$C_{y\delta_a}$	Variation of side-force with aileron deflection.
$C_{y\delta_r}$	Variation of side-force with rudder deflection.

The three moments, *L*, *M*, and *N*, are defined to be about the body axes.

$$L = qS_w b_w C_l \tag{C-11}$$

$$M = qS_w \bar{c}_w C_m \tag{C-12}$$

$$N = qS_w b_w C_n \tag{C-13}$$

The coefficients C_l, C_m, and C_n are defined below in equations C-14 through C-16. The stability and control derivatives are defined in tables C-3 through C-5.

$$C_l = C_{l_\beta}\beta + \frac{b}{2u_o}C_{l_p}p + \frac{b}{2u_o}C_{l_r}r + C_{l_{\delta a}}\delta_a + C_{l_{\delta r}}\delta_r \tag{C-14}$$

$$C_m = C_{m0} + C_{m_\alpha}\alpha + \frac{\bar{c}_w}{2u_o}C_{m_{\dot{\alpha}}}\dot{\alpha} + \frac{\bar{c}_w}{2u_o}C_{m_q}q + C_{m_{\delta e}}\delta_e \tag{C-15}$$

$$C_n = C_{n_\beta}\beta + \frac{b}{2u_o}C_{n_p}p + \frac{b}{2u_o}C_{n_r}r + C_{n_{\delta a}}\delta_a + C_{n_{\delta r}}\delta_r \tag{C-16}$$

Table C-3. The Rolling Moment Stability and Control Derivatives

Derivative	Description
C_{l_β}	The variation in the rolling moment with variations in side-slip.
C_{l_p}	The variation in the rolling moment with variations in roll rate.
C_{l_r}	The variation in the rolling moment with variations in yaw rate.
$C_{l_{\delta a}}$	The variation in the rolling moment with aileron deflection.
$C_{l_{\delta r}}$	The variation in the rolling moment with rudder deflection.

Table C-4. The Pitching Moment Stability and Control Derivatives

Derivative	Description
C_{m_0}	The zero AoA pitching moment.
C_{m_α}	The variation in the pitching moment with variations in α.
$C_{m_{\dot{\alpha}}}$	The variation in the pitching moment with variations in $\dot{\alpha}$.
C_{m_q}	The variation in the pitching moment with variations in pitch rate.
$C_{m_{\delta e}}$	The variation in the pitching moment with elevator deflection.

Table C-5. The Yawing Moment Stability and Control Derivatives

Derivative	Description
C_{n_β}	The variation in the yawing moment with variations in sideslip.
C_{n_p}	The variation in the yawing moment with variations in roll rate.
C_{n_r}	The variation in the yawing moment with variations in yaw rate.
$C_{n_{\delta a}}$	The variation in the yawing moment with aileron deflection.
$C_{n_{\delta r}}$	The variation in the yawing moment with rudder deflection.

APPENDIX D—LINEARIZATION OF LONGITUDINAL DYNAMICS

To perform classical feedback control analysis of the aircraft dynamics, a linear model must be developed for the longitudinal dynamics. This section outlines the development of the model and the associated stability and control derivative definitions.

From the development of the equations of motion, the relevant longitudinal equations are assembled in first order form so that the derivative terms are isolated. The four states for the system are $\begin{bmatrix} u & w & q & \theta \end{bmatrix}^T$:

$$\dot{u} = \frac{X}{m} - gS_\theta - qw + rv \tag{D-1}$$

$$\dot{w} = \frac{Z + mgC_\theta C_\phi}{m} - pv + qu \tag{D-2}$$

$$\dot{q} = \frac{M}{I_y} - rp\frac{\left(I_x - I_z\right)}{I_y} - \frac{I_{xz}}{I_y}\left(p^2 - r^2\right) \tag{D-3}$$

$$\dot{\theta} = qC_\phi - rS_\phi \tag{D-4}$$

First, simplify the expressions by setting lateral directional terms (p, r, ϕ) to zero:

$$\dot{u} = \frac{X}{m} - gS_\theta - qw \tag{D-5}$$

$$\dot{w} = \frac{Z + mgC_\theta C_\phi}{m} + qu \tag{D-6}$$

$$\dot{q} = \frac{M}{I_y} \tag{D-7}$$

$$\dot{\theta} = qC_\phi - rS_\phi \tag{D-8}$$

A formal linearization process requires that the partial derivative of each expression be taken numerous times. To maintain proper bookkeeping on terms, some implicit expressions are defined to represent equations D-5 through D-8. Because the applied forces and moments (X, Z, M) are also functions of control inputs, control input terms, which are not state variables, must also be included:

$$\dot{u} = f_u\left(u, w, q, \theta, \dot{u}, \dot{w}, \dot{q}, \dot{\theta}, \delta_e, \delta_p\right) \tag{D-9}$$

$$\dot{w} = f_w\left(u, w, q, \theta, \dot{u}, \dot{w}, \dot{q}, \dot{\theta}, \delta_e, \delta_p\right) \tag{D-10}$$

$$\dot{q} = f_q\left(u, w, q, \theta, \dot{u}, \dot{w}, \dot{q}, \dot{\theta}, \delta_e, \delta_p\right) \tag{D-11}$$

$$\dot{\theta} = f_\theta\left(u, w, q, \theta, \dot{u}, \dot{w}, \dot{q}, \dot{\theta}, \delta_e, \delta_p\right) \tag{D-12}$$

Linearization is implicitly represented by equations D-13 through D-16. Whereas it is possible for the linearized expressions to have terms that are a function of the derivatives of states, in only one instance does this actually occur $\left(\Delta\dot{w}\right)$. To simplify the expressions, only the existing term is included. The '$_o$' subscript is used to indicate a function, derivative, or state variable evaluated at the reference condition:

$$\dot{u}\big|_o + \Delta\dot{u} \cong f_u\big|_o + \frac{\partial f_u}{\partial u}\bigg|_o \Delta u + \frac{\partial f_u}{\partial w}\bigg|_o \Delta w + \frac{\partial f_u}{\partial q}\bigg|_o \Delta q + \frac{\partial f_u}{\partial \theta}\bigg|_o \Delta\theta + \frac{\partial f_u}{\partial \delta_e}\bigg|_o \Delta\delta_e + \frac{\partial f_u}{\partial \delta_p}\bigg|_o \Delta\delta_p \tag{D-13}$$

$$\dot{w}\big|_o + \Delta\dot{w} \cong f_u\big|_o + \frac{\partial f_w}{\partial u}\bigg|_o \Delta u + \frac{\partial f_w}{\partial w}\bigg|_o \Delta w + \frac{\partial f_w}{\partial q}\bigg|_o \Delta q + \frac{\partial f_w}{\partial \theta}\bigg|_o \Delta\theta + \frac{\partial f_w}{\partial \delta_e}\bigg|_o \Delta\delta_e + \frac{\partial f_w}{\partial \delta_p}\bigg|_o \Delta\delta_p \tag{D-14}$$

$$\dot{q}\big|_o + \Delta\dot{q} \cong f_u\big|_o + \frac{\partial f_q}{\partial u}\bigg|_o \Delta u + \frac{\partial f_q}{\partial w}\bigg|_o \Delta w + \frac{\partial f_q}{\partial q}\bigg|_o \Delta q + \frac{\partial f_q}{\partial \theta}\bigg|_o \Delta\theta + \frac{\partial f_q}{\partial \dot{w}}\bigg|_o \Delta\dot{w} + \frac{\partial f_q}{\partial \delta_e}\bigg|_o \Delta\delta_e + \frac{\partial f_q}{\partial \delta_p}\bigg|_o \Delta\delta_p \tag{D-15}$$

$$\dot{\theta}\big|_o + \Delta\dot{\theta} \cong f_u\big|_o + \frac{\partial f_\theta}{\partial u}\bigg|_o \Delta u + \frac{\partial f_\theta}{\partial w}\bigg|_o \Delta w + \frac{\partial f_\theta}{\partial q}\bigg|_o \Delta q + \frac{\partial f_\theta}{\partial \theta}\bigg|_o \Delta\theta + \frac{\partial f_\theta}{\partial \delta_e}\bigg|_o \Delta\delta_e + \frac{\partial f_\theta}{\partial \delta_p}\bigg|_o \Delta\delta_p \tag{D-16}$$

Because the value of a particular function at the reference condition is by definition equal to the reference value of its derivative (e.g., $\dot{u}\big|_o = f_u\big|_o$), these terms can be eliminated from the expressions:

$$\Delta\dot{u} \cong \frac{\partial f_u}{\partial u}\bigg|_o \Delta u + \frac{\partial f_u}{\partial w}\bigg|_o \Delta w + \frac{\partial f_u}{\partial q}\bigg|_o \Delta q + \frac{\partial f_u}{\partial \theta}\bigg|_o \Delta\theta + \frac{\partial f_u}{\partial \delta_e}\bigg|_o \Delta\delta_e + \frac{\partial f_u}{\partial \delta_p}\bigg|_o \Delta\delta_p \tag{D-17}$$

$$\Delta\dot{w} \cong \frac{\partial f_w}{\partial u}\bigg|_o \Delta u + \frac{\partial f_w}{\partial w}\bigg|_o \Delta w + \frac{\partial f_w}{\partial q}\bigg|_o \Delta q + \frac{\partial f_w}{\partial \theta}\bigg|_o \Delta\theta + \frac{\partial f_w}{\partial \delta_e}\bigg|_o \Delta\delta_e + \frac{\partial f_w}{\partial \delta_p}\bigg|_o \Delta\delta_p \tag{D-18}$$

$$\Delta\dot{q} \cong \frac{\partial f_q}{\partial u}\bigg|_o \Delta u + \frac{\partial f_q}{\partial w}\bigg|_o \Delta w + \frac{\partial f_q}{\partial q}\bigg|_o \Delta q + \frac{\partial f_q}{\partial \theta}\bigg|_o \Delta\theta + \frac{\partial f_q}{\partial \dot{w}}\bigg|_o \Delta\dot{w} + \frac{\partial f_q}{\partial \delta_e}\bigg|_o \Delta\delta_e + \frac{\partial f_q}{\partial \delta_p}\bigg|_o \Delta\delta_p \tag{D-19}$$

$$\Delta\dot{\theta} \cong \left.\frac{\partial f_\theta}{\partial u}\right|_o \Delta u + \left.\frac{\partial f_\theta}{\partial w}\right|_o \Delta w + \left.\frac{\partial f_\theta}{\partial q}\right|_o \Delta q + \left.\frac{\partial f_\theta}{\partial \theta}\right|_o \Delta\theta + \left.\frac{\partial f_\theta}{\partial \delta_e}\right|_o \Delta\delta_e + \left.\frac{\partial f_\theta}{\partial \delta_p}\right|_o \Delta\delta_p \qquad \text{(D-20)}$$

Therefore, there are 17 potential stability derivatives (those that are a function of state variables) for the longitudinal dynamics and eight potential control derivatives. Tables D-1 through D-4 contain the various stability derivatives. In cases of q, w, and θ, these are usually assumed to be small; however, u_o, the reference speed of the aircraft, is not neglected. As is convention, where mass properties are present, the mass terms are included in the definition of the derivative.

Table D-1. Derivatives of f_u

Derivative	Description
$\frac{\partial f_u}{\partial u}$	$= \frac{1}{m}\frac{\partial X}{\partial u} = X_u$
$\frac{\partial f_u}{\partial w}$	$= \frac{1}{m}\frac{\partial X}{\partial w} - q_o = X_w - q_o = X_w$ (q_o reference pitch rate is zero)
$\frac{\partial f_u}{\partial q}$	$\frac{1}{m}\frac{\partial X}{\partial q} - w_o = -w_o = 0$ (w_o reference z-axis velocity is zero)
$\frac{\partial f_u}{\partial \theta}$	$\frac{1}{m}\frac{\partial X}{\partial \theta} - gC_{\theta_o} = -gC_{\theta_o} = -g$

Table D-2. Derivatives of f_w

Derivative	Description
$\frac{\partial f_w}{\partial u}$	$\frac{1}{m}\frac{\partial Z}{\partial u} + q_o = Z_u + q_o = Z_u$
$\frac{\partial f_w}{\partial w}$	$\frac{1}{m}\frac{\partial Z}{\partial w} = Z_w$
$\frac{\partial f_w}{\partial q}$	$\frac{1}{m}\frac{\partial Z}{\partial q} + u_o = u_o$
$\frac{\partial f_w}{\partial \theta}$	$= \frac{1}{m}\frac{\partial Z}{\partial \theta} - gS_\theta = -gS_\theta = 0$

Table D-3. Derivatives of f_q

Derivative	Description
$\frac{\partial f_q}{\partial u}$	$\frac{1}{I_y}\frac{\partial M}{\partial u} = M_u$
$\frac{\partial f_q}{\partial w}$	$\frac{1}{I_y}\frac{\partial M}{\partial w} = M_w$
$\frac{\partial f_q}{\partial q}$	$\frac{1}{I_y}\frac{\partial M}{\partial q} = M_q$
$\frac{\partial f_q}{\partial \theta}$	$\frac{1}{I_y}\frac{\partial M}{\partial \theta} = 0$
$\frac{\partial f_q}{\partial \dot{w}}$	$\frac{1}{I_y}\frac{\partial M}{\partial \dot{w}} = M_{\dot{w}}$

Table D-4. Derivatives of f_θ

Derivative	Description
$\frac{\partial f_\theta}{\partial u}$	0
$\frac{\partial f_\theta}{\partial w}$	0
$\frac{\partial f_\theta}{\partial q}$	1
$\frac{\partial f_\theta}{\partial \theta}$	0

$$\Delta\dot{u} \cong X_u \Delta u + X_w \Delta w - g\Delta\theta + X_{\delta_e}\Delta\delta_e + X_{\delta_p}\Delta\delta_p \tag{D-21}$$

$$\Delta\dot{w} \cong Z_u \Delta u + Z_w \Delta w + u_o \Delta q + Z_{\delta_e}\Delta\delta_e + Z_{\delta_p}\Delta\delta_p \tag{D-22}$$

$$\Delta\dot{q} \cong M_u \Delta u + M_w \Delta w + M_q \Delta q + M_{\dot{w}}\Delta\dot{w} + M_{\delta_e}\Delta\delta_e + M_{\delta_p}\Delta\delta_p \tag{D-23}$$

$$\Delta\dot{\theta} \cong \Delta q \tag{D-24}$$

Because Δw is not as convenient as using AoA, one final change is made. Using the approximation for AoA shown in equation D-25, a new expression is determined. At this level Δw and $\Delta\alpha$ can be thought to differ only in magnitude by a static constant u_o:

$$\alpha = \tan^{-1}\frac{w}{u} \approx \frac{w}{u} \qquad \Delta\alpha \cong \frac{\Delta w}{u} \rightarrow \Delta w \cong u_o \Delta\alpha \tag{D-25}$$

Additionally, the derivatives are defined to have the following relationships:

$$Z_\alpha = u_o Z_w \qquad M_\alpha = u_o M_w \qquad M_{\dot{\alpha}} = u_o M_{\dot{w}}$$

Modifying equation D-21 results in equation D-26:

$$\Delta\dot{u} \cong X_u \Delta u + X_w u_o \Delta\alpha - g\Delta\theta + X_{\delta_e}\Delta\delta_e + X_{\delta_p}\Delta\delta_p \tag{D-26}$$

Modifying equation D-22 results in equation D-27.

$$u_o \Delta\dot{\alpha} \cong Z_u \Delta u + Z_w u_o \Delta\alpha + u_o \Delta q + Z_{\delta_e}\Delta\delta_e + Z_{\delta_p}\Delta\delta_p$$

$$u_o \Delta\dot{\alpha} \cong Z_u \Delta u + Z_\alpha \Delta\alpha + u_o \Delta q + Z_{\delta_e}\Delta\delta_e + Z_{\delta_p}\Delta\delta_p$$

$$\Delta\dot{\alpha} \cong \frac{Z_u}{u_o}\Delta u + Z_u \Delta u + \frac{Z_\alpha}{u_o}\Delta\alpha + \Delta q + \frac{Z_{\delta_e}}{u_o}\Delta\delta_e + \frac{Z_{\delta_p}}{u_o}\Delta\delta_p \tag{D-27}$$

Modifying equation D-23 results in equation D-28.

$$\Delta\dot{q} \cong M_u \Delta u + M_w \Delta w + M_q \Delta q + M_{\dot{w}} u_o \Delta\dot{\alpha} + M_{\delta_e}\Delta\delta_e + M_{\delta_p}\Delta\delta_p$$

$$\Delta\dot{q} \cong M_u \Delta u + M_w \Delta w + M_q \Delta q + M_{\dot{\alpha}} \Delta\dot{\alpha} + M_{\delta_e}\Delta\delta_e + M_{\delta_p}\Delta\delta_p \tag{D-28}$$

One problem with the expressions is the inclusion of the $\Delta\dot{\alpha}$ term in the pitch rate equation. To eliminate this problem, the $\Delta\dot{w}$ equation is substituted into the pitch rate equation:

$$\Delta\dot{q} \cong M_u \Delta u + M_w \Delta w + M_q \Delta q + M_{\dot{\alpha}}\left(\frac{Z_u}{u_o}\Delta u + \frac{Z_\alpha}{u_o}\Delta\alpha + \Delta q + \frac{Z_{\delta_p}}{u_o}\Delta\delta_p\right) + M_{\delta_e}\Delta\delta_e + M_{\delta_p}\Delta\delta_p \tag{D-29}$$

$$\Delta\dot{q} \cong M_u \Delta u + M_w u_o \Delta\alpha + M_q \Delta q + \frac{M_{\dot{\alpha}} Z_u}{u_o}\Delta u + \frac{M_{\dot{\alpha}} Z_\alpha}{u_o}\Delta\alpha + M_{\dot{\alpha}}\Delta q + \frac{M_{\dot{\alpha}} Z_{\delta_e}}{u_o}\Delta\delta_e + \frac{M_{\dot{\alpha}} Z_{\delta_p}}{u_o}\Delta\delta_p + M_{\delta_e}\Delta\delta_e + M_{\delta_p}\Delta\delta_p$$

$$\Delta\dot{q} \cong \left(M_u + \frac{M_{\dot{\alpha}} Z_u}{u_o} \right) \Delta u + \left(M_\alpha + \frac{M_{\dot{\alpha}} Z_\alpha}{u_o} \right) \Delta\alpha + \left(M_q + M_{\dot{\alpha}} \right) \Delta q + \left(M_{\delta_e} + \frac{M_{\dot{\alpha}} Z_{\delta_e}}{u_o} \right) \Delta\delta_e$$

$$+ \left(M_{\delta_p} + \frac{M_{\dot{\alpha}} Z_{\delta_p}}{u_o} \right) \Delta\delta_p$$

Arranging in state space form leads to equation D-30.

$$\begin{bmatrix} \Delta\dot{u} \\ \Delta\dot{\alpha} \\ \Delta\dot{q} \\ \Delta\dot{\theta} \end{bmatrix} = \begin{bmatrix} X_u & X_w u_o & 0 & -g \\ \frac{Z_u}{u_o} & \frac{Z_\alpha}{u_o} & 1 & 0 \\ M_u + \frac{M_{\dot{\alpha}} Z_u}{u_o} & M_\alpha + \frac{M_{\dot{\alpha}} Z_\alpha}{u_o} & M_q + M_{\dot{\alpha}} & 0 \\ 0 & 0 & 1 & 0 \end{bmatrix} \begin{bmatrix} \Delta u \\ \Delta\alpha \\ \Delta q \\ \Delta\theta \end{bmatrix}$$

$$+ \begin{bmatrix} X_{\delta_e} & X_{\delta_p} \\ \frac{Z_{\delta_e}}{u_o} & \frac{Z_{\delta_p}}{u_o} \\ M_{\delta_e} + \frac{M_{\dot{\alpha}} Z_{\delta_e}}{u_o} & M_{\delta_p} + \frac{M_{\dot{\alpha}} Z_{\delta_p}}{u_o} \\ 0 & 0 \end{bmatrix} \begin{bmatrix} \Delta\delta_e \\ \Delta\delta_p \end{bmatrix} \tag{D-30}$$

D.1 DERIVATIVE ANALYSIS.

The prior section developed the need for eight dimensional derivatives to complete the model. This section provides the development of these terms. The moment equations agree with the classical definitions, but the force definitions in some cases are different. For this reason, the force equations are derived.

D.2 FORCE EXPRESSIONS.

D.2.1 X_u.

The term X_u represents X force change with forward velocity. The X force equation is shown implicitly in equation D-31.

$$\frac{\partial X}{\partial u} = \frac{\partial}{\partial u} \left(T - DC_\beta C_\alpha - YS_\beta C_\alpha + LS_\alpha \right) \tag{D-31}$$

Some basic engine effects were included in our definition, so substitute equation D-32 was substituted for thrust:

$$T = \frac{550\eta_p P}{u} \tag{D-32}$$

Instead of u, V was used in our expression for dynamic pressure to simplify the mathematics:

$$\frac{\partial X}{\partial u} = \frac{\partial}{\partial u}\left(\frac{550\eta_p P}{u} - \frac{1}{2}\rho u^2 S_w\left(C_{D_o} + KC_L{}^2\right)C_\beta C_\alpha + \frac{1}{2}\rho u^2 S_w\left(C_L\right)S_\alpha\right)$$

$$\frac{\partial X}{\partial u} = \frac{\partial}{\partial u}\left(\frac{550\eta_p P}{u} + \frac{1}{2}\rho u^2 S_w\left(C_L S_\alpha - \left(C_{D_o} + KC_L{}^2\right)C_\beta C_\alpha\right)\right)$$

$$\frac{\partial X}{\partial u} = \frac{\partial}{\partial u}\left(\frac{-550\eta_p P}{u} + \rho u S_w\left(C_L S_\alpha - \left(C_{D_o} + KC_L{}^2\right)C_\beta C_\alpha\right)\right)$$

Collecting terms, adding in the mass properties, and discounting irrelevant terms lead to equation D-33.

$$X_u = \frac{1}{m}\left(\left.\frac{-550\eta_p P}{u}\right|_o + \frac{2}{u}qS_w\left(C_L S_\alpha - \left(C_{D_o} + KC_L{}^2\right)C_\alpha\right)\Big|_o\right) \tag{D-33}$$

$$X_u = \frac{1}{m}\left(\left.\frac{-550\eta_p P}{u}\right|_o - qS_w\left.\frac{2C_D}{u}\right|_o\right) \tag{D-34}$$

<u>D.2.2 X_w</u>.

The term X_w represents X force change with the w body velocity. This velocity is directly related to α, and it is more convenient to initially work with α. The X force derivative is shown implicitly in equation D-35:

$$\frac{\partial X}{\partial u} = \frac{\partial}{\partial u}\left(\frac{550\eta_p P}{u} - qS_w C_D C_\alpha + qS_w\left(C_L\right)S_\alpha\right) \tag{D-35}$$

Taking the derivative,

$$\frac{\partial X}{\partial \alpha} = \frac{\partial}{\partial \alpha}\left(\frac{550\eta_p P}{u} - qS_w C_D C_\alpha + qS_w\left(C_L\right)S_\alpha\right)$$

$$\frac{\partial X}{\partial u} = \left(-qS_w C_{D_\alpha} C_\alpha + qS_w C_D S_\alpha + qS_w C_L C_\alpha + qS_w \frac{dC_L}{d\alpha} S_\alpha\right)$$

Converting to *w* and adding in the mass term leads to equation D-38.

$$\frac{\partial X}{\partial \frac{w}{u_o}} = \frac{1}{m}\left(-qS_w C_{D_\alpha} C_\alpha + qS_w C_D S_\alpha + qS_w C_L C_\alpha + qS_w \frac{dC_L}{d\alpha} S_\alpha\right) \tag{D-36}$$

$$X_w = \frac{1}{mu_o}\left(-qS_w C_{D_\alpha} C_\alpha + qS_w C_D S_\alpha + qS_w C_L C_\alpha + qS_w \frac{dC_L}{d\alpha} S_\alpha\right)\Bigg|_o \tag{D-37}$$

$$X_w = \frac{-qS_w}{mu_o}\left(C_{D_\alpha} C_\alpha - C_D S_\alpha - C_L C_\alpha - \frac{dC_L}{d\alpha} S_\alpha\right)\Bigg|_o \tag{D-38}$$

If α is assumed to be small, the expression reduces to equation D-39:

$$X_w = \frac{-qS_w}{mu_o}\left(C_{D_\alpha} - C_L\right) \tag{D-39}$$

An explicit expression for C_{D_α} can be computed from the drag polar and is shown in equation D-40:

$$\begin{aligned}
C_{D_\alpha} &= \frac{\partial}{\partial \alpha}\left(C_{D_o} + KC_L{}^2\right) \\
C_{D_\alpha} &= 2KC_L \frac{dC_L}{d\alpha} \\
C_{D_\alpha} &= 2KC_L C_{L_\alpha} \\
C_{D_\alpha} &= 2KC_L C_{L_\alpha}\Big|_o
\end{aligned} \tag{D-40}$$

D.2.3 Z_u.

The derivative Z_u relates change in Z force with changes in speed:

$$Z = -DS_\alpha - LC_\alpha \tag{D-41}$$

$$Z = -\frac{1}{2}\rho u^2 S_w C_D S_\alpha - \frac{1}{2}\rho u^2 S_w C_L S_\alpha \tag{D-42}$$

Taking the derivative leads to equation D-43:

$$\frac{\partial Z}{\partial u} = -\rho u S_w C_D S_\alpha - \frac{1}{2}\rho u^2 S_w C_{D_u} S_\alpha - \frac{1}{2}\rho u^2 S_w C_{L_u} C_\alpha - \rho u S_w C_L C_\alpha$$

$$Z_u = -\rho u S_w \left(C_D S_\alpha + C_L C_\alpha\right) - \frac{1}{2}\rho u^2 S_w \left(C_{D_u} S_\alpha - C_{L_u} C_\alpha\right) \tag{D-43}$$

Assuming a small AoA leads to equation D-44:

$$Z_u = -\frac{2q}{u_o} S_w \left(C_L\right) - qS_w \left(-C_{L_u}\right)$$

$$Z_u = -qS_w \left(\frac{2C_L}{u_o} + C_{L_u}\right) \tag{D-44}$$

D.2.4 Z_α.

The term Z_α relates the change in Z-force to changes in AoA. Taking the derivative leads to equation D-45:

$$Z = -DS_\alpha - LC_\alpha$$

$$Z = -qS_w C_D S_\alpha - qS_w C_L C_\alpha$$

$$\frac{\partial Z}{\partial u} = \frac{\partial}{\partial u}\left(-qS_w C_D S_\alpha - qS_w C_L C_\alpha\right)$$

$$\frac{\partial Z}{\partial u} = -qS_w C_D C_\alpha - qS_w C_{D_\alpha} S_\alpha + qS_w C_L S_\alpha - qS_w C_{L_\alpha} C_\alpha$$

$$Z_\alpha = -qS_wC_DC_\alpha - qS_wC_{D_\alpha}S_\alpha + qS_wC_LS_\alpha - qS_wC_{L_\alpha}C_\alpha \tag{D-45}$$

Assuming a small AoA leads to equation D-46.

$$\frac{\partial Z}{\partial u} = -qS_wC_D - qS_wC_{L_\alpha}$$

$$Z_\alpha = \frac{-qS_w}{m}\left(C_D + C_{L_\alpha}\right) \tag{D-46}$$

D.3. DERIVATIVE SUMMARY.

Tables D-5 and D-6 contain summaries of the derivatives used.

Table D-5. Summary of Dimensional Derivatives

Derivative
$X_u = \frac{1}{m}\left(\left.\frac{-550\eta_p P}{u^2}\right\|_o + \frac{2}{u}qS_w\left(C_LS_\alpha - \left(C_{D_o} + KC_L{}^2\right)C_\alpha\right)\Big\|_o\right)$
$X_w = \frac{-qS_w}{mu_o}\left(C_{D_\alpha}C_\alpha - C_DS_\alpha - C_LC_\alpha - \frac{dC_L}{d\alpha}S_\alpha\right)\Big\|_o$
$Z_u = -\rho uS_wC_DS_\alpha - \frac{1}{2}\rho u^2S_wC_{D_u}S_\alpha - \rho uS_wC_LC_\alpha - \frac{1}{2}\rho u^2S_wC_{L_u}C_\alpha\Big\|_o$
$Z_\alpha = -qS_wC_DC_\alpha - qS_wC_{D_\alpha}S_\alpha + qS_wC_LS_\alpha - qS_wC_{L_\alpha}C_\alpha\Big\|_o$
$M_u = C_{m_u}\frac{qS_w\bar{c}}{u_oI_y}$
$M_\alpha = C_{m_\alpha}\frac{qS_w\bar{c}}{I_y}$
$M_\alpha = C_{m_\alpha}\frac{qS_w\bar{c}}{I_y}\left(\frac{\bar{c}}{2u_o}\right)$
$M_q = C_{m_q}\frac{qS_w\bar{c}}{I_y}\left(\frac{\bar{c}}{2u_o}\right)$

Table D-6. Summary of Dimensional Derivatives Assuming Small Alpha

Derivative
$X_u = \frac{1}{m}\left(\left.\frac{-550\eta_p P}{u^2}\right\|_o - qS_w \left.\frac{2C_D}{u}\right\|_o \right)$
$X_w = \frac{-qS_w}{mu_o}\left(C_{D_\alpha} - C_L\right)$
$Z_u = -qS_w\left(\frac{2C_L}{u_o} + C_{L_u}\right)$
$Z_\alpha = \frac{-qS_w}{m}\left(C_D + C_{L_\alpha}\right)$
$M_u = C_{m_u}\frac{qS_w\bar{c}}{u_o I_y}$
$M_\alpha = C_{m_\alpha}\frac{qS_w\bar{c}}{I_y}$
$M_\alpha = C_{m_\alpha}\frac{qS_w\bar{c}}{I_y}\left(\frac{\bar{c}}{2u_o}\right)$
$M_q = C_{m_q}\frac{qS_w\bar{c}}{I_y}\left(\frac{\bar{c}}{2u_o}\right)$

APPENDIX E—LINEARIZATION OF LATERAL DYNAMICS

To perform classical feedback control analysis of the aircraft dynamics, a linear model must be developed for the lateral dynamics. This section outlines the development of the model and the associated stability and control derivative definitions.

From the development of the equations of motion (EOMs) of the main document, the relevant longitudinal equations are assembled in first order form so that the derivative terms are isolated. The four states for the system are $[v\ p\ r\ \phi]^T$. It is assumed that the product of inertia, I_{xz}, is small.

The nonlinear EOMs are represented in equations E-1 through E-4.

$$\dot{v} = \frac{Y}{m} + gC_\theta S_\phi - ru + pw \tag{E-1}$$

$$\dot{p} = \frac{L}{I_x} - qr\frac{\left(I_z - I_y\right)}{I_x} \tag{E-2}$$

$$\dot{r} = \frac{N}{I_z} - pq\frac{\left(I_y - I_x\right)}{I_z} \tag{E-3}$$

$$\dot{\phi} = p + qS_\phi T_\theta + rC_\phi T_\theta \tag{E-4}$$

The formal linearization process requires that the partial derivative of each expression be taken numerous times. To maintain proper bookkeeping on terms, some implicit expressions are defined to represent equations E-1 through E-4. Derivatives are listed in tables E-1 through E-7.

$$\dot{v} = f_v\left(v, p, r, \phi, \delta_a, \delta_r\right) \tag{E-5}$$

$$\dot{p} = f_p\left(v, p, r, \phi, \delta_a, \delta_r\right) \tag{E-6}$$

$$\dot{r} = f_r\left(v, p, r, \phi, \delta_a, \delta_r\right) \tag{E-7}$$

$$\dot{\phi} = f_\phi\left(v, p, r, \phi, \delta_a, \delta_r\right) \tag{E-8}$$

$$\dot{v}\Big|_o + \Delta\dot{v} = f_v\Big|_o + \frac{\partial f_v}{\partial v}\Big|_o \Delta v + \frac{\partial f_v}{\partial p}\Big|_o \Delta p + \frac{\partial f_v}{\partial r}\Big|_o \Delta r + \frac{\partial f_v}{\partial \phi}\Big|_o \Delta\phi + \frac{\partial f_v}{\partial \delta_a}\Big|_o \Delta\delta_a + \frac{\partial f_v}{\partial \delta_r}\Big|_o \Delta\delta_r \tag{E-9}$$

$$\dot{p}\Big|_o + \Delta\dot{p} = f_p\Big|_o + \frac{\partial f_p}{\partial v}\Big|_o \Delta v + \frac{\partial f_p}{\partial p}\Big|_o \Delta p + \frac{\partial f_p}{\partial r}\Big|_o \Delta r + \frac{\partial f_p}{\partial \phi}\Big|_o \Delta\phi + \frac{\partial f_p}{\partial \delta_a}\Big|_o \Delta\delta_a + \frac{\partial f_p}{\partial \delta_r}\Big|_o \Delta\delta_r \tag{E-10}$$

$$\dot{r}\Big|_o + \Delta\dot{r} = f_r\Big|_o + \frac{\partial f_r}{\partial v}\Big|_o \Delta v + \frac{\partial f_r}{\partial p}\Big|_o \Delta p + \frac{\partial f_r}{\partial r}\Big|_o \Delta r + \frac{\partial f_r}{\partial \phi}\Big|_o \Delta\phi + \frac{\partial f_r}{\partial \delta_a}\Big|_o \Delta\delta_a + \frac{\partial f_r}{\partial \delta_r}\Big|_o \Delta\delta_r \tag{E-11}$$

$$\dot{\phi}\Big|_o + \Delta\dot{\phi} = f_\phi\Big|_o + \frac{\partial f_\phi}{\partial v}\Big|_o \Delta v + \frac{\partial f_\phi}{\partial p}\Big|_o \Delta p + \frac{\partial f_\phi}{\partial r}\Big|_o \Delta r + \frac{\partial f_\phi}{\partial \phi}\Big|_o \Delta\phi + \frac{\partial f_\phi}{\partial \delta_a}\Big|_o \Delta\delta_a + \frac{\partial f_\phi}{\partial \delta_r}\Big|_o \Delta\delta_r \tag{E-12}$$

$$\Delta\dot{v} = \frac{\partial f_v}{\partial v}\Big|_o \Delta v + \frac{\partial f_v}{\partial p}\Big|_o \Delta p + \frac{\partial f_v}{\partial r}\Big|_o \Delta r + \frac{\partial f_v}{\partial \phi}\Big|_o \Delta\phi \tag{E-13}$$

$$\Delta\dot{p} = \frac{\partial f_p}{\partial v}\Big|_o \Delta v + \frac{\partial f_p}{\partial p}\Big|_o \Delta p + \frac{\partial f_p}{\partial r}\Big|_o \Delta r + \frac{\partial f_p}{\partial \phi}\Big|_o \Delta\phi \tag{E-14}$$

$$\Delta\dot{r} = \frac{\partial f_r}{\partial v}\Big|_o \Delta v + \frac{\partial f_r}{\partial p}\Big|_o \Delta p + \frac{\partial f_r}{\partial r}\Big|_o \Delta r + \frac{\partial f_r}{\partial \phi}\Big|_o \Delta\phi \tag{E-15}$$

$$\Delta\dot{\phi} = +\frac{\partial f_\phi}{\partial v}\Big|_o \Delta v + \frac{\partial f_\phi}{\partial p}\Big|_o \Delta p + \frac{\partial f_\phi}{\partial r}\Big|_o \Delta r + \frac{\partial f_\phi}{\partial \phi}\Big|_o \Delta\phi \tag{E-16}$$

Table E-1. Derivatives of f_v

Derivative	Description
$\frac{\partial f_v}{\partial v}$	$= \frac{1}{m}\frac{\partial Y}{\partial v} = Y_v$
$\frac{\partial f_v}{\partial p}$	$= \frac{1}{m}\frac{\partial Y}{\partial p} + w_o = Y_p + w_o \cong Y_p$
$\frac{\partial f_v}{\partial r}$	$= \frac{1}{m}\frac{\partial Y}{\partial r} - u_o = Y_r - u_o$
$\frac{\partial f_v}{\partial \phi}$	$= \frac{1}{m}\frac{\partial Y}{\partial \phi} + gC_\theta C_\phi = gC_\theta C_\phi \Big\vert_o$
$\frac{\partial f_v}{\partial \delta_a}$	$= \frac{1}{m}\frac{\partial Y}{\partial \delta_a} = 0$
$\frac{\partial f_v}{\partial \delta_r}$	$= \frac{1}{m}\frac{\partial Y}{\partial \delta_r} = Y_{\delta_r}$

Table E-2. Derivatives of f_p

Derivative	Description
$\frac{\partial f_p}{\partial v}$	$= \frac{1}{I_x}\frac{\partial L}{\partial v} = L_v$
$\frac{\partial f_p}{\partial p}$	$= \frac{1}{I_x}\frac{\partial L}{\partial p} = L_p$
$\frac{\partial f_p}{\partial r}$	$= \frac{1}{I_x}\frac{\partial L}{\partial r} = L_r$
$\frac{\partial f_p}{\partial \phi}$	$= \frac{1}{I_x}\frac{\partial L}{\partial \phi} = 0$
$\frac{\partial f_p}{\partial \delta_a}$	$= \frac{1}{I_x}\frac{\partial L}{\partial \delta_a} = L_{\delta_a}$
$\frac{\partial f_p}{\partial \delta_r}$	$= \frac{1}{I_x}\frac{\partial L}{\partial \delta_r} = L_{\delta_r}$

Table E-3. Derivatives of f_r

Derivative	Description
$\frac{\partial f_r}{\partial v}$	$= \frac{1}{I_z}\frac{\partial N}{\partial v} = N_v$
$\frac{\partial f_r}{\partial p}$	$= \frac{1}{I_z}\frac{\partial N}{\partial p} = N_p$
$\frac{\partial f_r}{\partial r}$	$= \frac{1}{I_z}\frac{\partial N}{\partial r} = N_r$
$\frac{\partial f_r}{\partial \phi}$	$= \frac{1}{I_z}\frac{\partial N}{\partial \phi} = 0$
$\frac{\partial f_r}{\partial \delta_a}$	$= \frac{1}{I_z}\frac{\partial N}{\partial \delta_a} = N_{\delta_a}$
$\frac{\partial f_r}{\partial \delta_r}$	$= \frac{1}{I_z}\frac{\partial N}{\partial \delta_r} = N_{\delta_r}$

Table E-4. Derivatives of f_ϕ

Derivative	Description
$\frac{\partial f_\phi}{\partial v}$	$qC_\phi T_\theta - rS_\phi T_\theta \big\|_o \cong 0$
$\frac{\partial f_\phi}{\partial p}$	$= 1$
$\frac{\partial f_\phi}{\partial r}$	$C_\phi T_\theta \big\| \cong 0$
$\frac{\partial f_\phi}{\partial \phi}$	$qC_\phi T_\theta - rS_\phi T_\theta \big\|_o \cong 0$
$\frac{\partial f_\phi}{\partial \delta_a}$	0
$\frac{\partial f_\phi}{\partial \delta_r}$	0

$$\begin{bmatrix} \Delta\dot{v} \\ \Delta\dot{p} \\ \Delta\dot{r} \\ \Delta\dot{\phi} \end{bmatrix} = \begin{bmatrix} Y_v & Y_p & Y_r - u_o & gC_\theta \\ L_v & L_p & L_r & 0 \\ N_v & N_p & N_r & 0 \\ 0 & 1 & 0 & 0 \end{bmatrix} \begin{bmatrix} \Delta v \\ \Delta p \\ \Delta r \\ \Delta\phi \end{bmatrix} + \begin{bmatrix} 0 & Y_{\delta_r} \\ L_{\delta_a} & L_{\delta_r} \\ N_{\delta_a} & N_{\delta_r} \\ 0 & 0 \end{bmatrix} \begin{bmatrix} \Delta\delta_a \\ \Delta\delta_r \end{bmatrix} \tag{E-17}$$

It is more convenient to work with the aircraft's sideslip angle than with the lateral velocity.

$$\Delta\beta = \tan^{-1}\frac{\Delta v}{u_o} \cong \frac{\Delta v}{u_o} \tag{E-18}$$

$$\begin{bmatrix} u_o\Delta\dot{\beta} \\ \Delta\dot{p} \\ \Delta\dot{r} \\ \Delta\dot{\phi} \end{bmatrix} = \begin{bmatrix} Y_v & Y_p & Y_r - u_o & gC_\theta \\ L_v & L_p & L_r & 0 \\ N_v & N_p & N_r & 0 \\ 0 & 1 & 0 & 0 \end{bmatrix} \begin{bmatrix} u_o\Delta\beta \\ \Delta p \\ \Delta r \\ \Delta\phi \end{bmatrix} + \begin{bmatrix} 0 & Y_{\delta_r} \\ L_{\delta_a} & L_{\delta_r} \\ N_{\delta_a} & N_{\delta_r} \\ 0 & 0 \end{bmatrix} \begin{bmatrix} \Delta\delta_a \\ \Delta\delta_r \end{bmatrix} \tag{E-19}$$

$$\begin{bmatrix} u_o\Delta\dot{\beta} \\ \Delta\dot{p} \\ \Delta\dot{r} \\ \Delta\dot{\phi} \end{bmatrix} = \begin{bmatrix} u_oY_v & Y_p & Y_r - u_o & gC_\theta \\ u_oL_v & L_p & L_r & 0 \\ u_oN_v & N_p & N_r & 0 \\ 0 & 1 & 0 & 0 \end{bmatrix} \begin{bmatrix} \Delta\beta \\ \Delta p \\ \Delta r \\ \Delta\phi \end{bmatrix} + \begin{bmatrix} 0 & Y_{\delta_r} \\ L_{\delta_a} & L_{\delta_r} \\ N_{\delta_a} & N_{\delta_r} \\ 0 & 0 \end{bmatrix} \begin{bmatrix} \Delta\delta_a \\ \Delta\delta_r \end{bmatrix} \tag{E-20}$$

$$\begin{bmatrix} u_o\Delta\dot{\beta} \\ \Delta\dot{p} \\ \Delta\dot{r} \\ \Delta\dot{\phi} \end{bmatrix} = \begin{bmatrix} Y_\beta & Y_p & Y_r - u_o & gC_\theta \\ L_\beta & L_p & L_r & 0 \\ N_\beta & N_p & N_r & 0 \\ 0 & 1 & 0 & 0 \end{bmatrix} \begin{bmatrix} \Delta\beta \\ \Delta p \\ \Delta r \\ \Delta\phi \end{bmatrix} + \begin{bmatrix} 0 & Y_{\delta_r} \\ L_{\delta_a} & L_{\delta_r} \\ N_{\delta_a} & N_{\delta_r} \\ 0 & 0 \end{bmatrix} \begin{bmatrix} \Delta\delta_a \\ \Delta\delta_r \end{bmatrix} \tag{E-21}$$

The final version of the lateral equations is shown in equation E-22.

$$\begin{bmatrix} \Delta\dot{\beta} \\ \Delta\dot{p} \\ \Delta\dot{r} \\ \Delta\dot{\phi} \end{bmatrix} = \begin{bmatrix} \frac{Y_\beta}{u_o} & \frac{Y_p}{u_o} & \frac{Y_r - u_o}{u_o} & \frac{gC_\theta}{u_o} \\ L_\beta & L_p & L_r & 0 \\ N_\beta & N_p & N_r & 0 \\ 0 & 1 & 0 & 0 \end{bmatrix} \begin{bmatrix} \Delta\beta \\ \Delta p \\ \Delta r \\ \Delta\phi \end{bmatrix} + \begin{bmatrix} 0 & \frac{Y_{\delta_r}}{u_o} \\ L_{\delta_a} & L_{\delta_r} \\ N_{\delta_a} & N_{\delta_r} \\ 0 & 0 \end{bmatrix} \begin{bmatrix} \Delta\delta_a \\ \Delta\delta_r \end{bmatrix} \tag{E-22}$$

Table E-5. Derivatives of Y

Derivative	Description
Y_β	$= \frac{qS_w}{m} C_{y\beta}$
Y_p	$= \frac{qS_w b_w}{2mu_o} C_{yp}$
Y_r	$= \frac{qS_w b_w}{2mu_o} C_{yr}$
Y_{δ_a}	$= \frac{qS_w}{m} C_{y\delta_a}$
Y_{δ_r}	$= \frac{qS_w}{m} C_{y\delta_r}$

Table E-6. Derivatives of L

Derivative	Description
L_β	$= \frac{qS_w b_w}{I_x} C_{l_\beta}$
L_p	$= \frac{qS_w b_w^2}{2I_x u_o} C_{l_p}$
L_r	$= \frac{qS_w b_w^2}{2I_x u_o} C_{l_r}$
L_{δ_a}	$= \frac{qS_w b_w}{I_x} C_{l_{\delta_a}}$
L_{δ_r}	$= \frac{qS_w b_w}{I_x} C_{l_{\delta_r}}$

Table E-7. Derivatives of *N*

Derivative	Description
N_β	$= \frac{qS_w b_w}{I_x} C_{n_\beta}$
N_p	$= \frac{qS_w b_w^2}{2I_z u_o} C_{n_p}$
N_r	$= \frac{qS_w b_w^2}{2I_z u_o} C_{n_r}$
N_{δ_a}	$= \frac{qS_w b_w}{I_x} C_{n_{\delta_a}}$
N_{δ_r}	$= \frac{qS_w b_w}{I_x} C_{n_{\delta_r}}$

APPENDIX F—AIRCRAFT MODEL NUMERICAL DATA

There were several flight-dynamics models used during the project. The principal model, JSBSim, was a full nonlinear 6-degree-of-freedom (6-DOF) model implemented in C++. JSBSim is an open-source model that follows the traditional formulation of the equations of motion and the buildup of the force models as characterized in appendix B. This simulation code was used to drive the cockpit simulator and the hardware-in-the-loop simulation that was used with the actual aircraft in the hangar. JSBSim also came with a fully populated model of a C-182, which appeared to be similar to the known C-182 data from Roskam. The C-182 data from JSBSim were necessarily more extensive in that a tabular drag polar for the aircraft was included and most of the stability and control derivatives had tabular values as a function of angle of attack (AoA). The tabular data showed good fidelity with the Roskam data to the extent that they could be evaluated. The one point of disagreement was in the predicted elevator effectiveness. JSBSim derivatives predicted more effectiveness than the Roskam. The JSBSim model was used as published without any changes.

Table F-1 shows a comparison between the Roskam and JSBSim longitudinal derivatives. Figures F-1 and F-2 show the tabular data characterizing the lift and drag properties of the model.

Table F-1. Comparison of Roskam and JSBSim Longitudinal Derivatives for the C-182

Derivative	Roskam Value	JSBSim Value
C_{L_α}	4.6	Table
C_{m_α}	-0.89	Table
$C_{L_{\dot{\alpha}}}$	1.7	1.7
C_{D_α}	0.13	Table
C_{L_q}	3.9	3.9
C_{m_q}	-12.4	-12.4
$C_{L_{\delta e}}$	0.06	0.43
$C_{m_{\delta e}}$	-1.28	-0.6220
C_{m_u}	0	0
C_{D_u}	0	0
C_{L_u}	0	0

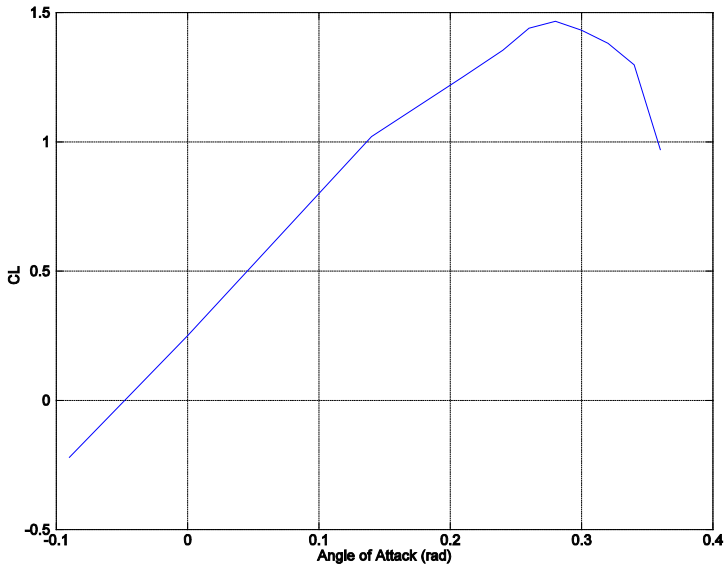

Figure F-1. The JSBSim C-182 Lift Coefficient as a Function of AoA

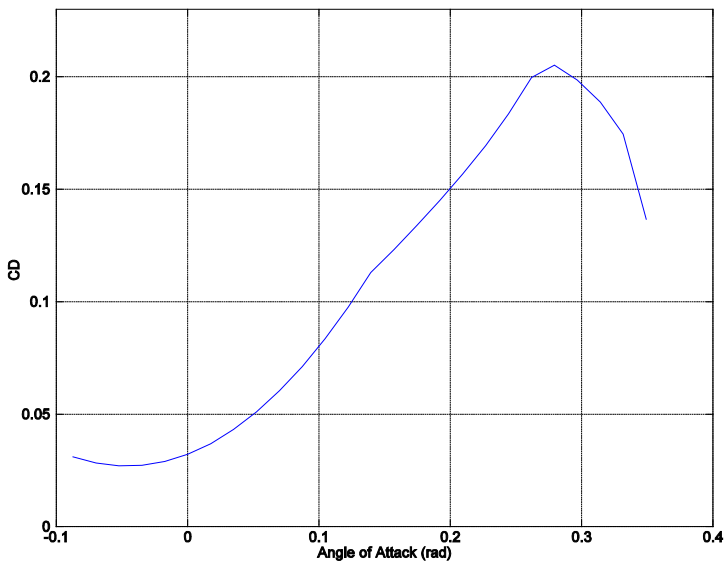

Figure F-2. The JSBSim C-182 Drag Coefficient as a Function of AoA

In cases for which the slopes of the lift and drag values are required, such as with C_{L_α} and C_{D_α}, the values are estimated from the lift-and-drag data based on the aircraft's current AoA.

Figures F-3 and F-4 show the variation of the pitching moment with AoA.

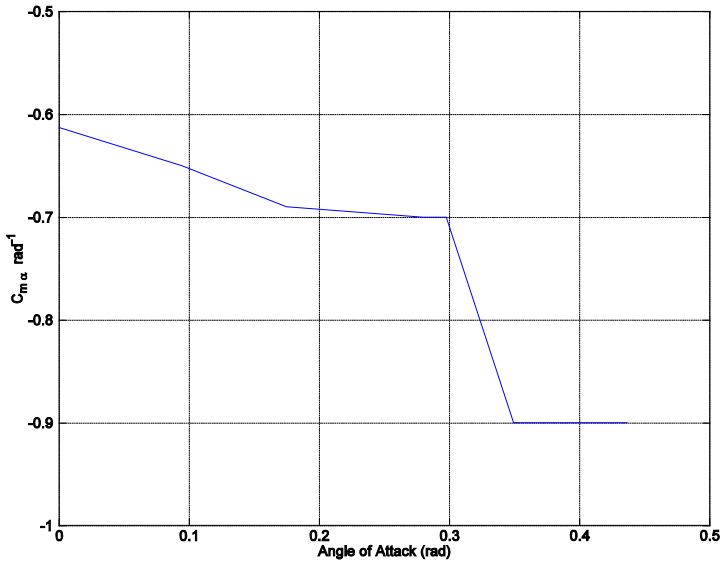

Figure F-3. The JSBSim Derivative C_{m_α} as a Function of AoA

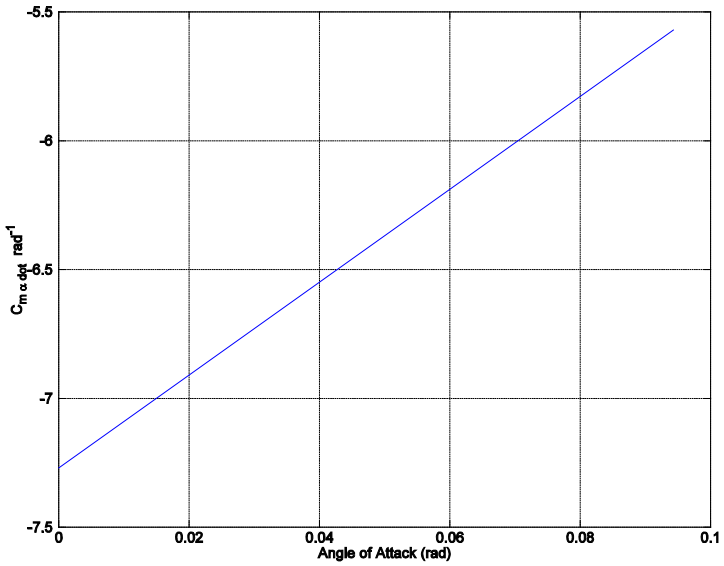

Figure F-4. The JSBSim Derivative $C_{m_{\dot{\alpha}}}$ as a Function of AoA

The lateral derivatives are shown in table F-2. A majority of the lateral stability and control derivatives from JSBSim are variable as a function of AoA, as opposed to the Roskam values, which are static. For values outside the range of 0 to 0.0943 rad (5.40°), JSBSim uses the value taken on at the extremes of that range (see table F-3). The radii of gyration and the basic weights and dimensions for the C-182 are shown in tables F-4 and F-5, respectively.

Table F-2. Comparison of Roskam and JSBSim Lateral Derivatives for the C-182

Derivative	Roskam Value	JSBSim Value
C_{l_β}	-0.089	Varies with α and β
C_{l_p}	-0.47	-0.484 + (-0.003 / .0943) α
C_{l_r}	0.096	0.0798 + (0.1071 / .0943) α
$C_{l_{\delta a}}$	0.178	-0.15
$C_{l_{\delta r}}$	0.0147	0.0147
C_{n_β}	0.065	0.0587 + (0.032 / .0943) α
C_{n_p}	-0.03	-0.0278 + (-0.0371 / .0943) α
C_{n_r}	-0.099	-0.0937 + (-0.0262 / .0943) α
$C_{n_{\delta a}}$	-0.053	-0.0216 + (-0.0288 / .0943) α
$C_{n_{\delta r}}$	-0.0657	-0.0645 + (-0.0160 / .0943) α
C_{y_β}	-0.31	-0.3930
C_{y_p}	-0.037	-0.0750 + (-0.0700 / .0943) α
C_{y_r}	0.21	0.2140 + (0.0530 / .0943) α
$C_{y_{\delta a}}$	0.0	0.0
$C_{y_{\delta r}}$	0.187	0.1870

Table F-3. C_{l_β} Two-Dimensional Lookup Table

Sideslip Angle β (rad)	AoA α (rad)	
	0.00	0.0943
-0.3490	0.0322	0.0312
0.0000	0.0000	0.0000
0.3490	-0.0322	-0.0312

Table F-4. Radii of Gyration for the C-182

R_{xx}	3.3971 ft
R_{yy}	4.0472 ft
R_{zz}	4.8929 ft

Table F-5. Basic Weights and Dimensions for the C-182

S_w (Wing Area)	174.0 ft
$\bar{c}_w$ (Mean Aerodynamic Chord)	4.9 ft
b_w (Wing Span)	35.8 ft
W_{empty} (Empty Weight)	1700 lb
W_{nom} (Nominal Weight)	2750 lb

APPENDIX G—LINEAR ANALYSIS OF CONTROL MODES

G.1 LONGITUDINAL LINEAR MODEL.

For the purposes of doing control system analysis, a linear model was constructed. This model was a state space representation of the dynamics implemented in a MATLAB/Octave environment in which classical control system techniques could be used with relative ease. The longitudinal model was based on equation G-1 (terms defined and derived in appendix B).

$$\begin{bmatrix} \Delta\dot{u} \\ \Delta\dot{\alpha} \\ \Delta\dot{q} \\ \Delta\dot{\theta} \end{bmatrix} = \begin{bmatrix} X_u & X_w u_o & 0 & -g \\ \dfrac{Z_u}{u_o} & \dfrac{Z_\alpha}{u_o} & 1 & 0 \\ M_u + \dfrac{M_{\dot{\alpha}} Z_u}{u_o} & M_\alpha + \dfrac{M_{\dot{\alpha}} Z_\alpha}{u_o} & M_q + M_{\dot{\alpha}} & 0 \\ 0 & 0 & 1 & 0 \end{bmatrix} \begin{bmatrix} \Delta u \\ \Delta\alpha \\ \Delta q \\ \Delta\theta \end{bmatrix} + \begin{bmatrix} X_{\delta_e} & X_{\delta_p} \\ \dfrac{Z_{\delta_e}}{u_o} & \dfrac{Z_{\delta_e}}{u_o} \\ M_{\delta_e} + \dfrac{M_{\dot{\alpha}} Z_{\delta_e}}{u_o} & M_{\delta_p} + \dfrac{M_{\dot{\alpha}} Z_{\delta_p}}{u_o} \\ 0 & 0 \end{bmatrix} \begin{bmatrix} \Delta\delta_e \\ \Delta\delta_p \end{bmatrix} \tag{G-1}$$

Because elevator deflection was the only longitudinal control input of consequence for the development of the autopilot, the *B* matrix was limited to just the first column:

$$\begin{bmatrix} \Delta\dot{u} \\ \Delta\dot{\alpha} \\ \Delta\dot{q} \\ \Delta\dot{\theta} \end{bmatrix} = \begin{bmatrix} X_u & X_w u_o & 0 & -g \\ \dfrac{Z_u}{u_o} & \dfrac{Z_\alpha}{u_o} & 1 & 0 \\ M_u + \dfrac{M_{\dot{\alpha}} Z_u}{u_o} & M_\alpha + \dfrac{M_{\dot{\alpha}} Z_\alpha}{u_o} & M_q + M_{\dot{\alpha}} & 0 \\ 0 & 0 & 1 & 0 \end{bmatrix} \begin{bmatrix} \Delta u \\ \Delta\alpha \\ \Delta q \\ \Delta\theta \end{bmatrix} + \begin{bmatrix} X_{\delta_e} \\ \dfrac{Z_{\delta_e}}{u_o} \\ M_{\delta_e} + \dfrac{M_{\dot{\alpha}} Z_{\delta_e}}{u_o} \\ 0 \end{bmatrix} \begin{bmatrix} \Delta\delta_e \end{bmatrix} \tag{G-2}$$

Using the aircraft stability and control data and mass properties from the nonlinear model, the numerical values for the aircraft can be calculated. The *C* and *D* matrices follow from the state variables presented. All four state variables are desired outputs along with altitude rate, which must be derived from the other states. The approximation for altitude rate is shown in equation G-3 and the output equation is shown in equation G-4.

$$\dot{h} = u_o \sin\gamma \cong u_o \sin(\theta - \alpha) \cong -u_o\alpha + u_o\theta \tag{G-3}$$

$$\begin{bmatrix} \Delta\dot{u} \\ \Delta\dot{\alpha} \\ \Delta\dot{q} \\ \Delta\dot{\theta} \\ \Delta\dot{h} \end{bmatrix} = \begin{bmatrix} 1 & 0 & 0 & 0 \\ 0 & 1 & 0 & 0 \\ 0 & 0 & 1 & 0 \\ 0 & 0 & 0 & 1 \\ 0 & -u_o & 0 & u_o \end{bmatrix} \begin{bmatrix} \Delta u \\ \Delta\alpha \\ \Delta q \\ \Delta\theta \end{bmatrix} + \begin{bmatrix} 0 \\ 0 \\ 0 \\ 0 \\ 0 \end{bmatrix} \begin{bmatrix} \Delta\delta_e \end{bmatrix} \tag{G-4}$$

APPENDIX H—EXPERIMENTAL SERVO COMPONENT DETAILS

Servo motor:
Mfg: Applied Motion
Part No. N0100-103-A-000
Size: NEMA 17
Type: Brushless
Feedback: 8000-count optical encoder
Max Continuous Torque: 2.8 inch-lb
Peak Torque: 8.4 inch-lb
Voltage: 24 volts
Website: http://www.applied-motion.com/products/servo-motors/n0100-103-a-000

Servo drive:
Mfg: Applied Motion
Part No: SV7-S-AF
Continuous Current: 7 amps
Peak Current: 14 amps
Website: http://www.applied-motion.com/products/series/sv7-servo-drives

Torque sensor:
Mfg: Futek
Part No. Sensor: TFF350
Part No. Signal Conditioning: CSG110
Torque Measurement: ± 150 inch-lb

Gears:
Material: Aluminum 2024-T4
Dropout Gear Material: Brass
Final Gear Ratio: 33.75 to 1
Design Notes:

- Gears were sized for the alpha prototype with the motor providing a peak power of 0.18 HP at 2,300 RPM, which was calculated from a speed torque curve of the motor.

- Gear ratio was chosen to provide for a maximum g-pull-up at Vne.

- Some of the gears were re-used in the beta prototype when the servo used the sprocket as an output.

- The final beta servo peak output torque was estimated to be approximately 166.5 in-lb, which would provide approximately 241 lb of linear force to the control cable.

APPENDIX I—FLIGHT TEST HAZARD ANALYSIS

A flight test hazard analysis developed in support of the flight test program reported in this appendix is included for future reference.

I.1 INTRODUCTION.

This document identifies potential hazards and planned mitigations for upcoming flight tests in support of autopilot development work under the General Aviation Basic Envelope Protection research and development effort.

The flight tests are to take place in a 1978 Cessna R182 aircraft, equipped with an experimental autopilot and display system.

Hazards have been identified and mitigations developed as detailed in this document. Hazards and mitigation have been informed by the author's previous avionics development, aviation, and flight test experience. In addition, all relevant hazards and mitigations contained in the National Aeronautics and Space Administration (NASA) Flight Test Safety Database have been included in section I.3.

I.2 HAZARDS AND MITIGATIONS.

I.2.1 Hazard 1: Loss of Aircraft Control System Integrity.

Discussion:

Integrity of the pilot's ability to maintain normal control of elevators and ailerons in the presence of installed experimental servos is paramount. The following mitigations to ensure continuous control authority are planned.

Planned Mitigations:

- Experimental autopilot servos are equipped with a shear-pin mechanism, allowing the pilot to physically isolate the servo internal mechanism from the flight control cables by imparting sufficient force to the yoke.

- Experimental autopilot servos are back-drivable and become passive after removal of electrical power.

- A servo disconnect switch to remove power from the experimental servos is available within easy reach of both the pilot and the flight test engineer.

I.2.2 Hazard 2: Aircraft Structure Over-Stressed by Experimental Autopilot.

Discussion:

During tests of an experimental autopilot, unexpected control deflections may occur. In particular, at speeds above design maneuvering speed, full elevator deflection could result in exceeding the aircraft's flight load factor limits.

Several layers of protection are planned to mitigate this risk.

Planned Mitigations:

- Use automatic g-disconnect system to remove power from experimental autopilot servos in the event that aircraft *Z*-axis acceleration exceeds +2.4g or is less than -0.9g.

- Conduct all flight test maneuvers during initial autopilot development flights at an indicated airspeed less than design maneuvering speed for the aircraft (112 knots indicated air speed (KIAS) at full gross weight of 3100 lb; 101 KIAS at 2550 lb; 89 KIAS at 2000 lb).

- Check AFCS disconnect function prior to each flight.

- Pilot to guard controls.

- Brief termination criteria and recovery technique. Termination criteria will include a maximum allowable airspeed and a minimum allowable altitude.

I.2.3 Hazard 3: Aircraft Structure Over-Stressed during Recovery from Unusual Attitude.

Discussion:

Unusual attitudes may result from either (1) unexpected autopilot behavior during testing of an experimental autopilot, or (2) deliberate pilot action to determine the envelope protection qualities of the system under development.

During manual or automatic recovery from unusual attitudes, airspeed may increase to values above design maneuvering speed, which allows the possibility of overstressing the aircraft structure if recovery controls are not applied in an appropriate and judiscious manner.

Planned Mitigations:

- Mitigations itemized for Hazard 2 in section I.2.2.

- Establish a minimum test start altitude (4,500 ft AGL is the planned minimum test start altitude).

- Establish minimum altitude for safe recovery (3,000 ft AGL is the planned floor.)

- Weather: VMC, Defined horizon.

I.2.4 Hazard 4: Stalls and Stall/Spins.

Discussion:

During the flight tests, the experimental system will be tested in near-stall and full-stall conditions at altitude. Under normal circumstances, the system should be capable of recovering the aircraft to normal flight. A potential hazard exists if the experimental system fails to perform as intended.

Planned Mitigations:

- Stall characteristics are well-established for the planned certified test aircraft.

- Check AFCS disconnect function prior to each flight.

- Stall and stall-spin recovery techniques briefed prior to flight.

- Pilot to disconnect autopilot and recover manually if uncoordinated/incipient spin conditions develop.

- Establish a minimum test start altitude (4,500 ft AGL is the planned minimum test start altitude).

- Establish minimum altitude for safe recovery (3,000 ft AGL is the planned floor).

- Weather: VMC, Defined horizon.

I.2.5 Hazard 5: Controlled Flight Into Terrain.

Discussion:

Controlled flight into terrain (CFIT) is an ever-present risk for many flight operations. During flight test activity, crew preoccupation with the tasks inherent in the tests increases the risk of CFIT, particularly during low-level maneuvering.

Planned Mitigations:

- The test floor for all flight test maneuvers during the planned flight tests is 3,000 ft AGL.

- Autopilot servos will be powered off during all phases of flight below the test floor altitude.

- The PIC will be solely responsible for flying the aircraft and will not interact with any item of test equipage below the test floor altitude.

- Weather: VMC, defined horizon.

I.2.6 Hazard 6: Aircraft Impacts the Ground due to Autopilot Malfunction.

Discussion:

This hazard involves an autopilot malfunction resulting in a sudden pitch-down of the aircraft close to the ground.

Planned Mitigations:

- The test floor for all flight test maneuvers during the planned flight tests is 3,000 ft AGL.

- Autopilot servos will be powered off during all phases of flight below the test floor altitude.

- Below 500 ft AGL, a crewmember's hands will be on the controls.

I.2.7 Hazard 7: Loss of Power.

Discussion:

The aircraft to be used for flight test is a single-engine propeller-driven aircraft. Loss of power from the single engine during particular phases of flight may result in the necessity to execute an off-airport landing. This risk is common to the operation of all aircraft and is part of normal training and preparation.

Planned Mitigations:

- Brief engine loss-of-power procedures from POH prior to each flight.

- Conduct normal preflight inspection to include fuel contamination and fuel quantity checks, including physical check of fuel quantity in both tanks with dipstick.

- Estimate and record flight time available given current fuel load prior to engine start.

- Conduct pre-takeoff magneto check to ensure proper operation of redundant magneto system.

- Use installed fuel totalizer to aid in estimating flight time remaining with current available fuel.

- Discontinue further testing and return to land when 1 hour of fuel remains.

- Use carburetor heat during low-power portions of flight.

- Conduct test maneuvers in location within gliding distance of suitable landing area.

I.2.8 Hazard 8: Mid-Air Collision.

Discussion:

Mid-air collision with another aircraft is an extremely remote risk. However, the see-and-avoid method of separation from other aircraft is compromised during flight test activities, generally because of the high-workload nature of the activity and the tendency to become preoccupied with the flight test maneuvers undertaken.

Planned Mitigations:

- Weather: VMC, defined horizon.

- The test floor for all flight test maneuvers during the planned flight tests is 3000 ft AGL.

- Clearing turns will be executed prior to initial flight test maneuvers.

- TIS traffic display will be monitored to assure awareness of other transponder-equipped aircraft in area.

- In the event TIS coverage is not available, flight following will be used from the appropriate radar-equipped facility.

I.2.9 Hazard 9: Loss of Aircraft Controllability (Unspecified Cause).

Discussion:

Aircraft loss of controllability will result in the flight crew's need to exit the aircraft prior to reaching an unacceptably low altitude.

Planned Mitigations:

- Quick-release door hinges will be installed and functional on the test aircraft.

- Test personnel will wear an appropriately sized parachute.

- Prior to each flight, test personnel will brief and practice required actions for exiting the aircraft during an in-flight emergency.

- Floor for regaining aircraft control following an emergency is 1,500 ft AGL; failure to regain control before reaching 1,500 ft AGL requires crew to exit aircraft.

- Flight tests are planned over sparsely populated areas to avoid risk to people and property on the ground.

I.3 NASA FLIGHT TEST SAFETY DATABASE ENTRIES

This appendix lists hazards and mitigations relevant to the planned flight tests that are contained in the NASA Flight Test Safety Database (available at http://ftsdb.grc.nasa.gov/TestHazardAnalysis).

THA No.	Maneuver Title	Hazard	Mitigations
386	Autopilot Development	Loss of all thrust	Cause 1: Second engine failure on one engine approach (not applicable) 1. Review dual engine flameout and emergency relight procedures prior to intentional single-engine operation (not applicable). 2. Conduct test in location within gliding distance of suitable landing area (applicable).
387	Autopilot Malfunctions	Controlled Flight Into Terrain	Cause 1: Pilots occupied with test-related tasks 1. Minimum crew for high-risk (low-altitude) points. 2. Check AFCS disconnect function prior to each flight. 3. Pilot to guard controls. 4. Brief termination criteria and recovery technique. 5. Safety pilot to monitor runway on approach conditions and make altitude callouts. 6. Establish a minimum safe test start altitude and “knock-it-off” altitude. 7. Weather: VMC, ground contact (low altitude points), defined horizon.

THA No.	Maneuver Title	Hazard	Mitigations
9292	Autopilot Malfunctions	Structural Failure	<u>Cause 1: Over-g during recovery</u> 1. Minimum crew increases learning carryover. 2. Check AFCS disconnect function prior to each flight. 3. Pilot to guard controls. 4. Brief termination criteria and recovery technique. 5. Establish a minimum test-start altitude. 6. Structures data monitored. 7. Logical buildup of conditions (high-to-low altitude; short-to-long reaction time). 8. Weather: VMC, ground contact (low-altitude points), defined horizon. 9. Practice recovery in simulator. <u>Cause 2: Autopilot hardover</u> 1. Minimum crew. 2. Check AFCS disconnect function prior to each flight. 3. Pilot to guard controls. 4. Brief termination criteria and recovery technique. 5. Establish a minimum test-start altitude. 6. Monitor data to determine A/C performance and stress levels. 7. Structures data monitored. 8. Logical build-up of conditions (high-to-low altitude; short-to-long reaction time).

THA No.	Maneuver Title	Hazard	Mitigations
			9. Weather: VMC, ground contact (low-altitude points), defined horizon. 10. Practice hardover recovery in the simulator.
11817	Autopilot Development	Structural Failure	<u>Cause 1: Speed excursion beyond Vne or Vd/Md</u> 1. Monitor airspeed excursion. Disconnect autopilot and recover prior to exceeding Vne or a speed midway between Vmo/Mmo and Vd/Md for airplanes with an established Vmo/Mmo. 2. Aircraft airspeed envelope must have been cleared to Vd/Md prior to performing this test. <u>Cause 2: Over-g on recovery</u> 1. Monitor data to determine A/C performance. 2. Monitor structures data. 3. Practice maneuvers and recovery in the simulator. <u>Cause 3: Hardover malfunction</u> 1. Aircraft airspeed envelope must have been cleared to Vd/Md prior to performing this test. 2. Monitor data to determine A/C performance and autopilot commands. 3. Monitor structures data.

THA No.	Maneuver Title	Hazard	Mitigations
11818	Autopilot Development	Stall	<u>Cause 1: Vstall reached during slow flight</u> 1. Verify stall characteristics prior to this testing. 2. Check AFCS disconnect function prior to each flight. 3. Pilot to guard controls. 4. Brief termination criteria and recovery technique. 5. Establish a minimum test start altitude. 6. Weather: VMC, ground contact (low altitude points), defined horizon. <u>Cause 2: Inappropriate maneuver recovery</u> 1. Do not pull past stall warning. 2. Brief termination criteria and recovery technique. 3. Check AFCS disconnect function prior to each flight. 4. Practice maneuver and recovery in simulator or similar certified aircraft. <u>Cause 3: Autopilot malfunction</u> 1. Pilot guards controls. 2. Practice malfunction recovery in simulator. 3. Establish minimum altitude for safe recovery.
11819	Autopilot Malfunctions	Aircraft Impacts the Ground	<u>Cause 1: Autopilot fails catastrophically and pitches aircraft down violently</u> 1. Autopilot will not be engaged or allowed to be engaged below 100 ft AGL. 2. Be aware of circuit breaker position to allow for immediate power removal in case autopilot fails to disengage. 3. Below 500 ft AGL, a crewmember's hands will be on the controls.

APPENDIX J—PREFLIGHT CHECKLIST FOR EXPERIMENTAL TEST FLIGHTS

This checklist was completed during the preflight briefing for experimental test flights conducted during this program. It is included here for future reference.

Preflight Procedure and Briefing Checklist
For GA Basic Envelope Protection Flight Tests

THIS CHECKLIST TO BE COMPLETED PRIOR TO ANY TEST FLIGHT

CHECKS TO BE ACCOMPLISHED PRIOR TO PREFLIGHT BRIEFING

DATE OF FLIGHT TEST _____
FLIGHT TEST SORTIE NUMBER _____

AIRCRAFT GENERAL PREFLIGHT

ITEM	STATUS
Fuel on board (gal)	
Estimated endurance (hours) at 13 gph	
Oil quantity (quarts)	
Aircraft W&B accomplished?	
Aircraft weight at start of flight	
Aircraft weight with 1 hr of fuel remaining	
Va at start of flight	
Va with 1 hour of fuel remaining	
General aircraft preflight accomplished?	

FLIGHT TEST EQUIPMENT PREFLIGHT

ITEM	STATUS
Aircraft controls smooth through full range of motion?	
Servo disconnect switch functional?	
Door quick-release pins installed on both sides?	
Door stops disconnected on both sides?	

PREFLIGHT BRIEFING

DATE OF FLIGHT TEST _____
FLIGHT TEST SORTIE NUMBER _____

TIME

Estimated time of departure	
Estimated duration of flight	
Fuel endurance	
Time of today's sunset	
Daylight remaining at departure time	

CREW

PIC	
FTE	
Observer 1	
Observer 2	
PIC current for VFR flight?	
PIC night current?	
PIC current for IFR flight?	

WEATHER

Local ceiling/visibility	
Local winds	
VMC available in test area at altitude?	
Any relevant TFRs?	

<u>GENERAL TEST PLAN BRIEFING</u>

Purpose of sortie _____
Specific maneuvers planned _____
Geographic area of testing _____

Crew resource management
- Role of PIC
- Role of FTE
- Role of Observers

RISK MITIGATIONS

Altitude floor for all test activity _____MSL (minimum 3000 ft AGL)
Altitude floor for start of any maneuver _____ MSL (minimum 4500 AGL)
Max airspeed for any maneuver start: _____ knots
Carb heat applied whenever MP < _____ in Hg

Knock-It-Off criteria and procedure

Mandatory knock-it-off criteria:
Abnormal servo function
Abnormal flight control feel
Any engine or aircraft abnormality
Other criteria _____

*** ANY AIRCRAFT OCCUPANT CAN CALL A "KNOCK-IT-OFF" WHEREUPON PIC MUST END TEST AND RETURN TO LAND. ***

Traffic avoidance
TIS available? _____
Flight following frequency _____
Will we use flight following for this flight? _____

EMERGENCY PROCEDURES BRIEFING

Procedure for loss of engine thrust:
Best-glide speed: _____ knots
Engine restart procedure (brief)
Off-airport touchdown procedure (brief)

Procedure for in-flight smoke/fire
Experimental pallet power OFF
Location of fire extinguisher

Bail-out option for this flight? Y/N
If "Yes":
Bail-out altitude _____ MSL (minimum 1500 ft AGL)
Bail-out procedure:
Bailout ANNOUNCE / VERIFY
Seats SLIDE BACK
Seatbelts UNBUCKLE
Doors UNLOCK
Headset DISCONNECT
Hinge Pin Handles PULL
EXIT AIRCRAFT then PULL RIP CORD

PRIOR TO TAKEOFF ROLL

Time now: _____
Estimated time when 1 hr fuel remaining: _____
Time of sunset: _____
Autopilot servos verified powered off? _____

NOTE: PIC dedicated to flying aircraft ONLY below 3000 ft AGL

Data Set	Maneuver Description	Notes/Observations

Actual time at conclusion of flight: _____

APPENDIX K—FLIGHT TEST DVD

A 17-minute flight test video on DVD highlighting the capabilities developed and tested in flight is available by request to the authors. John Wilson may be reached at jwilson210@earthlink.net. Mark Peters may be reached at mark.peters.533@gmail.com.